ISAS - SCUOLA
INTERNAZIONALE
SUPERIORE
STUDI AVANZATI
TRIESTE
Strada Costiera 11

ISAS - INTERNATIONAL SCHOOL FOR ADVANCED STUDIES

"Ab-initio Study of Si-Ge Alloys and Ultra-thin Superlattices"

Thesis submitted for the degree of
Doctor Philosophiae

Candidate:
QTEISH Abdallah

Supervisor:
RESTA Raffaele
Prof.

December 1987

TRIESTE

Ab-initio Study of Si-Ge Alloys and Ultra-thin Superlattices

Thesis submitted for the degree of Doctor Philosophiae,
at the International School for Advanced Studies, Trieste,Italy.

Dec. 1987

To My Parents

Acknowlegments

I would like to express my gratitude to Prof. R. Resta for his co-operation and his friendly guidance throughout this work. I also wish to express my appreciation for Prof. A. Baldereschi for his continuous help and many fruitful discussions. I am indebted to Prof. E. Tosatti for his continuous encouragement and support. I would like to thank Prof.'s S. Baroni, A. Balzarotti and N. Motta for several helpful discussions. Finally, I want to thank Cav. S. Stabile for his valuable technical help.

Contents

This Thesis

This thesis is devoted to the study of Si_xGe_{1-x} alloys and ultra-thin superlattices, using the state-of-art density functional theory and norm-conserving pseudopotentials. The present work is the only available ab-initio study for Si-Ge alloys. For the alloy phase, we have introduced a model for the microscopic atomic structure based on the tetrahedron approximation. Nine different ordered structures (each corresponding to a different configuration of the tetrahedra) have been studied.

These ab-initio calculations allowed us to study the structural properties (lattice parameter, bond length alternation and their variation with x), bond ionicity and its dependence on the chemical environment, stability of the bulk ordered structures and (assuming completely random distribution of atoms at the lattice site) the energy of mixing of Si_xGe_{1-x} alloys.

Using our previously calculated formation energies of the tetrahedra configurations, and solid state statistical mechanical methods (cluster variation method and a modified quasi-chemical approximation), the entropy, enthalpy, Gibbs free energy and other thermodynamical functions are calculated from first-principles, as functions of x and temperature. Since bulk ordered structures are found to be unstable, only disordered alloys have been studied. From the calculated free energy of mixing, the phase diagram has been constructed and the critical temperature is deduced. Also, the tendency to clustering in these materials has been studied. Furthermore, the effects of the pressure on the above properties have been studied, by performing similar calculation under hydrostatic pressure.

The band structure and its pressure dependence for Si, Ge, And Si_xGe_{1-x} alloys have been studied using the same approach. For the alloys, the calculations are performed within the virtual crystal approximation (VCA) and the supercell approach; the latter is done by performing different supercell calculation at ($x = 0.5$), from which we were able to study the effects of ordering,

charge density distribution and microscopic structural relaxation on the band structure. The pressure coefficients of the band gaps at the high symmetry points have been determined for Si and Ge; for the alloys this has been done only at $(x = 0.5)$, within VCA and Zinc-blend structure.

Finally, we have studied the stability and the electronic structure along the high symmetry lines of two Si_2Ge_2 superlattices, having (111) and (001)-orientations. The (110)-oriented superlattice has the same crystal structure as the (001)-oriented one. Therefore, the three high symmetry directions are considered in our study of the above superlattice. The total crystal charge densities and that corresponding to the lowest conduction band states are displayed, and the electronic confinement of the conduction band states is studied.

The material of this thesis is divided into four chapters, in addition to the introduction. Each of the chapters 2-5 is treated as an independent report having its own introduction, and a summary of the main results and conclusions.

The results reported in Ch. 2 are the subject of a paper accepted in final by the Physical Review B, and now in press. Those reported in Ch. 3 are the subject of a paper accepted (subject to a miner revision) by Physical Review B. The results of Ch.'s 4 and 5 are the subject of further papers, which are presently being written.

Chapter 1

Introduction

The possibility of producing new materials with designed optical and electrical properties makes the study of semiconducting alloys and superlattices of paramount importance. Specially if one is talking about alloys and superlattices of Si and Ge which have great potentials for device applications. Recently, new important developments have been achieved in the field of semiconductor alloys. Here, we will start by mentioning some of these developments which have a direct connection with the subject of the thesis.

- The observation of the long-range ordering in some of strained and unstrained semiconductor alloys superlattices, by annealing the grown layers [1-7]. For example, the observed tetragonal structure in $Ga_{0.5}Al_{0.5}As$ [2] superlattice grown on GaAs substrate. Previously, they were known to form disordered alloys with positive interaction parameter (i.e. to be thermodynamically unstable). Srivastava, Martins and Zunger [9] have shown how this can be possible, through ab-initio total energy calculations, while Martins and Zunger [10] have studied the effects of strain in stabilizing the ordered structures observed in strained alloys superlattices. However, this is still a controversial subject, since Kunc and Batra [11] and Ciraci and Batra [12,13] have shown that the observed ordered

structures, in $Ga_{1-x}Al_xAs$ and Si_xGe_{1-x} alloys, can be described as a moderate tendency towards *segregation* into isolated regions having only bulk properties.

- The developments in the high precision growth techniques, such as, the molecular beam epitaxy (MBE) and metalorganic chemical vapor deposition (MOCVD). The degree of control is now so advanced that novel synthetic structures, with layer thicknesses down to one monolayer have been grown [14-16]. The stability [11-13,17,18] and the electronic structure properties [19] of the ultra-thin superlattices are now of current interest. They have been found to have different electronic structure properties than random alloys having the same concentration.

  - The folding of the Brillouin zone may lead to a new optical transitions, as the new quasi-direct transitions observed in Si_4Ge_4 (001)-oriented superlattice grown on Si substrate [14].
  - The energy gaps of the ultra-thin layered superlattices are usually smaller than that of random alloys [7,20,21]. In Fig. 1.1 we show the photoluminescence spectra of $(InAs)_1(GaAs)_1$ superlattice and of $In_{0.5}Ga_{0.5}As$ alloys, where the difference is very clear.

- Extended X-ray absorption fine structure (EXAFS) measurements [22-26] have shown that the bond lengths of the different bonds are neither equal among themselves nor equal to the corresponding ones in the pure materials, being however much closer to the latter, and having weak dependence on the alloy composition. These observations provide a direct evidence for the existence of structural disorder, in addition to the chemical disorder (i.e. random distribution of the atoms at the lattice sites) which usually exists in such materials. The structural properties of alloys are also of current interest for the variety of problems connected with them such as, the energy gap bowing [8], stability and other thermodynamic properties [9,28,27],... etc.

- Previously, the thermodynamic properties of semiconductor alloys were studied using only phenomenological approaches. The major aim for this type of calculations is to calculate the energy of mixing, which can be split

into elastic and chemical contributions. In these approaches only one of the contributions (chemical [29-32] or elastic [33-35]) is often considered in an approximate way. Both contributions are considered in some cases [27]. The new development is the determination of the structure configurational energy [36-40] using the state-of-art density functional theory (DFT) [41,42], which takes properly into account both of the above contributions on the same footing. In this type of calculations, the alloy is considered to be formed from basic building blocks (basic clusters) consisting of a small number of atoms. The basic assumption is that each configuration of the basic clusters can be realized by an ordered structure, consisting only of clusters of this configuration. Therefore, the problem of determining the thermodynamic properties is divided neatly into two steps:

1. The calculation of the ground state properties such as, the total energy of each configuration of the basic cluster which is the key quantity. Because of the above assumption, this can be done using a first-principle approach.

2. The calculation of the thermodynamic properties (such as entropy, enthalpy, ...), starting from the calculated energies in the previous step, and using the methods of solid state statistical mechanics (e.g cluster variation method).

It has been shown by Zunger and co-workers [36,37,38] that proper account for both the elastic and chemical contributions is essential and leads to new features in the phase diagram. Up to now, only the solid phase is considered. The determination of the above properties for the liquid phase is lacking behind, and requires new developments.

Recently, Si_xGe_{1-x} alloys properties of the bulk and in the form of superlattices have became a subject of increasing interest. The strained Si/Si_xGe_{1-x} superlattices have been found to have very intriguing transport, structural and electronic structure properties, such as the observed strong low-temperature mobility enhancement in selectively doped Si/Si_xGe_{1-x} [43], the long-range or-

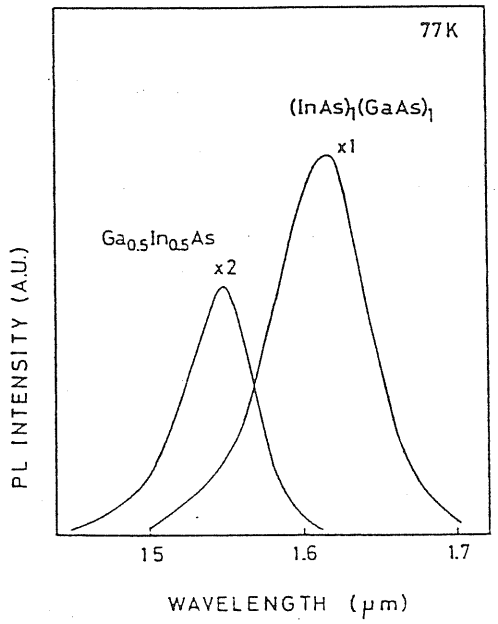

Figure 1.1: The photoluminescence spectra of $(InAs)_1(GaAs)_1$ superlattice and $In_{0.5}Ga_{0.5}As$ alloys at 77 K. (from Ref. 21)

dering observed in $Si/Si_{0.46}Ge_{0.54}$ [1] and the new quasi-direct optical transitions observed in ordered Si_4Ge_4 [14] strained-layer superlattices.

In this thesis we will focus on Si_xGe_{1-x} alloys. Both Si and Ge belong to the same group IV of the periodic table, which contains in addition to them C, Sn and Pb. Among all the possible binary compounds of this group only SiC is known to exist in stable ordered structures, while Si and Ge are known to form random alloys with positive interaction parameter. The lattice constants of pure Si and Ge are mismatched by 4%; this implies that the microscopic structures of Si_xGe_{1-x} are usually strained. Only very limited EXAFS measurements for these alloys are available [25,26]. Whereas from the experimental point of view, the band structure of Si_xGe_{1-x} is well established [44,45].

Here, the structural, thermodynamic and electronic structure properties of random alloys, and the stability and the electronic structure of Si_2Ge_2 (001) and (111)-oriented superlattices have been studied. The calculations are performed using the local density approximation (LDA) [46] of (DFT) and norm-conserving (NC) pseudopotentials [47,48]. To our knowledge this is the most complete and detailed study for these materials.

The calculations of the ground state properties of solids has advanced significantly in recent years. It is now possible to carry out within a unified theory (based on DFT-LDA and NC pseudopotentials) accurate calculations of the static [49], dynamic [50] and other ground state properties. The fundamental quantity in this theory is the total energy. If one is able to calculate the total energy for a given ionic configuration, the calculation of the experimentally measurable quantities can be easily carried out. In DFT, the Kohn-Sham eigenvalues are only meant to be used in the total energy calculations. However, they have been used as excitation energies. The calculated gaps of semiconductors in this way are underestimated by 20 - 50 %. The discrepancy is now understood as a consequence of a discontinuity in the exchange and correlation potential [51]. This method is now a standard technique in solid state physics. Excellent review articles are available in the literature [52-56]. For this reason and because of space limitations, the method will not be reviewed here. It should be mentioned at this point that very recently Car and Parrinello [57] have combined LDA with molecular dynamic simulations, providing in this way the basis for new interesting and exciting developments.

The thesis is divided mainly into four chapters, each one having its own introduction, and a summary of the related main results and conclusions are given at the end of the chapter. In the following we give a very brief summary about the contents of each one:

Ch. 2 is devoted to studying the structural properties (such as bond length alternation and the variation of lattice constants and bond lengths with x), and the stability of ordered and random Si_xGe_{1-x} alloys. This has been done first within the virtual crystal approximation (VCA). It has been shown that the obtained results are far from being satisfactory. In order to go beyond VCA a model for the atomic microscopic structure of binary alloys has been introduced. Within this model the 5-site tetrahedron is taken as basic cluster. Nine ordered structures (each corresponding to different configuration) have been studied. The total energy as a function of the lattice parameter a (including local structural relaxation) has been determined. Therefore, the first step in the determination of the thermodynamic properties is done. None of the above ordered structures is found to be stable. Good agreement between

the x variation of the bond lengths of Ge-Ge and Ge-Si pairs and the available theoretical and experimental results has been found, the one of the Si-Si pairs is predicted. The ionicity of the Si-Ge is found to be very small and unaffected by the chemical environment. The energy of mixing and the interaction parameter of random alloys are calculated, by assuming random distribution of the tetrahedra. The calculated interaction parameter at $x = 0.5$ is found to be in very good agreement with the available experimental data. The convergence of our calculations has been checked by recalculating the energy of mixing within the pair approximation (considering the bond as basic cluster).

In Ch. 3 we complete the calculation of the thermodynamic properties of Si_xGe_{1-x}, using the energies calculated in Ch. 2, and the methods of solid state statistical mechanics. Since the long-range ordered structures are found to be unstable, only disordered alloys are studied. Two approximations for the configurational entropy have been used, which are the cluster variation method (CVM) [58,59] and a modified quasi-chemical approximation (QCA) [60]. As a consequence of our structural model, only constrained CVM calculations can be performed. The thermodynamic function such as entropy, enthalpy, free energy and others are calculated as functions of temperature and composition. The phase diagram is also calculated and the critical temperature is predicted to be around 360 K. The tendency to clustering is found to be very small, which provides further support for the instability of ordered bulk Si-Ge structures. The effects of the pressure on the phase diagram, thermodynamic functions and clustering have been studied. For the phase diagram, it has been found that by increasing the pressure the instability region shrinks and moves toward the Ge-side while the critical temperature increases, and it has drastic effects on the other studied properties.

In Ch. 4 we digress from random alloys to study the stability and the electronic structure of Si_2Ge_2 (001) and (111)-oriented superlattices. The (110)-oriented superlattice has the same crystal structure as that of the (001)-oriented one. It has been found that they are thermodynamically unstable. The (111)-oriented superlattice is found to be relatively more stable than the other one which, in turn, is more stable than the zinc-blende structure (Si_1Ge_1 superlattice along both directions). This shows clearly the tendency of Si-Ge systems

toward segregation. The band structure of the equilibrium structures has been calculated, and compared with that of $Si_{0.5}Ge_{0.5}$ alloys within VCA and zinc-blende structure. It has been found that both of the two superlattices are indirect gap semiconductors. The mixing between the conduction band states is found to be appreciable, and has direct effects on the conduction band structure. The level charge density of the lowest conduction band levels at the high symmetry points is displayed.

In Ch. 5 we go back to random alloys to study their band structure and its pressure dependence. It has been found that if the band structure of Si and Ge are calculated at the calculated equilibrium volumes, desirable results within LDA can be obtained. The underestimation of the band gaps of the two elements are found to be comparable, and correct topology for the band structure of Ge is found. Using VCA meaningful variation of the band gaps of Si_xGe_{1-x} alloys with x has been found, the crossover point in the lowest optical transition from Ge-like (at L-point) and Si-like (at Δ-line) is found to be at $x = 0.12$, in good agreement with the experimental value $x = 0.15$ [44]. To go beyond VCA some supercell calculations at $x = 0.5$ have been performed; the effects of ordering, charge density distribution and microscopic structural relaxation are discussed. The pressure coefficients of the band gaps of Si, Ge and $Si_{0.5}Ge_{0.5}$ alloys within VCA and zinc-blende structure have been calculated. Our calculated values for the pure elements are in very good agreement with experiment and with other self-consistent calculations. For the alloy (at $x = 0.5$) our calculated results are closer to Ge than to Si.

Chapter 2

Structure Properties and Stability

Extended X-ray absorption fine-structure (EXAFS) measurements have shown that the bond lengths in alloys are not strictly equal to $\frac{\sqrt{3}}{4}a$ (where a is the lattice constant of the alloy), but different type of bonds have different bond-lengths which are closer to that of the corresponding pure materials. This has been found in several pseudobinary alloys [1-5]. As a consequence there is structural disorder in addition to the chemical disorder (random distribution of the atoms in the lattice sites) which usually exists in these materials. The determination of these properties is of current interest for variety of problems connected with the structural disorder such as:

- It has been shown by Jaffe and Zunger [8] that major part of the energy gap bowing is due to such kind of disorder.
- The energy of mixing is a direct measure of the alloy stability. It can be split as a sum of elastic and chemical contributions. By definition the chemical term is due to the electronic density redistribution and local

structural relaxation. Bublik et al. [61] have shown that the chemical contribution to the interaction parameter can be determined experimentally by X-ray diffuse scattering technique; for Si_xGe_{1-x} it is found to be x-independent.

- For excitons bound to isoelectronic impurities (such as $GaP_xAs_{1-x}:N$ and $Ga_xIn_{1-x}P:N$) it has been found that the chemical disorder around N modifies the exciton lineshape (broadening and shift) and induces migration of the exciton from site to site [62]. The excitonic transfer occurs as a consequence of the different energies associated to the different nearest-neighbors configuration of the atoms surrounding nitrogen which, in turn, is connected with the bond length alternation.

Another interesting aspect is the recently observed long-range ordering in semiconducting alloys superlattices, which is a novel feature in semiconducting alloys. Previously they were known to form disordered alloys with positive interaction parameter. This has been observed in strained Si_xGe_{1-x} [1] grown on Si substrate, and unstrained (or weakly strained) $Al_xGa_{1-x}As$ [2] grown on GaAs, $GaAs_xSb_{1-x}$ [3] and $In_xGa_{1-x}As$ along $< 100 >$[4], $< 110 >$ [5] and $< 111 >$-directions [6] grown on InP substrate. These observations have raised important questions concerning the equilibrium phases of these alloys at low temperature and the thermal stability of the ultra-thin superlattices grown by molecular beam epitaxy (MBE) or metalorganic chemical vapor deposition (MOCVD). It has been found theoretically that coherent ordered structures could be stable [9,63], despite the positive interaction parameter of the disordered phase. The ordered semiconducting alloys are new materials which have different properties from the disordered phase having the same composition [20,21,43]. Understanding the mechanism behind the stability of ordered structures is of paramount importance from the conceptual and practical point of views.

This chapter is devoted to the study of the structural properties (lattice parameter, bond length alternation and their variation with x), bond ionicity, stability of bulk ordered structures and energy of mixing of the random Si_xGe_{1-x} alloys. The calculations are performed using the state-of-art density functional theory [41,42], within the local density approximation [46] and norm-conserving

pseudopotentials [47,48]. In order that the calculations can be performed at the first-principle level, a model for binary alloys based on the tetrahedron approximation has been introduced in the spirit of the model for ternary semiconducting alloys recently proposed by Srivastava, Martins and Zunger [9]. Nine different ordered structures (each belonging to different configurationsof tetrahedra) are studied. None of them is found to be thermodynamically stable, and this has been attributed to the very small ionicity of Si-Ge bond. Such a feature contrasts the large ionicity of the Si-C bond, which was found to stabilize the Si-C ordered structures [64]. Furthermore, the Si-Ge bond is found to be localized (the ionicity is unaffected by changes in concentration and chemical environment), in full agreement with the experimental finding that the chemical term in the interaction parameter is x-independent [61]. The variation of the bond lengths of Si-Ge and Ge-Ge pairs with x are found to be in good agreement with the available experimental [25,26] and theoretical [35] results, and the variation of the Si-Si bond length is predicted. Assuming completely random distribution of tetrahedra the energy of mixing and hence the interaction parameter are calculated as functions of x. At $x = 0.5$ the interaction parameter is found to be equal to 1.05 kcal/mol (mole referred to a formula unit with one atom throughout the thesis) in good agreement with the experimentally estimated value 1.21 [33] and 0.97 kcal/mol [65] Whereas, around 20% of the interaction parameter is found to be x-dependent, in contradiction with the regular solution model which assumes constant interaction parameter.

For completeness, we have performed independent calculations using the virtual crystal approximation (VCA). Our main finding is that VCA gives unsatisfactory results. The energy of mixing and the x-variation of the lattice parameter are in large disagreement with the experimental results. This demonstrates the necessity of going beyond VCA.

The rest of the chapter is organized as follows. In Sec. 2.1 we report and discuss the results obtained using VCA. In Sec. 2.2 we describe the structural model and the way used to deduce results for random alloys from calculations performed for periodic structures. In Sec. 2.3 we describe the crystal structure of the simplest coherent periodic structures which realize the tetrahedra configurations. In Sec. 2.4 we give details on the calculations and results for the

periodic structures. Sec. 2.5 is devoted to the study of bond lengths (alternation and x-dependence) and bond ionicity. In Sec. 2.6 we consider the energy of mixing and the interaction parameter of the completely random alloys. Finally, Sec. 2.7 contains summary of our main results and conclusions.

2.1 Virtual crystal approximation (VCA)

As we have mentioned above there are two kinds of disorder exist in alloys. 1) Chemical disorder which is related to the random distribution of the constituent atoms at the lattice sites. 2) Structural disorder which is related to the bond length alternation. Because of disorder it is very difficult to attack frontly the problem of the alloys. Different approximations have been proposed to describe alloys, such as VCA, coherent potential approximation (CPA) [66], molecular CPA [67] and the cluster averaging approximation [27]. Due to its attractive simplicity, VCA is widely used in the literature to describe alloys. Specially in the band structure calculations. Some VCA calculations [68] of the structural properties have been also performed for Si_xGe_{1-x} alloys. However, these calculations are not at the first-principle level.

VCA is a very crude approximation. Even if the structural disorder is neglected, it is valid only when the difference in the potentials of the constituent materials is very small [69]. In VCA the chemical identities of the individual alloyed elements and bonds are eliminated by assuming that

- The atoms are occupying without vacancies the lattice sites of perfect zinc-blende structure. Thus, the structural disorder is completely neglected.
- The potential is a weighted average of the ionic potentials at the alloyed lattice sites. For binary alloys it is given simply as

$$V = xV_A + (1-x)V_B,$$

  where V_A and V_B are the ionic potentials of the constituent materials.
- As a consequence of the previous points, the alloy has the same point group symmetry as that of the end materials.

The ground state properties of Si_xGe_{1-x} for $0 < x < 1$ in steps of 0.1 of the alloy composition x, have been determined self-consistently in the framework of density functional theory [41,42], using the local density approximation [46] and norm-conserving pseudopotentials [47,48]. For the exchange and correlation we use the results of Ceperley and Alder [70], as parametrized by Perdew and Zunger [71]. The pseudopotentials are taken from the tabulation of Bachelet et al. [72]. The special-point technique [73] is used to obtain the density from the Brillouin-Zone integration, where the two Chadi-Cohen [74] special points have been used. The one-particle wave functions are expanded in plane waves (PW's) with a constant energy cutoff E_{cut}. Self consistency has been achieved to better than 10^{-5} Ry/atom where the variational expression for the total energy has been used.

For each of the above mentioned concentrations, the total energy has been calculated at several values of the lattice parameter a around the equilibrium. In this study we use $E_{cut} = 17.5$ Ry. The results are least-square fitted to Murnagham's equation of state [75]

$$E(V) = \frac{B_0 V}{B_0'} \left(\frac{(\frac{V_0}{V})^{B_0'}}{(B_0' 1)} + 1 \right) + const. \qquad (2.1)$$

where V_0 is the equilibrium volume, B_0 and B_0' are the bulk-modulus and its pressure derivative at V_0. The results of the fit are shown in Tab. 2.1. In Fig. 2.1 we show the calculated lattice parameter within VCA (diamond), compared with Vegard's law variation (straight line) and experiment (solid curve); to draw this curve, we have simply scaled the experimental results to match to the theoretical end points. The calculated lattice parameter shows upward bowing, in contradiction with the experimental variation which show small downward bowing [76]. In Fig. 2.2 we show the calculated bulk moduli (diamond); the straight line is drawn to guide the eyes. It shows downward bowing, which is also in contradiction with experiment, since the elastic constants experimentally obtained are larger than the weighted average of the corresponding values of pure Si and Ge [61]. Such a feature is however consistent with the fact that the calculated lattice parameter is larger than experiment (implying larger compressibility).

Another important discrepancy between theory at the VCA level and experiment is due to the energy of mixing. The interaction parameter Ω at $x = 0.5$

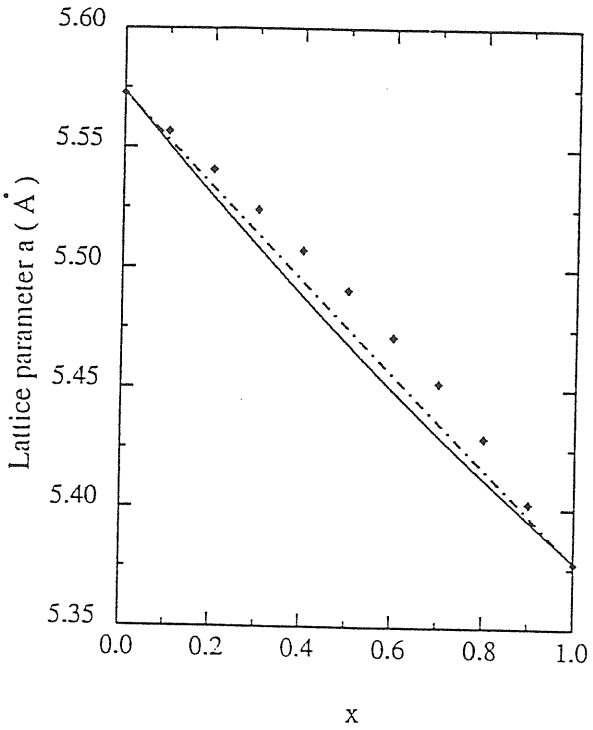

Figure 2.1: Equilibrium lattice parameter as a function of x. Dashed-dotted line: Vegard's law; diamond: this work, first-principle calculation within virtual crystal approximation; solid line: experimental deviation from Vegard's law [76]; to draw this curve, we have simply scaled the experimental results to match the theoretical end points.

is equal to four times the energy of mixing. Our calculated value for $\Omega(0.5)$ is is 11.15 kcal/mol, one order of magnitude larger than the indirectly estimated experimental value 1.21 kcal/mol [33].

Therefore, it is evident that VCA is a poor approximation for the structural properties of Si_xGe_{1-x} alloys. In addition to the fact that the informations we get using VCA are limited, they are in contradiction with the experimentally observed results. However, we will show in Ch. 3 that VCA is a good approximation for optical properties and band structure calculations. In order to go beyond VCA, we will introduce in the following section a model for binary alloys based on the tetrahedron approximation.

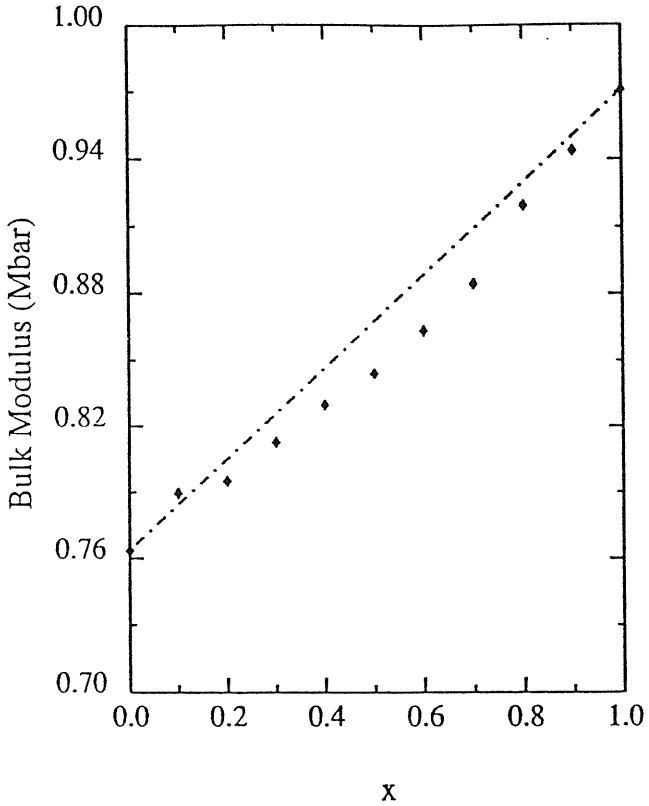

Figure 2.2: The bulk modulus of Si_xGe_{1-x} as a function of x. Diamond: the calculated values within virtual crystal approximation; dashed-dotted line: linear variation (drawn to guide the eyes).

Composition x	Lattice parameter (Å)	Bulk modulus (Mbar)	B_0'
0.0	5.38	0.97	4.34
0.1	5.40	0.94	4.27
0.2	5.43	0.92	4.50
0.3	5.45	0.88	4.06
0.4	5.47	0.86	4.20
0.5	5.49	0.84	4.17
0.6	5.51	0.83	3.92
0.7	5.53	0.81	4.30
0.8	5.54	0.80	4.27
0.9	5.56	0.79	4.80
1.0	5.57	0.76	4.83

Table 2.1: The calculated values of the equilibrium lattice parameter a_{eq}, bulk modulus B_0 and its pressure derivative B_0', within the virtual crystal approximation, at different values of the alloy composition x.

2.2 Microscopic model for binary alloys

We will start by discussing some features of ternary semiconducting alloys (say, $A_xB_{1-x}C$ alloys). X-ray diffraction measurements [77] have shown that, in general, they posses zinc-blende (ZB) like structure: one of the fcc-sublattices is occupied by the cations (the C atoms) and the other is shared by the anions (A and B atoms). The variation of the lattice parameter $a(x)$ is almost linear, therefore fulfilling Vegard's law. Two conflicting models have been proposed for the description of the the microscopic arrangement of the atoms in the ZB structure.

- The approximation that the atoms occupy the ideal ZB sites [78], i.e. all the bond lengths are equal.
- Pauling and Hugins model [79], which assumes the conservation of the bond length (the bond lengths of the alloyed bonds equal to the corresponding ones in the pure materials), leading therefore to a distorted ZB structure when the atomic radii of the constituents are different.

Recently EXAFS measurements [22-24] for this class of materials have shown that they are intermediate between the equal-bond-lengths and Pauling-Hugins pictures, being closer to the latter. The main results of the EXAFS measurements are the following:

- The cation sublattice is weakly distorted (the average deviation is about 1% from the equal bond length structure).
- The first nearest-neighbor anions distances are closer to the corresponding ones in the pure materials (bond length alternation), and they have very weak x-dependence (the bond lengths change by less than 2% over the whole range of x, the larger bond being reduced and the smaller increased).

Therefore, EXAFS measurements show clearly that the structures of these materials are not strictly ZB like structure. But in the other hand, they don't

provide ready answer what does a real atomic-scalestructure of these materials look like.

To study the microscopic atomic structure and the energy of mixing of the above materials a microscopic model has recently been proposed [9,28]. The basic assumption in this model is that the mixed sublattice remains undistorted, the other sublattice being allowed to relax to accommodate different bond lengths. Under this assumption the basic unit of the crystal lattice is a tetrahedron with the cations at the vertices and the anions inside. There are five different configurations of such tetrahedra, according to the number $n = 0, 1, 2, 3, 4$ of A-atoms at their vertices. Knowing the probability distribution of the tetrahedra $P_n(x)$ the average bond length, energy of mixing and other thermodynamic properties (see Ch. 3) can be calculated.

The binary alloys A_xB_{1-x} have different features from the ternary alloys. There are three types of bonds, one of them (the A-B bond) being created in the formation of the alloy and strongly affecting its properties [64]. Both sublattices are alloyed. As in the case of ternaries, the bond length alternation has been observed [25,26] in Si_xGe_{1-x} alloy, but there is no experimental data available for the second nearest-neighbor relaxation. A complete study of the possible local structures would involve energy minimization over a very large number of independent structural parameters. In this work we wish to maintain the problem tractable at first-principle level, and yet to get some insight into local structures, bonding and alloying in Si_xGe_{1-x}. To this aim, we have exploited the simplifying features of the above model for ternary alloys, by assuming that one of the sublattices (arbitrarily chosen) is undistorted, while the other sublattice is allowed to relax. We perform in this way only constrained energy minimization, where in a sense we study relaxation at the level of first neighbors as a function of the local configurations, but we ignore second neighbor relaxation.

The basic assumption of the model implies that all of the possible local structures can be realized in coherent periodic structures having very few atoms per unit cell (up to eight). The building unit is a tetrahedron, whose vertices belong to the undistorted f.c.c sublattice having lattice constant a; the inside atom is allowed to relax. As for periodic structures, we assume the smallest

possible unit cell and the highest symmetry. The distortion of the inside atom is thus determined by a single scalar parameter δ. Since the atom inside the tetrahedron can be either A or B type, there are ten local configurations which we denote A_n and B_n : A (B) refers to the inside atom and $n = 0, 1, 2, 3, 4$ is the number of A atoms at the vertices. Therefore A_4 and B_0 correspond to the pure materials, A_0 and B_4 both correspond to zinc-blende structure and are equivalent; the remaining six configurations describe the other possible bonding geometries within the present model. The crystal structure of the simplest periodic structures which realize the local configurations A_n and B_n are described in the next section. Within this model, each of the tetrahedra contains one or two types of bond, and each of the pure (A-A or B-B) bonds appears in only four configurations. Considering the 5-site tetrahedron as a basic unit makes this model analogous to the central atoms model of Lupis and Elliot [80] or the surrounding atom model of Mathieu and co-workers [81]. Very recently a similar model has been introduced to calculate the frequency-dependent dielectric function of Si_xC_{1-x} alloys [82].

The first-principle theory is used to calculate the formation energy of the periodic structures as a function the structural parameters

$$\Delta E_{A_n}(a,\delta) = E_{A_n}(a,\delta) - \left(\frac{4+n}{8}E_A + \frac{4-n}{8}E_B\right)$$

and

$$\Delta E_{B_n}(a,\delta) = E_{B_n}(a,\delta) - \left(\frac{n}{8}E_A + \frac{8-n}{8}E_B\right) \tag{2.2}$$

where the energies of the pure materials E_A and E_B in Eq. (2.2) are evaluated at the appropriate equilibrium geometries for the disordered alloys. Assuming complete random distribution of the atoms at the lattice sites, the probability distribution of a type of tetrahedra (say, A_n) is equal to the probability of the inside atom of being A-type times the probability of having n A-atoms at the vertices. The latter is assumed to be Bernouillan. We get therefore

$$P_{A_n}(x) = \binom{4}{n} x^{n+1}(1-x)^{4-n},$$

$$P_{B_n}(x) = \binom{4}{n} x^{n}(1-x)^{5-n}, \tag{2.3}$$

which obviously satisfy

$$\sum_{n=0}^{4} (P_{A_n} + P_{B_n}) = 1 \tag{2.4}$$

It should be noticed that this distribution is system, temperature (T) and pressure (P) independent, which is valid only at very high temperatures. In the next chapter we will show how T and P-dependent probability can be evaluated by minimizing the free energy of mixing. Throughout this chapter complete randomness is assumed.

In order to evaluate the average energy of mixing of the alloy, we start from the expression for the periodic systems, Eq. (2.2), where the dependence on the structural parameters a and δ is explicit. We find ΔE strongly dependent on a, but only very weakly on δ (see Sec. 2.4). We notice that, at a given alloy concentration x, the local structures are in general strained in Si_xGe_{1-x} alloys. We use the concentration-weighted lattice constant

$$\bar{a}(x) = x a_A + (1-x) a_B \tag{2.5}$$

to get the energy contribution of each kind of tetrahedra at a given concentration, i.e. :

$$\Delta E_{A_n}(x) = \Delta E_{A_n}(\bar{a}(x), \delta_{eq}), \tag{2.6}$$

where δ_{eq} is the defined in the Sec. 2.4. The average energy of mixing of the disordered alloy $\Delta E(x)$ in terms of the formation energies of the ordered structures is then

$$\Delta E(x) = \sum_{n=0}^{4} \left(P_{A_n}(x) \Delta E_{A_n}(x) + P_{B_n}(x) \Delta E_{B_n}(x)\right). \tag{2.7}$$

We finally mention that correlation between tetrahedra is neglected within our model; the goodness of this approximation is checked below, where it is shown that the charge redistribution in Si_xGe_{1-x} alloys is very small (see Fig. 2.14). More details and discussion about the this will be given in Sec. 2.7.

2.3 Crystal structures

In the previous section we have shown that there are ten different configurations of the 5-site tetrahedra A_n and B_n. As it has been already mentioned, the basic assumption of the above models that all the possible local structures can be realized in coherent periodic structures. In this section we will describe the crystal structure of the simplest periodic structures which realize the local configurations of binary alloys.

2.3.1 A_4 and B_0 configurations

In these configurations the vertices and inside atoms are of the same type. So, they correspond to $x = 1$ and 0 respectively. Since all the bonds are equivalent, there will be no structural relaxation. The periodic structure which realize these configurations is the diamond ($O_h, Fm3m$) structure, with two atoms per unit cell, shown in Fig. 2.3. The unit vectors and the atomic positions are shown in the same figure. The first Brillouin zone (BZ) is shown in Fig. 2.4 by solid lines. All over this work the integration over the BZ is performed using the special points technique. The Chadi-Cohen two special points (3/4, 1/4, 1/4) and (1/4, 1/4, 1/4) have been used, with weight factors 3/4 and 1/4 respectively [74].

2.3.2 A_3 and B_1 configurations

In these configurations the inside atoms is surrounded by three atoms of the same type and one of the other. In other words, it has three homopolar bonds and one heteropolar bond. They correspond to $x = 0.875$ and 0.125 respectively. The simplest periodic structure which realize these configurations is a simple cubic, with eight atoms per unit cell, shown in Fig. 2.5. The symmetry point group is (T_d, F$\bar{4}$3m). The unit vectors and the atomic positions are shown in the same figure. According to our model (which does not allow for the second neighbor relaxation) and by symmetry reasons, only the inside atoms

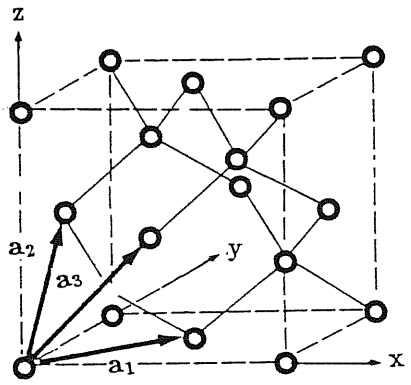

Figure 2.3: Diamond structure which realize the configurations A_4 abd B_0 (see text). a_i (i = 1, 2, 3) are the unit vectors, and they are $\mathbf{a}_1 = a(1/2,1/2,0)$, $\mathbf{a}_2 = a(1/2,0,1/2)$ and $\mathbf{a}_3 = a(0,1/2,1/2)$. Here, a is the lattice parameter. The two basic atoms are located at $a(0,0,0)$ and $a(1/4,1/4,1/4)$.

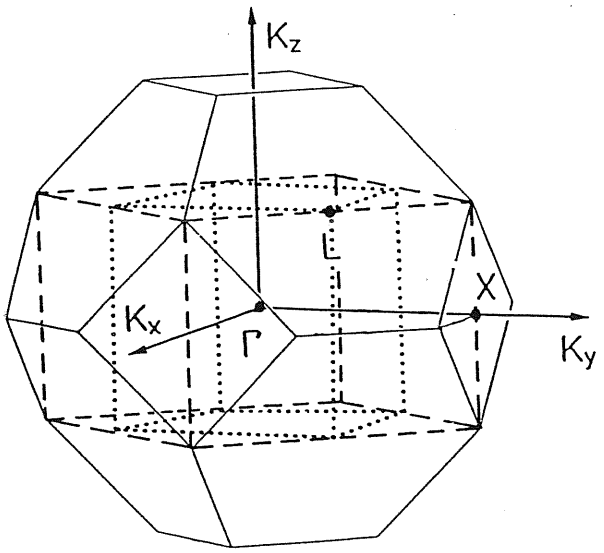

Figure 2.4: Brillouin zones of the studied ordered structures. Solid lines: diamond and zinc-blende structures (shown in Fig.'s 2.3 and 2.8); dashed lines: simple tetragonal (shown in Fig. 2.6); dotted lines: simple cubic (shown in Fig.'s 2.5 and 2.7).

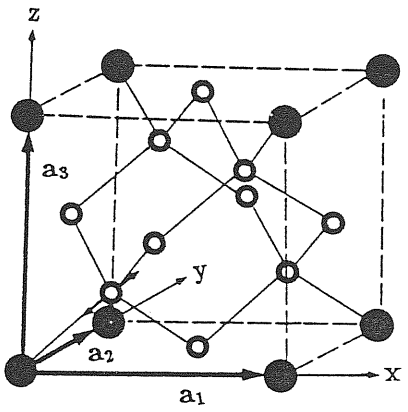

Figure 2.5: The simple cubic structure which realize the A_3 and B_1 configurations. a_i $(i = 1, 2, 3)$ are the unit vectors, and they are $\mathrm{a}_1 = a$ (1, 0, 0), $\mathrm{a}_2 = a$(0,1,0) and $\mathrm{a}_3 = a$(0,0,1). Here, a is the lattice parameter. The eight basic atoms are located at (origin at the center of the cube) a(1/2,1/2,1/2) for B, and a(-1/4,-1/4,-1/4), a(1/4,1/4,-1/4), a(1/4,-1/4,1/4), a(-1/4,1/4,1/4), a(1/2,0,0), a(0,1/2,0) and a(0,0,1/2) for A.

relax by moving along the heteropolar bond. The direction of the relaxation depends on the bond lengths of the involved bonds; if the heteropolar bond is longer than the homopolar bond, the inside atom will relax by moving toward the equivalent three atoms and vice versa. This is shown in the figure by small arrows. The relaxation parameter is defined bd $\delta = d/d_0$, where d and d_0 are the bond lengths of the heteropolar bond before and after ralaxation, respectively. The BZ of this structure is shown in Fig. 2.4 by dotted lines. Using the method of Monkhorst and Pack [83] and the crystal symmetry, the two Chadi-Cohen points for the diamond structure correspond only to one point (1/4,1/4.1/4) in our present case.

2.3.3 A_2 and B_2 configurations

In these configurations the inside atoms is surrounded by two atoms of the same type and two of the other. They correspond to $x = 0.75$ and 0.25 respectively. The simplest periodic structure which realize these configurations is simple

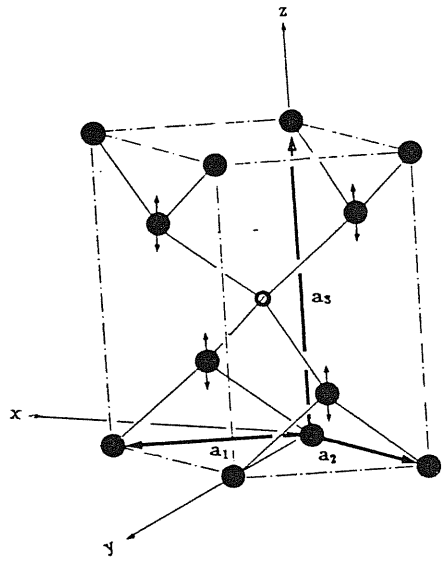

Figure 2.6: The simple tetragonal structure which realize the A_2 and B_2 configurations. a_i (i = 1, 2, 3) are the unit vectors, and they are a_1 = a (1/2,-1/2,0), a_2 = a(-1/2,1/2,0) and a_3 = a(0,0,1). Here, a is the lattice parameter. The four basic atoms are located at a(0,0,0), a(1/4,1/4,1/4), a(1/4,3/4,3/4) for A, and (0,1/2,1/2) for B.

tetragonal, with four atoms per unit cell, shown in Fig. 2.6. The unit vectors and the atomic positions are shown simultaneously in the figure. The symmetry point group is (D_{2d}, P$\bar{4}$2m). In this structure the relaxations occurs by moving the atoms at the center of the faces up or down in the same plane, toward the atoms which form shorter bonds with the relaxing atoms. The relaxation parameter is defined in this case by $\delta = d/d_0$, where d_0 and d are the interplanar distances before and after relaxation between two adjacent layers, with (100) interfaces, having the same type of atoms. The BZ of this crystal structure is shown in Fig. 2.4 by dashed lines. The two Chadi-Cohen special of the diamond structure are the same points in our present case, but with weight factors 1/2 and 1/2, respectively.

2.3.4 A_1 and B_3 configurations

In these configurations the inside atoms is surrounded by one atom of the same type and three of the other. They correspond to x = 0.625 and 0.375 respectively. The simplest periodic structure which realize these configurations

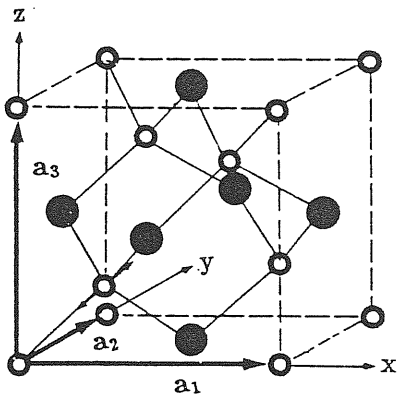

Figure 2.7: The simple cubic structure which realize the A_1 and B_3 configurations. a_i (i = 1, 2, 3) are the unit vectors, and they are a_1 = a (1,0,0), a_2 = a(0,1,0) and a_3 = a(0,0,1). Here, a is the lattice parameter. The eight basic atoms are located at (origin at the center of the cube) a(1/2,1/2,1/2), a(-1/4,-1/4,-1/4), a(1/4,1/4,-1/4), a(1/4,-1/4,1/4), a(-1/4,1/4,1/4) for A, and a(1/2,0,0), a(0,1/2,0) and a(0,0,1/2) for B.

is a simple cubic, with eight atoms per unit cell, shown in Fig. 2.7. The unit vectors and the atomic positions are shown in the figure as well. The symmetry point group, BZ and the special points are the same as that described in Sec. 2.3.2. But the relaxation in this case occurs by moving the inside atom along the homopolar bond. The relaxation parameter in this case is defined by $\delta = d/d_0$, where d_0 and d are the bond lengths of the homopolar bonds before and after relaxation.

2.3.5 A_0 and B_4 configurations

In these configurations the inside atoms is surrounded by four atoms of other type. Both correspond to $x = 0.5$. The periodic structure which realize these configuration is the zinc-blende structure, with two atoms per unit cell, shown in Fig. 2.8. The unit vectors and the atomic positions are shown in the same figure. Because all the bonds are of the same type, there is no structural relaxation. The BZ and the special points are the same as in the case of the

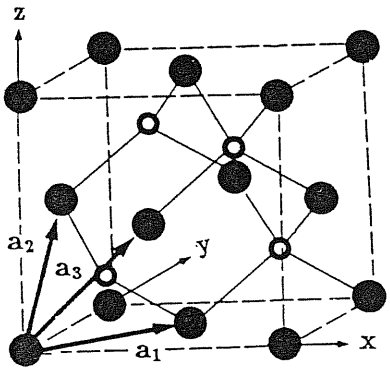

Figure 2.8: The zinc-blende structure which realize the A_0 and B_4 configurations. a_i (i = 1, 2, 3) are the unit vectors, and they are a_1 = a (1/2,1/2,0), a_2 = a(1/2,0,1/2) and a_3 = a(0,1/2,1/2). Here, a is the lattice parameter. The two basic atoms are located at a(0,0,0) for A, and a(1/4,1/4,1/4) for B or vice versa.

diamond structure.

The ground state properties of the above ordered structures are calculated self-consistently. The details of the calculation and the results are given in the following section.

2.4 Calculations and results for periodic structures

The prototypical geometries we have considered for the periodic structures are described in the previous section; their unit cell have from two to eight atoms. The technical details of the calculations are exactly the same as described in Sec. 2.1, except the following

- For simple tetragonal and simple cubic structures, equivalent sets of special points (see Sec. 2.3) to the two Chadi-Cohen points (in the case of diamond structure) have been used.

System	Lattice parameter (Å)	Bulk modulus (Mbar)	ΔE_{ZB} (mRy/atom)
Si			
$E_{cut} = 12$	5.394	.81	
$E_{cut} = 17.5$	5.378	.98	
$E_{cut} = 24^*$	5.378	.98	
Exp.	5.431	.99	
Ge			
$E_{cut} = 12$	5.593	.77	
$E_{cut} = 17.5$	5.572	.77	
$E_{cut} = 24^*$	5.573	.77	
Exp.	5.660	.77	
SiGe(ZB)			
$(E_{cut} = 12)$	5.496	.76	.68
$E_{cut} = 17.5$	5.370	.87	.66
$E_{cut} = 24^*$	5.472	.87	.70

Table 2.2: Theoretical values of the equilibrium lattice constant, calculated at different energy cutoffs (this work; the values marked with an asterisk are taken from Ref. 10), and compared to the experiment. The theoretical formation energy for the zinc-blende structure $Si_{0.5}Ge_{0.5}$ is also shown.

- More convenient constant energy cutoff is chosen.

We show in Table 2.2 the calculated lattice constants and bulk moduli of Si, Ge and SiGe in the zinc-blende structure for several values of E_{cut}, as compared to the experimental data. The formation energy of the zinc-blende SiGe is also shown, where the positive value reflects instability of this compound toward segregation. It is evident from Tab. 2.2 that $E_{cut} = 12Ry$ provides good structures and energies. All of the calculations reported in the following are performed using such cutoff, which leads to approximately 90 - 120 PW's per atom.

Unlike the case of VCA the ZB structure has formation energy a little bit smaller than the energy of mixing of random alloys [33,65]. This is expected since in random alloys having the same lattice parameter, other strained local configurations are possible and these increase the energy of mixing. Furthermore, it is worth to mention that the formation energy calculations [68] based on perturbation theory (including in an approximate way the effect of the third

System	Lattice parameter (Å)	Bulk modulus (Mbar)	Formation energy (mRy/atom)	Relaxation parameter
Si_4	5.394	.81	0.00	1.0000
Si_3	5.408	.86	0.18	0.9917
Si_2	5.429	.78	0.47	0.9972
Si_1	5.462	.66	0.66	1.0084
Si_0	5.496	.68	0.68	1.0000
Ge_0	5.496	.68	0.68	1.0000
Ge_1	5.521	.71	0.71	1.0099
Ge_2	5.542	.77	0.44	1.0082
Ge_3	5.565	.91	0.51	0.9905
Ge_4	5.593	.77	0.00	1.0000

Table 2.3: Theoretical values of the equilibrium lattice parameter, bulk modulus,formation energy and relaxation parameter for the ordered structures (see text), calculated using constant energy cutoff $E_{cut} = 12$ Ry.

and forth order terms) have led to the conclusion that disordered Si_xGe_{1-x} alloy within VCA is relatively more stable than the ZB structure, in contradiction with our first-principle results. This demonstrates that such kind of calculations are not trustable.

The total energy of each of the periodic structures has been calculated according to the following procedure. First, the energy of the unrelaxed ($\delta = 1$) structures is calculated as a function of the lattice constant a at nine points over a 10% range around equilibrium and fitted to Murnagham's equation of state, Eq. (2.1). The results of the fit are shown in Fig. 2.9 and Tab. 2.3, for the nine periodic structures corresponding each to a different concentration x (multiple of 0.125); the oscillatory behavior of the bulk modulus is due to the relatively small energy cutoff we are forced to use here (see also Tab. 2.2), and we will show below that this has negligible effect on the energy of mixing of disordered alloys. Then, at fixed equilibrium volume, we vary the internal relaxation parameter δ (five different calculations for each structure) and we fit the relaxation energy $\Delta E^R(\delta)$ to a parabola; this is shown in Fig. 2.10. We thus get the equilibrium relaxation δ_{eq} at $a = a_{eq}$. We also checked that

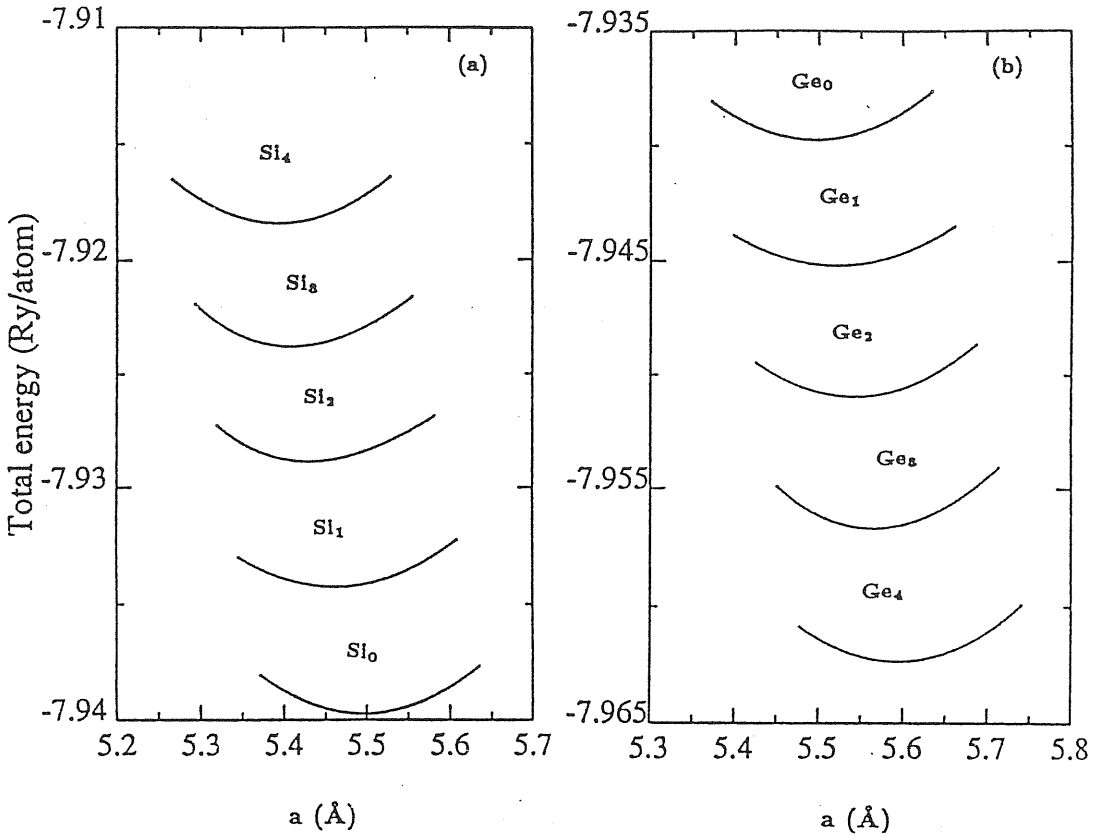

Figure 2.9: Total energies of the unrelaxed periodic structures. Notice the different scales in the two panels; Ge_0 and Si_0 are identical (zinc-blende structure).

$\Delta E^R(\delta)$ has a very weak volume dependence: for instance in case of Ge_2 we get $\delta_{eq} = 1.0082$ and $\Delta E^R(\delta_{eq}) = 0.09$ mRy/atom, while performing the same fit at $a = 5.398$ Å(i.e. at a fixed volume far from equilibrium) we get $\delta_{eq} = 1.0070$ and $\Delta E^R(\delta_{eq}) = .07$ mRy/atom. Energy differences of such order of magnitude cannot affect our calculated values of lattice constants and bulk moduli. Therefore, in the following of this work we neglect the a-dependence of both δ_{eq} and $\Delta E^R(\delta_{eq})$, and we use for each structure a constant value of ΔE^R (calculated at equilibrium volume). A further reason for performing such approximation is that it basically does not affect the calculated energy of mixing of the disordered alloys, owing both to the weight factor in Eq. (2.7) and to the order of magnitude of the strain energy involved.

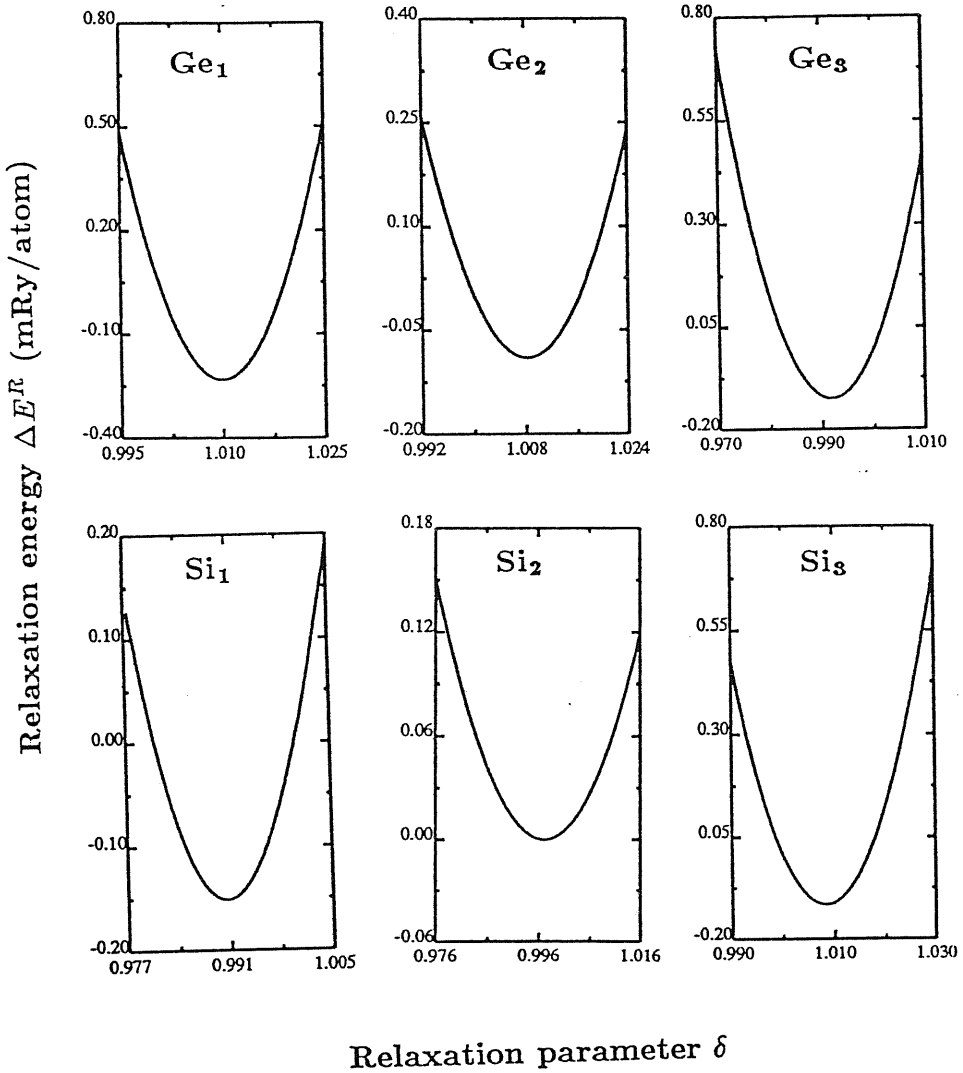

Figure 2.10: Relaxation of the periodic structures (see text).

2.5 Bond lengths and bond ionicity

As it has been mentioned before, EXAFS measurements have revealed that the nearest-neighbor bond lengths are not equivalent (unless there is no lattice mismatch between the end materials), but they are closer to the corresponding bond lengths in the pure materials. This has been observed for different phases of Si_xGe_{1-x} by Minomura et al [25], and for a-Si_xGe_{1-x} by Incoccia et al [26]. In Fig. 2.11 we show the results of Ref. 25. It is clear that the variation of the bond lengths of Ge-Ge and Si-Ge pairs is larger in the case of crystalline phase. The small variation of the amorphous phase is also confirmed by the work of Incoccia et al. This could be due to the stronger structural constraints in the crystalline phase.

We show in Fig. 2.12 the calculated lattice constant as a function of x, together with the experimental data [76]. With respect to Vegard's law (straight line) both theory and experiment show a small downward bowing. The theory exaggerates such bowing for $x > 0.5$, but the overall agreement is nevertheless good. We show in Fig. 2.13 the calculated bond-lengths of Ge-Ge, Ge-Si and Si-Si pairs for each of the periodic structures; the fit of these data to straight lines is also shown (dashed lines). Despite some scattering in the individual calculated points (and the availability of very few points for the homopolar bonds) the quality of the fit is quite good: this is demonstrated by the near parallelness of the three dashed lines in Fig. 2.13, which have been independently fitted. The structures Ge_2 and Si_2 have the largest deviation from the fit; this is probably an artifact of the microscopic model and we speculate that it could be overcome using larger supercells and geometrical freedom.

Extrapolation of our results toward the end concentrations gives $R_{SiGe}(1) \simeq 2.36$ Å(dilute Ge impurities in Si) and $R_{SiGe}(0) \simeq 2.40$ Å(dilute Si impurities in Ge). We follow Ref. 35 in defining a dimensionless relaxation parameter ϵ (different from our previous δ), which gives the "stiffness" of the Si-Ge bond in dilute alloys:

$$\epsilon_{Si:Ge} = \frac{R_{SiGe}(1) - R_{SiSi}(1)}{R_{SiGe}(0.5) - R_{SiSi}(1)}; \quad \epsilon_{Ge:Si} = \frac{R_{SiGe}(0) - R_{GeGe}(0)}{R_{SiGe}(0.5) - R_{GeGe}(0)}, \qquad (2.8)$$

where $R_{SiGe}(0.5)$ is evaluated for the zinc-blende structure. Our first- principle results gives $\epsilon_{Si:Ge} \simeq 0.50$ and $\epsilon_{Ge:Si} \simeq 0.57$, while a valence-force field model calculation [84] indicates 0.58 and 0.63, respectively. Our theoretical values are however strongly sensitive to the extrapolated values of $R_{SiGe}(0)$ and $R_{SiGe}(1)$. However, the two calculations show the same trend.

We show in Fig. 2.14a a contour plot of the valence electronic density for zinc-blende SiGe : the most prominent feature to be noticed is the extremely small ionicity of this compound. This is at variance with the case of SiC, where it has been recently shown that the bonds are strongly polar [64]. A comparison between the bond charge densities of the two bonds is shown in Fig. 2.15. The large ionicity of the Si-C bond is the responsible for the stability of the SiC ordered structures [64] known as polytypes. Here we argue that the small ionicity of the Si-Ge bond makes this bond weaker than the average of Ge-Ge and Si-Si bonds, leading to unstable bulk Si-Ge ordered structures. According to Miedema theory [29] (see also next chapter), the electronic energy contribution is split into two contributions (1) positive term, which is due to the electronic density mismatch (the energy needed to remove the unphysical discontinuity in the charge density) (2) negative term, which is due to the electronic redistribution. Because the second term is very small (see Fig. 2.14(a)) both ordered and disordered Si-Ge alloys are unstable. We show in Fig. 2.14(b) an analogous plot for a different structure (tetragonal Si_3), calculated at the same lattice parameter. Fig. 2.14 then demonstrates that the electronic charge density is weakly affected by the local environment. This is in full agreement with the experimental finding that the chemical contribution to the interaction parameter is x-independent.

Switching now from the periodic structures to the random alloy, a scheme for calculating average bond lengths has been proposed by Balzarotti et al [85] and used in the literature [9,27]

$$\bar{R}_{AB}(x) = \frac{\sum_{n=0}^{4}(N_{AB}^{n}P_{A_n}(x)R_{AB}(x) + N_{BA}^{n}P_{B_n}(x)R_{BA}(x))}{\sum_{n=0}^{4}(N_{AB}^{n}P_{A_n}(x) + N_{BA}^{n}P_{B_n}(x))},$$

$$\bar{R}_{AA}(x) = \frac{\sum_{n=0}^{4}(N_{AA}^{n}P_{A_n}(x)R_{AA}(x))}{\sum_{n=0}^{4}(N_{AA}^{n}P_{A_n}(x))}$$

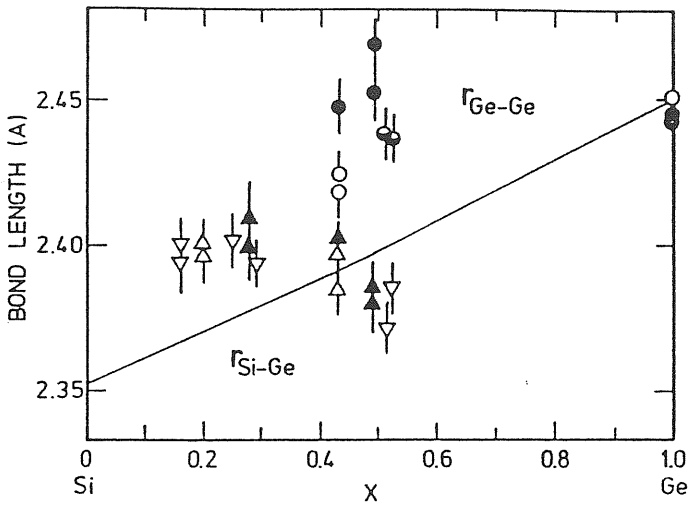

Figure 2.11: Variations of bond lengths of Ge-Ge and Si-Ge pairs
○, △ : c-$Si_{1-x}Ge_x$,
●, ▲ : a-$Si_{1-x}Ge_x$,
⊖, ▽ : a-$Si_{1-x}Ge_x$:H,
—— : from lattice constant
(from Ref. 25)

and

$$\bar{R}_{BB}(x) = \frac{\sum_{n=0}^{4}(N_{BB}^{n}P_{B_n}(x)R_{BB}(x))}{\sum_{n=0}^{4}(N_{BB}^{n}P_{B_n}(x))} \tag{2.9}$$

where N_{ij}^{n} is the number of the ij bonds in the i_n tetrahedra and R_{ij} is the bond length in the corresponding tetrahedra. The bond lengths obtained in such way are shown in Fig. 2.13 as solid lines. The most prominent feature is that bond lengths deviate from those of pure materials much more in the disordered phase; this is shown in Fig. 2.13 by the steepness of the lines. This feature is in close agreement with the finding of Ref. 9 for ternary alloys. The available [25] EXAFS measurements are also shown in the same figure (solid symbols). Although being very few and very poor (large error bars), they can be said to be in agreement with our calculations. The non-monotonical behavior of the Si-Ge bond length suggested by these data is not safely outside experimental error, has no explanation and is not reproduced by the theory, which gives basically linear behavior.

2.6 Energy of mixing of random alloys

Assuming completely random distribution of the atoms in the lattice sites and making use of the the formation energies of the different configurations of tetrahedra calculated in the previous section, we calculate the energy of mixing of Si_xGe_{1-x} random alloys, from Eq. (2.7). It should be noticed that this distribution is system, temperature and pressure independent(in the following chapter

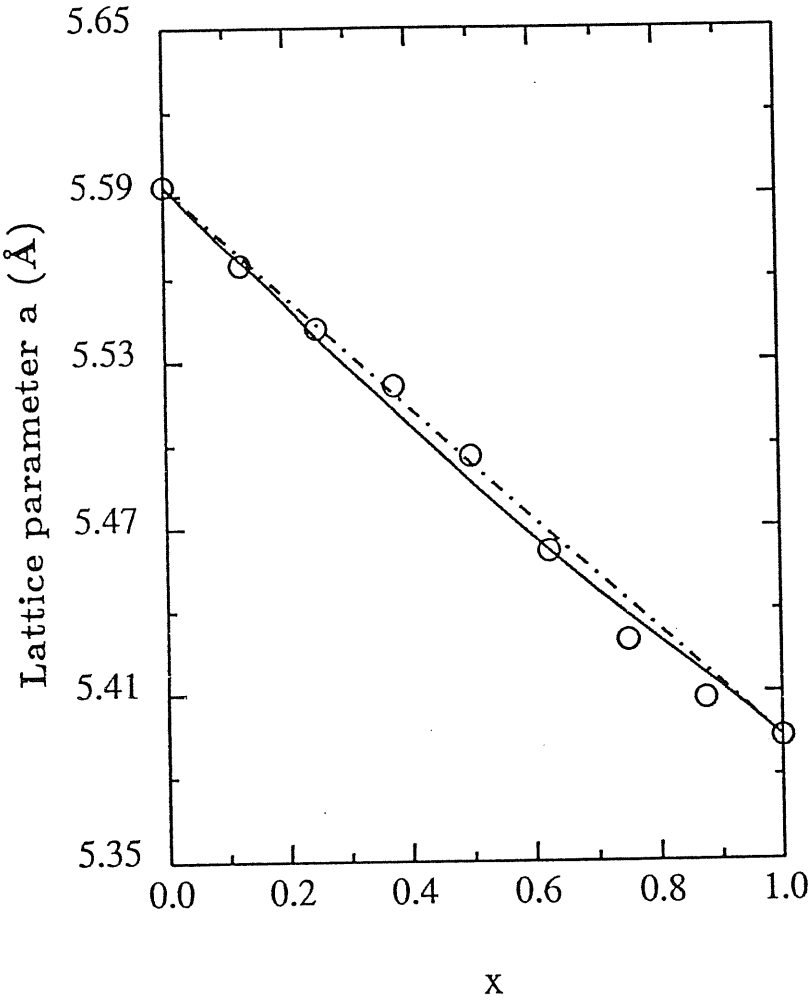

Figure 2.12: Equilibrium lattice constant as a function of x. Dash-dotted straight line: Vegard's law. Circles: this work, first-principle calculations. Solid line: experimental deviation from Vegard's law (Ref. 76); to draw this curve, we have simply scaled the experimental results to match to the theoretical end points.

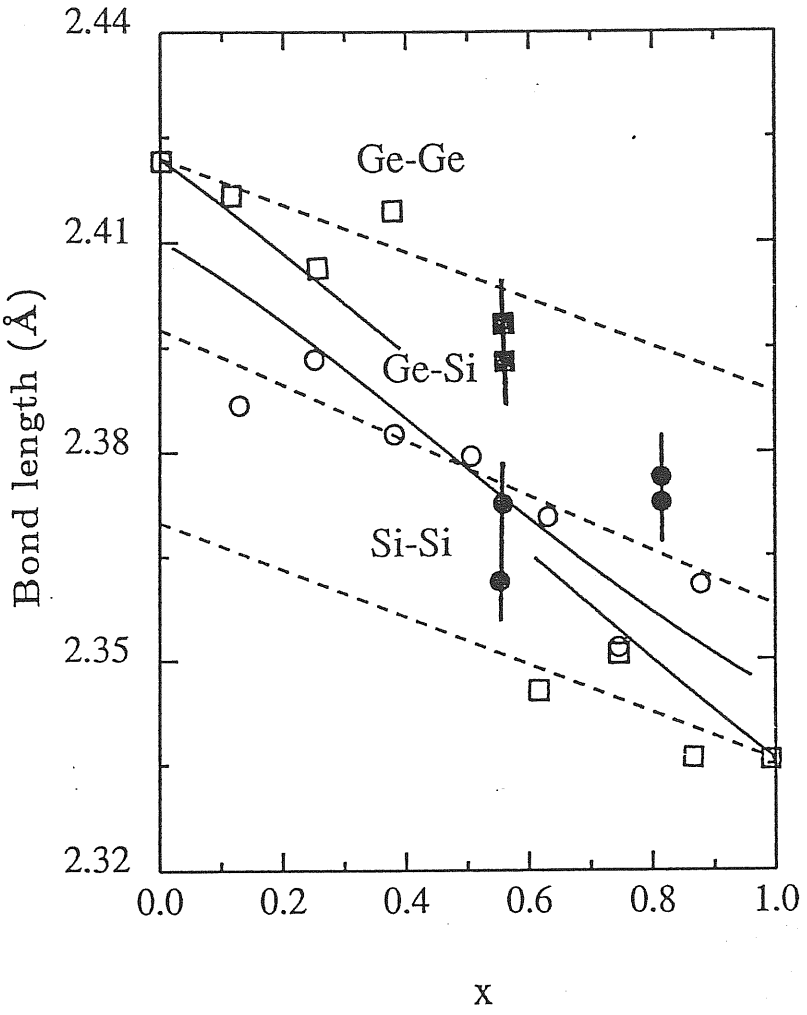

Figure 2.13: Bond-lengths as a function of x. Open squares : this work, homopolar bonds Si-Si and Ge-Ge. Open circles: this work, heteropolar bond Si-Ge. Straight dashed lines: best fit to the calculated values for ordered structures. solid curves: average bond lengths of the disordered alloys, using the method of Ref. 85. The experimental measurements from Ref. 25, are also shown with their (vertical) error bars. Full squares: Ge-Ge bond. Full circles: Si-Ge bond. To draw these points the experimental lattice parameter of Ge is scaled to match the theoretical value.

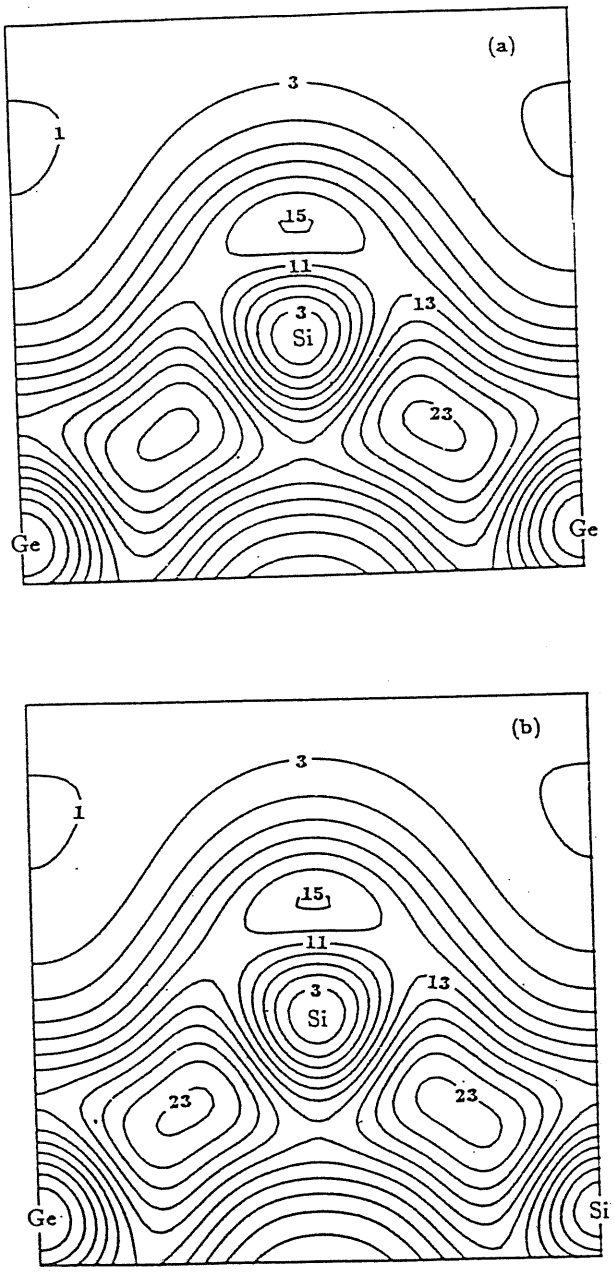

Figure 2.14: Contour plot of the electronic density (electron/unit cell of zinc-blende) of Si-Ge bond in the plane of two bonds, calculated for two different structures at the same lattice parameter. a) $Si_{0.5}Ge_{0.5}$, zinc-blende structure. b) $Si_{0.75}Ge_{0.25}$, tetragonal structure.

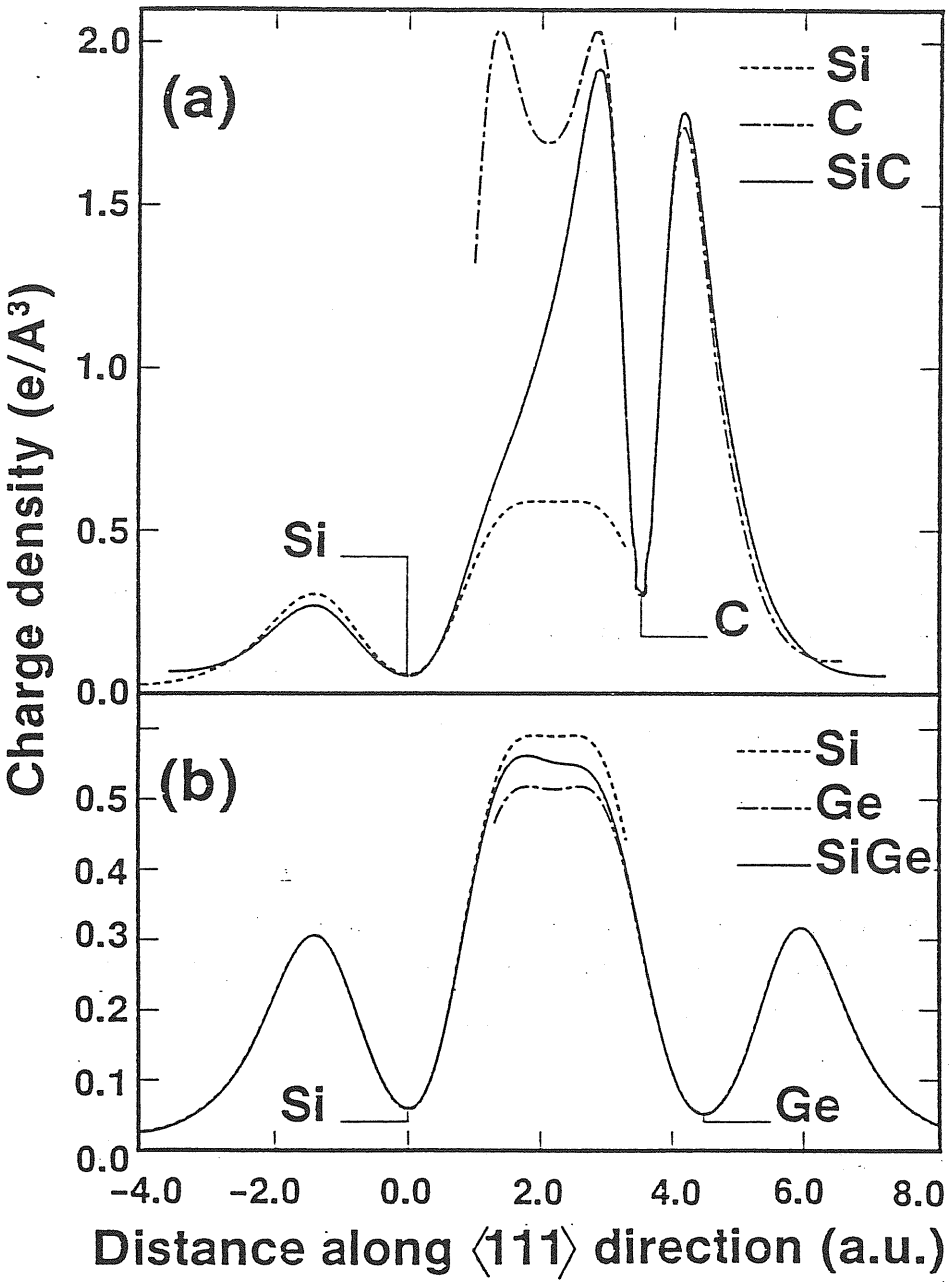

Figure 2.15: The charge densities of C, SiC, Si, SiGe and Ge are compared along the bond direction. For clarity of display, the densities of C, Si, and Ge are shown only in the side of the bond where the atomic positions coincide. (from Ref. 10)

Author	Ω (kcal/mol)
Van Vechten [30]	1.67
Stringfellow (DLP) [33]	1.19
Fedders and Muller [34]	0.89
Martins and Zunger [35]	1.63, 0.89
Present work (at x=.5)	1.05
Experiment [33]	1.21*
Bublik and Leikin (at x=.5) [65]	0.97*

Table 2.4: Interaction parameter Ω of Si_xGe_{1-x} alloys calculated using different models, compared with the results obtained through fitting to experimental data (marked by asterisk).

temperature and pressure dependent probability distributions of the tetrahedra of Si_xGe_{1-x} alloys will be calculated by minimizing the free energy). Our results for the energy of mixing are ploted in Fig. 2.16 (solid line), where the formation energies of each of the periodic structures (circles) are also shown. Within the regular solution model the energy of mixing is written as

$$\Delta E(x) = \Omega x(1-x), \tag{2.10}$$

where Ω is called the interaction parameter. The second derivative of our curve at its maximum, $x = 0.5$, gives a value of Ω of 1.05 kcal/mol, to be compared to an experimental [33] figure of 1.21 kcal/mol. However the experimental measurements are only indirect. It is should be mentioned that Bublik and Leikin [65] have obtained good fitting to the experimental liquidus and solidus curves (usually within 10%), using interaction parameter of the form

$$\Omega(x) = .89 + .16x, \tag{2.11}$$

where the x-dependent term is due to the elastic contribution. A comparison between the values of interaction parameter of Si_xGe_{1-x} alloys calculated using different methods is shown in Tab. 2.4. It is evident that our self-consistent result is in fair agreement with the values obtained through direct fitting to the experimental liquidus and solidus curves. This agreement is much better than all other theoretical approaches. Our calculations also indicate that Ω has an x-dependence of the order of 20%, shown in the figure by the dashed line.

Having calculated the average bond lengths in Sec. 2.5, the average energy of mixing of random Si_xGe_{1-x} can also be calculated in the pair approximation, in which the bond is taken as the basic unit. The energy of mixing within this approximation is given by

$$\Delta E(x) = 2P_{AB}(x)E_{AB}(x) + P_{AA}E_A(x) + P_{BB}E_b(x) - (xE_A(0) + (1-x)E_B(1)), \quad (2.13)$$

where E_{AB}, E_A and E_B are the total energies of the zinc-blende structure and the pure materials A and B, respectively, which have bond lengths equal to the corresponding average bond lengths in the random alloys. $P_{ij}(x)$ is the probability distribution of the the ij bond at the alloy composition x. For random alloys we have

$$P_{AB}(x) = x(1-x), \quad P_{AA}(x) = x^2 \quad and \quad P_{BB}(x) = (1-x)^2. \quad (2.14)$$

The resulting energy of mixing is shown in Fig 2.15 by dotted curve. The small difference between the energies of mixing calculated within the tetrahedron and the pair approximations demonstrates the good convergence of our calculation with respect to the size of the basic unit.

We checked at this point the sensitivity of our results to the quality of the fitting of the total energies to the Murnagham's equation of states. For the simplest periodic structures (i.e. $Si_0 = Ge_4$, Si_4 and Ge_0) completely converged results are available to us: we replaced these results in the corresponding terms of Eq. (2.7), keeping the other terms unchanged. Our final results for both $\Delta E(x)$ and $\Omega(x)$ change upon replacement by less than 1% over the whole range of x, which demonstrates the reliability of our calculations.

The interaction parameter can be unambiguously split in the sum of two terms, one purely elastic and one purely chemical (see e.g. Ref. 36). Experimental evidence [61] has been given that the chemical part of Ω in Si_xGe_{1-x} alloys is x-independent. While most of the theoretical work assumes Ω as x-independent, we naturally account in this work for the x-dependence of the elastic term in the interaction parameter. First-principle theory, in fact, deals with chemical and elastic energies on the same ground.

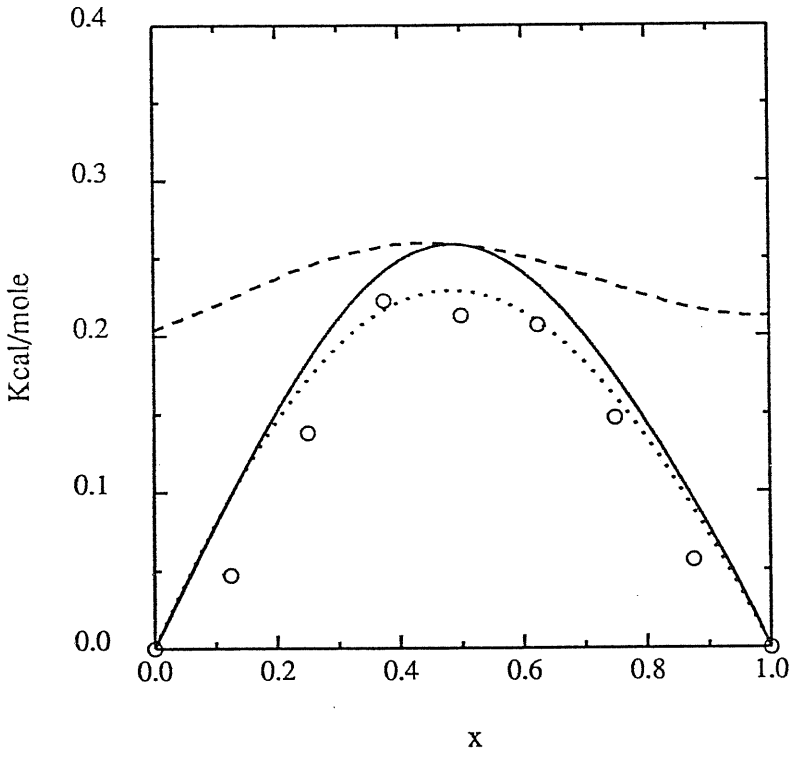

Figure 2.16: The energy of mixing as a function of x. Solid line: for random alloys within the tetrahedron approximation; dotted line: for random alloys within the pair approximation. Circles: for periodic structures. The x variation of the interaction parameter Ω (divided by four) is also shown to the same scale (dashed line).

Srivastava at al. [9] have put a lot of emphasis on the elastic contribution to the energy of mixing, while our calculations indicate that the energy difference between disordered and ordered Si_xGe_{1-x} alloys at a given concentration is fairly small. In fact the elastic energy in our system is one order of magnitude smaller than found by Srivastava et al. for $GaP - InP$ alloys (after Fig.3b in Ref. 9, noticing the difference in units). This fact is due to two reasons: First, our material has a lattice mismatch twice smaller; secondly, the formation energies of the ordered structures are positive in our case, and increase with the number of mixed bonds, thus making less visible the effect of strain. In order to better explain this, let us consider $x = 0.5$: the contribution to the energy of mixing of the disordered phase from each of the (strained ordered) structures Ge_0, Ge_1, Ge_2, Ge_3, Si_1, Si_2, Si_3 and Si_4 is, respectively 1.11, 0.85, 0.70, 0.78, 0.76, 0.87, 0.96 and 1.10 mRy/atom; the corresponding equilibrium values are given in Tab. 2.3. We thus get $\Delta E(0.5) = 0.83$ mRy/atom, while the ordered zinc-blende structure ($Si_0 = Ge_4$) gives 0.68, only 0.15 mRy/atom lower.

2.7 Conclusions and discussion

We have introduced a microscopic model for binary alloys to study the random Si-Ge alloys. We have studied, at a first-principle level, nine different model structures for Si_xGe_{1-x}, using density-functional theory within the local-density approximation and norm-conserving pseudopotentials. Independent calculations have performed with the virtual crystal approximation (VCA). We draw the following main conclusion:

- In addition to the fact that the informations we get within VCA are limited, they are in large disagreement with the observed results. This demonstrates the importance of going beyond VCA.

- None of the ordered structures we have studied is stable towards segregation. According to theory of Miedema [29], the very small ionicity of the Si-Ge bond is responsible for the instability of any ordered structure. Our first-principle calculations of the electronic charge distribution (see

Fig. 2.14) indeed confirm the extreme nonionicity of the Si-Ge bond. The same conclusion comes from previous work of Zunger and Martins [10].

- Our calculations also show that the electronic charge distribution is negligibly affected by changes in concentration and chemical environment. This explains well the experimental finding [61] that the chemical term in the energy of mixing is basically concentration independent in this material.

- We calculate the interaction parameter Ω and we find a remarkable agreement with the experiment. To the best of our knowledge, this is the first ab-initio calculation of Ω for Si-Ge alloys. Previous calculation of Ω where based on models or empirical theories.

- We explicitly account for the x-dependence of the elastic term in the interaction parameter. To date there is no experiment to compare to. Most of the previous theoretical work assumes x-independence; some authors [31] have proposed linear x-dependence. Our work shows that the x-dependence is strongly nonlinear.

- The calculated lattice constant as a function of the concentration shows only very small deviation from linear behavior (Vegard's law), in close agreement with the experimental findings.

- We calculated the bond-lengths of Si-Si, Si-Ge and Ge-Ge pairs as a function of concentration. Very few experimental data are available at present, and only for Si-Ge and Ge-Ge; the agreement with our calculation is good.

- Finally some words about the accuracy of our structural model are in order. Our approximation of assuming one of the two sublattices as undistorted (despite the physical equivalence of the two sublattices in binary alloys) amounts to study relaxation at the level of the first neighbors only. This is indeed a very good approximation, as is discussed in the following. The energy of mixing can be unambiguously split in two parts (see e.g. Ref. 36): (1) the volume deformation contribution, which is the elastic energy needed to stretch and expand the lattice constants of the constituent materials to match that of the alloy, and is model independent; (2) the

chemical contribution, which is the remaining term, due to both charge transfer and relaxation of the bond angles and bond lengths. The charge transfer is pretty small and independent of the local environment, while the local geometrical relaxation gives very tiny contributions. The first principle theory deals with all the terms on the same ground; our approximation, roughly speaking, accounts completely for the elastic term and for the charge-transfer part of the chemical term, while the remaining local relaxation is partly accounted for. Our results compare favorably with the experiment, while the virtual crystal approximation gives energies of mixing one order of magnitude off.

Chapter 3

Thermodynamic Properties

The thermodynamic properties of semiconducting alloys are a subject which still requires a lot of developments. In spite of the technological importance of these materials, the present understanding of their thermodynamic properties is far from satisfactory. Very recently, the state-of-art electronic structure calculations within the local density approximation (LDA) [46] have been combined with statistical mechanics methods to calculate from first-principles the entropy and other thermodynamic properties of these materials [36-40] This type of calculations is based on the assumption that the random alloy is built up of random distributions of basic clusters, and each configuration of these basic clusters can be realized by a periodic structure which consists only of this configuration. This means that the effects of correlations among clusters are completely neglected. We have shown that at least for Si_xGe_{1-x} alloys this is a very good approximation (see Sec. 2.7). As it has been already mentioned, the problem of calculating the thermodynamic properties is divided into two steps: (1) The calculations of the the ground state properties of each configuration of the chosen basic cluster, the most important being the total energy. (2) The calculation of the thermodynamic properties, using the results of step 1 and the

methods of solid state statistical mechanics (e.g. the cluster variation method).

It should be emphasized that the electronic structure calculations are able to provide accurate energies, while they deal with both elastic and chemical energies on the same footing. Previously, only phenomenological approaches were undertaken [28-35] which can be considered as incomplete, since they do not account properly for the all aspects of the problem. The most recent first-principle work of Mbaye, Ferreira and Zunger has shown [36-38] that proper account for the chemical and elastic energies is essential and leads to new features in the phase diagram.

In the previous chapter we have introduced a model for the local atomic structure of binary semiconducting alloys; in this model the basic unit is a 5-site tetrahedron. Nine different ordered structures (each corresponding to different configuration of tetrahedra) have been studied using local density approximation (LDA) [46] and norm-conserving (NC) pseudopotentials [68]. For the disordered materials, the energy of mixing and hence the interaction parameter have been calculated by assuming a completely random distribution of the atoms at the lattice sites (Bernoulli distribution of tetrahedra) which is temperature and system independent, and linear variation of the lattice constant (Vegard's law). Since these materials are usually prepared at high temperatures and quenched (rapid cooling), they maintain the stable atomic distribution at the high temperatures (the random distribution). Therefore, the above assumption is a good one for direct comparison with experiment.

Using the formation energies of the configurations calculated previously, we calculate in this work the probability distribution of tetrahedra, as functions of concentration (x) and temperature (T), in the framework of two different approximations. The first is the modified quasi-chemical approximation (sometimes referred to as third order quasi-chemical approximation [28]) (QCA) [59] The second approximation we use is the cluster variation method (CVM) [57,58]. Since no ordered structure has been found to be stable at $T = 0$, and increasing the temperature is not expected to stabilize any of them, we will study only the disordered Si_xGe_{1-x} alloys. Due to our structural model, which distinguishes between the sites of the two sublattices, only constrained

CVM calculations can be performed, while QCA calculations do not present any problem. The enthalpy, entropy, free energy, interaction parameter and the tendency to clustering as functions of x and T are calculated. The phase diagram has been calculated and the critical temperature is predicted to be around 360 K at zero pressure. We have performed similar study under hydrostatic pressure: our main findings are that the thermodynamic quantities and the phase diagram are strongly affected by pressure.

The rest of this chapter is organized as follows. In Sec. 3.1 we give brief survey and discussion about the used theoretical method to calculate the thermodynamic properties. Sec. 3.2 we give detailed description for the configurational entropy and free energy. In Sec. 3.3 we give the basic equations and definitions of the thermodynamic functions. In Sec. 3.4 we report and discuss the results obtained at zero pressure. In Sec 3.5 we discuss the effects of applying a hydrostatic pressure on the thermodynamic properties. Sec. 3.6 is devoted to discuss the tendency to clustering in these materials. Finally, Sec. 3.7 contains a summary of our main results and conclusions.

3.1 Theoretical Approaches

The determination of the thermodynamic properties, in particular the energy of mixing, is an intriguing aspect with long history. Theoretically very different approaches have been employed. As it has been already mentioned the energy of mixing can be thought of as a sum of chemical and elastic energies, which have opposite effects. The elastic term is positive, so it has the effect of destabilizing the system. Whereas, the chemical term is negative and tends to stabilize it. Therefore, the stability of the system depends on a delicate energy balance between the two terms. It has been shown that proper account for both terms is essential and leads to new features in the phase diagram. In this section we give a critical survey and discuss the used theoretical approaches. Bearing in mind the above splitting of the energy of mixing they can be classified into the following categories.

- **Models considering only the elastic term.** These models assume that the energy of mixing is due to the mismatch in the lattice parameters of the constituent materials. Among these models one finds

    1. The delta lattice parameter model (DLP) of Stringfellow [33], which assumes that the interaction parameter is proportional to the square of the lattice parameter mismatch. The proportionality constant is found by least-square fitting to the available experimental data. The idea behind this model is that the binding energy is proportional to the band gap which, in turn, is proportional to a power of the lattice constant. Because of the direct fitting to the experimental results and the correlation between the lattice-lattice mismatch-distortion and charge density distribution, the chemical term is partly taken into account in this empirical model. This explains the remarkable agreement between the DLP and experiment. This model has been extended recently to take clustering into account by Mardenf and Guillaume [86].
    2. The elastic model of Fedder and Muller [34], which assumes that the energy of mixing can be calculated from the macroscopic elastic

properties. Since only the elastic contribution is considered, the calculated values are 4-5 times greater than the observed values. When empirically scaled, this model gives reasonable results.

3. The valence-force field based model of Martins and Zunger [35]: this model takes into account the structural relaxation (bond alternation), but it neglects any electronic charge redistribution, by assuming the transferability of the bond charge density. The agreement with experiment is almost the same as the DLP model and the scaled elastic Fedder-Muller model.

It should be noticed that these models don't distinguish between the ordered and disordered alloys. Recently first-principle calculations have shown that contrary to the prediction of the above models ordered structures alloys can be thermodynamically stable, despite the positive energy of mixing for the disordered alloys. This has been confirmed experimentally in some semiconducting alloys.

- **Models considering only the chemical term.** In these models the energy of mixing is assumed to be due to the difference in bonding energies and electronegativity of the constituent materials, and the charge density redistribution. Among these models one finds

  1. The theory of Miedema et al. [29]. They characterize each element in the periodic table by two co-ordinates ϕ^* and $\rho^{1/3}$; the energy of mixing of a binary AB alloy is then written (in the simplest case) as:

$$\Delta E = -P(\Delta\phi^*)^2 + Q(\Delta\rho^{1/3})^2, \tag{3.1}$$

  where P and Q are positive constants. The attractive term depends on the difference in the elemental work functions, $\Delta\phi$, (latter modified to $\Delta\phi^*$) and is similar in spirit to Pauling's electronegativity contribution. The repulsive term depends on the difference in the cubic root of the electron densities at the elemental Wigner-Seitz sphere boundaries, $\Delta\rho^{1/3}$, and it was argued to arise from the distribution of the charge density across the AB interface. Equation (3.1) has been useful in providing quantitative values for the energy

of mixing, and it is found to be most successful in the treatment of binary *transition*-metal alloys

2. The Van Vechten model [30]. In this model the energy of mixing is calculated from the energy band gaps bowing, using the spectroscopic theory of the heat of formation.

3. Regular solution model (RSM), which assume that the energy of mixing is due to the difference between bonding energies of the homopolar and heteropolar second nearest-neighbor bonds, namely

$$\Omega = 6N_0(2\epsilon_{12} - \epsilon_{11} - \epsilon_{22}), \tag{3.2}$$

where ϵ_{ij} are the bonding energies. The quasi-chemical approximation is a more realistic version of RSM, which doesn't assume the random distribution. Using this model Jones, Porod and Ferry [31] were able to get some insight about clustering in some semiconducting alloys.

4. The more formal models, such as Kikuchi model [32]. In these models the entropy of mixing is calculated approximately by taking certain clusters as basic units, while the internal energy is calculated as a sum of a pairwise interactions. In this approach the calculation of the entropy is satisfactory. But in addition to the pairwise approximation of the interaction, the volume deformation and the structural relaxation contributions are also neglected.

- **Phenomenological models considering both chemical and elastic contributions** [28]. Recently Balzarotti et al. have introduced a model which takes into consideration both the chemical and elastic contributions. In the configurational energy calculations the elastic energy is calculated using a simplified the valence force-field model: they neglect both the bond bending and second-neighbor relaxation which found to have opposite effects and almost equal contribution. Whereas, the electronic term is calculated from the experimental interaction parameter. This gives a positive chemical contribution for ordered structures, contrary to the present understanding.

- **Ab-initio calculations** [36-40] The calculation of the enthalpy of mixing using the self-consistent band structure techniques is the most ambitious and accurate approach; in this framework the elastic and the chemical contributions are treated on the same footing. Since this type of calculations requires a boundary conditions, the disordered alloy is thought of as constructed from a random distribution of some basic clusters. The basic assumption is that all possible local structures can be realized in coherent periodic structures, each corresponding to a different possible configuration of the basic cluster. The accuracy of this approach increases by increasing the size of the basic cluster. Up to now the largest cluster considered is a 5-site tetrahedron. In the case of ternary alloys it reduces to a 4-site tetrahedron (since one the sublattices is alloyed). As shown in Sec. 2.6 reliable results can be obtained by considering clusters of this size. The properties of the disordered alloys can be calculated from the results obtained for the ordered ones if the probability distribution of the basic clusters are known. Some authors assume a random (Bernoulli) distribution, which is temperature and system independent, while in principle it should be calculated through free energy minimization.
  adopted here.

The effects of the elastic and chemical contributions on the phase-diagrams of semiconducting and metallic alloys have been studied recently by Ferreira, Mbaye and Zunger [36-38]. We show in Fig. 3.1 their results for the phase-diagram with (a) and without (b) including the elastic term, and also using positive chemical energy of mixing (c). The drastic difference between the first and the other two phase-diagrams demonstrates the importance of taking properly into account both chemical and elastic contributions to the enthalpy of mixing; this can be done using self-consistent ab-initio calculations.

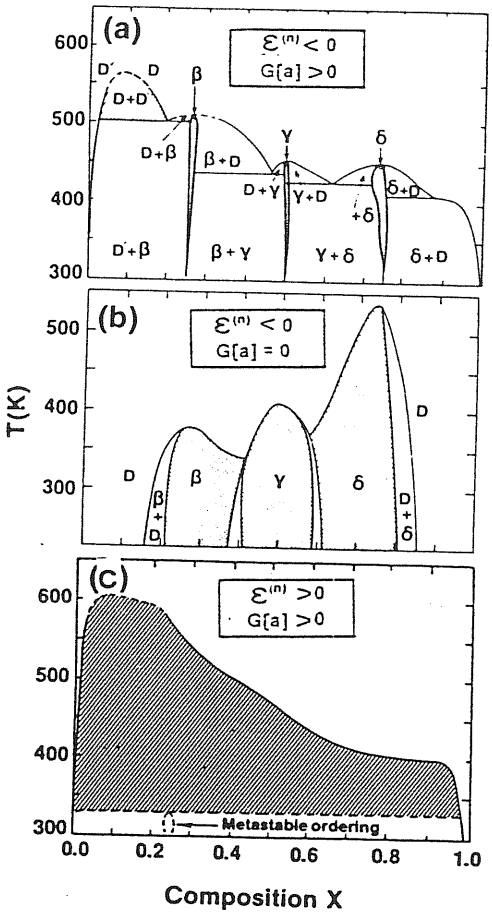

Figure 3.1: Phase diagram of $Ga_xIn_{1-x}P$: (a) first principle chemical $\epsilon^{(n)}$ and elastic $G[n]$ energies; (b) chemical energies only; (c) elastic-energy dominant. Shaded areas: single ordered phases; dashed: miscibility gap. (from Ref.'s 36 and 38)

3.2 Configurational entropy and free energy

The key quantity in statistical mechanics is the partition function, which is defined as a sum over the probability of all possible states of the system

$$f = \sum_{states} e^{-E(state)/k_B T}, \tag{3.3}$$

where the energies $E(state)$ contain configurational, vibrational and electronic contributions. For simplicity and following most of the workers in the field we will consider only the configurational contribution. The other contributions are assumed to be configuration-independent and they are usually neglected in the calculation of the configuration-related properties. For a binary system of N lattice sites, there are 2^N possible configurations. Usually not all of them are different, so Eq. (3.3) can be rewritten as

$$f = \sum_i g_i e^{-E_i/k_B T}, \tag{3.4}$$

where g_i is the number of possible configurations having the same energy E_i (from hereon referred to as degeneracy factor) which, in turn, can be rewritten as

$$f = \sum_i e^{-F_i/k_B T}, \tag{3.5}$$

where the non-equilibrium free energy F is

$$F_i = E_i - TS_i \tag{3.6}$$

and the configuration entropy is

$$S_i = k_B ln g_i. \tag{3.7}$$

The equilibrium Helmholtz free energy is

$$F_{eq} = -k_B T ln f \tag{3.8}$$

In the case of solids and liquids the Helmholtz and Gibbs free energies are equivalent, since the difference term PV has a negligible effect. Therefore, one can also write

$$G_{eq} = -k_B T ln f, \tag{3.9}$$

where G_{eq} is the equilibrium Gibbs free energy.

The sum over all possible different states in Eq.(3.4) is formidable task; the sum is therefore usually replaced by the largest term. In effect, the fluctuations about the most probable state are thereby neglected. The equilibrium Gibbs free energy is then obtained approximately by minimizing the non-equilibrium free energy function

$$G_{eq} \cong min_{\{i\}} F_i. \tag{3.10}$$

Even after using the above simplifying feature the calculation of G_{eq} is still a very difficult task and exact solutions are not possible (since complete sets of $\{i\}$ configurations are unavailable); to proceed one has to make some approximations. Instead of dealing with the whole system, we consider small clusters of sites (subsystems) known as basic clusters. The accuracy increases by increasing the size of the basic clusters. But in the other hand, the computational effort increases rapidly. Therefore, usually the size of the basic clusters is chosen to compromise between the accuracy and the computational efforts.

In our structural model described in Sec. 2.2, the basic cluster was a 5-site tetrahedron. Taking into consideration our basic cluster, approximate entropy can be calculated using a modified quasi-chemical approximation (QCA) of Guggenheim [60] or more accurately using the cluster variation method (CVM) of Kikuchi [58,59].

3.2.1 Modified quasi-chemical approximation

In strictly regular solution (SRS) model the atoms of the constituent materials are randomly distributed at the lattice sites. In spite of the fact that this is valid only at very high temperatures, SRS has been widely used in the literature to describe alloys. The QCA is a more realistic model, which allows to study clustering effects [31] in random alloys. The basic assumptions of the latter model are:

- Even in the case of liquids some sort of lattice is assumed, or in other words, each atom is attributed to a lattice point.

- Only the chemical energy contribution is taken into account, the lattice relaxation and the volume deformation energy contributions being completely neglected.
- Usually the effects of the first neighbors only are considered and pairwise interactions are assumed.
- Instead of assuming a random distribution of atoms (as in SRS), we assume a random distribution of pairs.

Thus, for a system of total number of N atoms having N_A atoms of type A and N_B atoms of type B, one can write

$$g' = \frac{\frac{1}{2}Z(N_A + N_B)}{N_{AA}!N_{BB}![(N_{AB}/2)!]^2}, \tag{3.11}$$

where Z is the number of the first nearest neighbors. Since random distribution of pairs overestimates the degeneracy factor g', one has to write

$$g = hg' \tag{3.12}$$

where h is a correction factor. This because the pairs can not truly distributed at random. The determination of h is discussed below.

In what is called modified QCA (or third order QCA [28]) the first assumption is kept (from hereon QCA refers to the modified QCA, while the former is referred to by *simple* QCA). Approximate entropy is calculated by assuming random distribution of clusters consisting of an atom and its surrounding atoms (5-site tetrahedron in our case). Taking our basic cluster as an example, the degeneracy factor g can be written as

$$g = h\frac{\prod_{i=1}^{2} N_i!}{\prod_{ijklm}(N_i z_{ijklm})!} \tag{3.13}$$

where z_{ijklm} is the concentration of the $ijklm$ tetrahedra having i as inside atom, $i, j, k, l, m = 1$ or 2. Here 1 refers to A and 2 refers to B-atom. h is the correction factor similar to that of simple QCA. To determine h, we note that if the atoms were distributed at random, we would have

$$g^{(B)} = h\frac{\prod_{i=1}^{2} N_i!}{\prod_{ijklm}(N_i z_{ijklm}^{(B)})!} = \frac{N_!}{\prod_i N_i!} \tag{3.14}$$

or

$$h = \frac{N_i}{(\prod_{i=1}^{2} N_i!)^2 \prod_{ijklm}(N_i z_{ijklm}^{(B)})!} \tag{3.15}$$

Thus,

$$g = \frac{N = i \ \prod_{ijklm}(N_i z_{ijklm}^{(B)})!}{\prod_{i=1}^{2} N_i! \prod_{ijklm}(N_i z_{ijklm})!} \tag{3.16}$$

here the superscript B refers to the Bernoulli distribution (completely random distribution of atoms at the lattice sites). The correction factor of the simple QCA can be determined following the same procedure. Using Stirling's approximation ($lnN! = NlnN - N$) the corresponding entropy is

$$S^{(QCA)} = -k_B \left(\sum_i x_i ln x_i + \sum_{ijklm} (z_{ijklm}^{(B)} ln z_{ijklm}^{(B)} - z_{ijklm} ln z_{ijklm}) \right) \tag{3.17}$$

In addition to the accuracy gained by increasing the size of the basic cluster in QCA, it allows for more realistic calculation of the enthalpy of mixing by including also the effects of some local structural relaxation. This has been done using different levels of approximations, ranging from the simple pair interaction to the ab-initio calculations.

3.2.2 Cluster variation method (CVM)

The CVM [58,59] is the most successful and accurate method for calculating approximate configurational entropy. Within this method the entropy is given in terms of the concentrations of the basic cluster and hierarchy of its subclusters. The major difficults encountered in CVM calculations are (1) the derivation of an expression for the degeneracy factor g suitable for the system and the chosen basic cluster, and (2) the computation of the equilibrium concentration of the basic cluster and its subclusters, which appear in the expression. Now, expressions have been derived for variety of crystal structures, considering basic clusters of different size and shape. Whereas, the natural iteration method [87] of Kikuchi, who originated and developed CVM, emerged as a practical and easy way for solving the set of nonlinear equations in a self-consistent manner. This is exactly the reason for the increasing interest in the CVM and its application to the solid solutions. For more details and discussion about the method see the review articles of de Fontaine [58] and Burley [59].

For our present case (binary alloys with two alloyed fcc-sublattices of zinc-blende type, within the tetrahedron approximation), an entropy expression do not exist in the literature, to our knowledge. In appendix A we give derivation of a suitable expression for this case in two different ways. The subclusters which give nonvanishing contributions are, in increasing order of complexity: points, first and second nearest neighbor pairs and tetrahedra surrounding an interstitial site in zinc-blende structure. We call the concentration of each of these clusters x_i, $y^{(1)}_{i,j}$, $y^{(2)}_{i,j}$ and w_{ijkl} respectively. In these notations the CVM expression is given as

$$S^{(CVM)} = -k_B \left(8 \sum_i x_i ln x_i + \sum_{ijklm} z_{ijklm} ln z_{ijklm} + \sum_{ijkl} w_{ijkl} ln w_{ijkl} \right.$$
$$\left. -2 \sum_{ij} y^{(1)}_{ij} ln y^{(1)}_{ij} - 6 \sum_{ij} y^{(2)}_{ij} ln y^{(2)}_{ij} \right) \qquad (3.18)$$

where x_i and z_{ijklm} have the same meaning as in Eq. (3.17) The explicit appearance of the concentrations of some of the clusters in $S^{(CVM)}$ takes care of the cooperative nature of the problem and makes CVM in principle more accurate than other approximations. However, in our present case only constrained CVM calculation can be done as we will see later .

3.3 Basic equations and definitions

In this section we show how the probability distribution of tetrahedra is calculated from the previously calculated energy of mixing for the different configurations of tetrahedra, as functions of the alloy composition x and temperature T; and we complete the definitions of the thermodynamic functions. According to Eq. (3.6) the Gibbs free energy of mixing is

$$\Delta G = \Delta H - TS, \qquad (3.19)$$

where ΔH is the enthalpy of mixing defined as

$$\Delta H = \sum_{ijklm} z_{ijklm} \Delta E_{ijklm} \qquad (3.20)$$

and S is the configurational entropy, which have been derived in the last section within QCA and CVM. The probability distribution of tetrahedra or the variables z can be determined by minimizing at fixed x and T the Gibbs free energy of mixing ΔG with respect to the variables z, under the constraint

$$\sum_{ijklm} (n_{ijklm} - 5x) z_{ijklm} = 0 \tag{3.21}$$

where n_{ijklm} is the number of A-atoms in the $ijklm$ cluster, which takes into account both the fixed concentration

$$x = \frac{1}{5} \sum_{ijklm} n_{ijklm} z_{ijklm} \tag{3.22}$$

and the normalization condition (the sum of the variables z is equal to one). Therefore, the free energy to be minimized is

$$G(x,T) = \sum_{ijklm} z_{ijklm}(x,T) \Delta E_{ijklm} - TS(x,T) + \sum_{ijklm} (n_{ijklm} - 5x) z_{ijklm}(x,T), \tag{3.23}$$

which should also be minimized at each values of x and T over the lattice parameter a. In the case of QCA, minimization of ΔG with respect to z_{ijklm} is straightforward and gives

$$z_{ijklm}(x,T) = \frac{\varsigma^{(n_{ijklm}-5x)} e^{-\Delta E_{ijklm}/k_B T}}{\sum_{ijklm} \varsigma^{(n_{ijklm}-5x)} e^{-\Delta E_{ijklm}/k_B T}} \tag{3.24}$$

where $\varsigma = e^{-\lambda/k_B T}$ is a positive and real quantity, which can be determined by solving the fifth order polynomial

$$\sum_{ijklm} (n_{ijklm} - 5x) \varsigma^{(n_{ijklm}-5x)} e^{-\Delta E_{ijklm}/k_B T} = 0. \tag{3.25}$$

For the case of CVM minimizing G with respect to the independent variables z_{ijklm} is more complicated and gives

$$z_{ijklm}(x,T) = \frac{X^{-5/8} Y_1^{1/2} Y_2 W^{-1} \varsigma^{(n_{ijklm}-5x)} e^{-\Delta E_{ijklm}/k_B T}}{\sum_{ijklm} X^{-5/8} Y_1^{1/2} Y_2 W^{-1} \varsigma^{(n_{ijklm}-5x)} e^{-\Delta E_{ijklm}/k_B T}} \tag{3.26}$$

where

$$X = x_i x_j x_k x_l x_m,$$

$$Y_1 = y_{ij}^{(1)} y_{ik}^{(1)} y_{ij}^{(1)} y_{im}^{(1)},$$

$$Y_2 = y_{jk}^{(2)} y_{jl}^{(2)} y_{jm}^{(2)} y_{kl}^{(2)} y_{km}^{(2)} y_{lm}^{(2)} \quad \text{and}$$

$$W = w_{ijkl}$$

The subcluster variables x, $y^{(1)}$, $y^{(2)}$ and w are dependent variables, which can be written in terms of the independent variables z as follows

$$y_{ij}^{(1)} = \sum_{klm} z_{ijklm}; \quad y_{jk}^{(2)} = \sum_{ilm} z_{ijklm}; \quad w_{jklm} = \sum_{i} z_{ijklm} \tag{3.27}$$

at a given concentration the variables x_i are in fact constants, and they don't need to be calculated. At given T , x and a, the system of nonlinear equations Eq. (3.26) can be solved numerically for the variables z, using the Newton-Raphson method, or more easily using the natural iteration method of Kikuchi[87]. The latter consists of the following steps:

- Start with initial guess values for the dependent variables x, $y^{(1)}$, $y^{(2)}$ and w, which could be that of the random distribution.
- Obtain the value of λ by solving the fifth order polynomial, Eq. (3.25).
- Calculate the independent variables z_{ijklm}, using Eq. (3.26).
- Obtain new values of the independent variables using Eq. (3.27).
- Use the the new values of the independent variables to calculate a new set of values for λ and the variables z, and so on so forth until good convergence is achieved.

It has been found that the calculated values of the first-neighbor mixed bond concentrations are not symmetric (e.i., $y_{12}^{(1)} \neq y_{21}^{(1)}$), this being a direct consequence of our structural model which distinguishes between the neighboring sites, or in other words, between the two fcc-sublattices of the crystal. Whereas,

in real disordered alloys they are equivalent. To go around this problem we have symmetrized them by assuming that each of the 5-sites of the tetrahedron could be an inside atom: in this way we allow for the inside atoms to belong to both of the sublattices. Thus, in our calculations Eq. (3.27) is modified to

$$y_{ij}^{(2)} = y_{ij}^{(2)} = \frac{1}{5}\sum_{klm}(z_{ijklm} + z_{mijkl} + z_{lmijk} + z_{klmij} + z_{jklmi})$$

and

$$w_{ijkl} = \frac{1}{5}\sum_{m}(z_{ijklm} + z_{mijkl} + z_{lmijk} + z_{klmij} + z_{jklmi}). \tag{3.28}$$

It should be noticed that the first and second nearest-neighbor pairs concentrations are equal after symmetrization. We found that this is unavoidable to get meaningful results.

Having calculated the tetrahedra concentration z, the thermodynamic functions can be calculated easily. The enthalpy of mixing is defined in Eq. (3.20); the entropy and the Gibbs free energy are given as in Eq. (3.17) or Eq. (3.18) and Eq. (3.6), respectively. The excess Gibbs free energy is

$$G^E(x,T) = G(x,T) - k_BT\left(xlnx + (1-x)ln(1-x)\right), \tag{3.29}$$

from which the interaction parameter Ω is calculated

$$\Omega(x,T) = \frac{G^E(x,T)}{x(1-x)}. \tag{3.30}$$

In the previous chapter we calculated a temperature independent $\Omega(x)$, where complete randomness was assumed. In present chapter we have T-dependence and an excess entropy contribution from the clustering effects.

3.4 Results and discussion at $P = 0$

Using the formation energy of different tetrahedral configuration $\Delta E_{ijklm}(a)$ calculated previously in Sec. 2.4., the tetrahedral concentrations z_{ijklm} are calculated using Eq. (2.24) after solving Eq. (2.25) for the case of QCA, and solving self-consistently Eq. (2.26) starting from random distribution of tetrahedra. The lattice parameter $a(x)$ is assumed to vary according to Vegard's law. In principle it should be calculated by a free energy minimization, but this is a very good approximation since the variation of a is experimentally found to be almost linear in these alloys. From the theoretical side, we have found previously (see Sec. 2.5 and Ref. 27) that Vegard's law is very well satisfied in the periodic structures at $T = 0$. Here we content ourselves by checking at $x = 0.5$ that the calculated a giving minimum G is 5.491 and 5.493 Å at T equal to 100 and 300 K, respectively, compared to 5.494 assumed by Vegard's law. In Fig. 3.2 we show the resultant P_{Si_n} and P_{Ge_n} (the multiplicity factor $\binom{4}{n}$ times the corresponding tetrahedra concentration) as a function of x for different values of T, using QCA (dotted curves) and CVM (dashed curves), compared with the random (Bernoulli) distribution (solid curves). The dominant features to be noticed are (1) the large difference between the CVM and the random distributions at high temperatures, which does not seem to vanish by increasing further the temperature (notice the small difference between the CVM distributions at 400 and 1400 K), (2) the small discrepancy between the CVM and QCA at low temperatures, which increases by increasing T, and (3) the symmetry of P_{Si_n} and P_{Ge_n} shown in the figure at $T = 100$ k. The results of CVM are obtained using the symmetrization procedure described in the last section. It should be mentioned that that taking simply the average of $y_{12}^{(1)}$ and $y_{21}^{(1)}$ leads to unphysical results (sudden and sharp decrease in the free energy at some x).

The Gibbs free energy as a function of x at different values of T, shown in Fig. 3.3a, has a quasi SRS-like behavior [88]. The concavity of the CVM free energy (solid curves) vanishes faster than that of QCA (dashed curves) leading to a lower critical temperature. Even if the behavior of the CVM free energy is reasonable, the relatively large deviation from randomness at very high

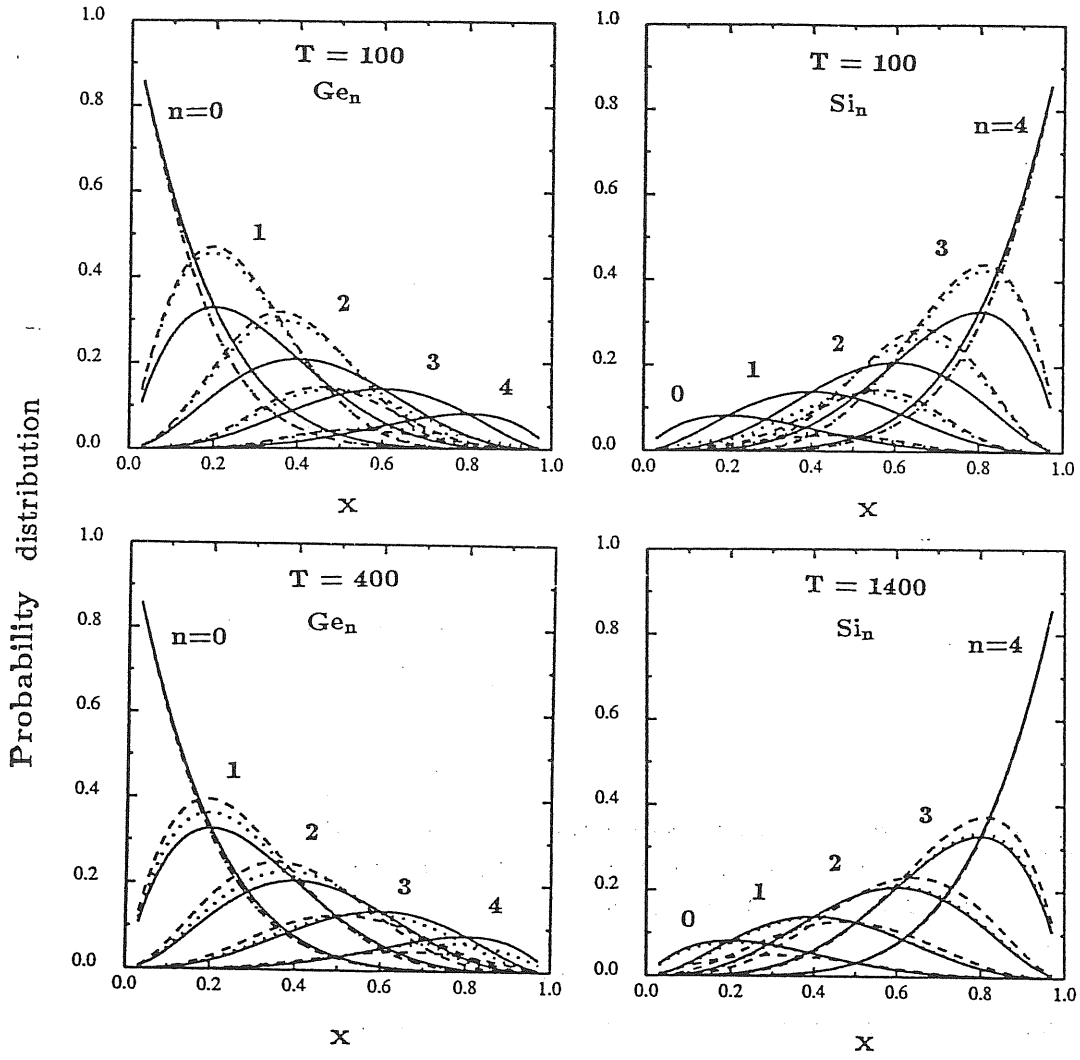

Figure 3.2: The probability distribution of the tetrahedral configurations as functions of the concentration at different temperatures and $P = 0$. Dashed curves: CVM results; dotted curves: QCA results, compared with the Bernoulli distribution (solid curves).

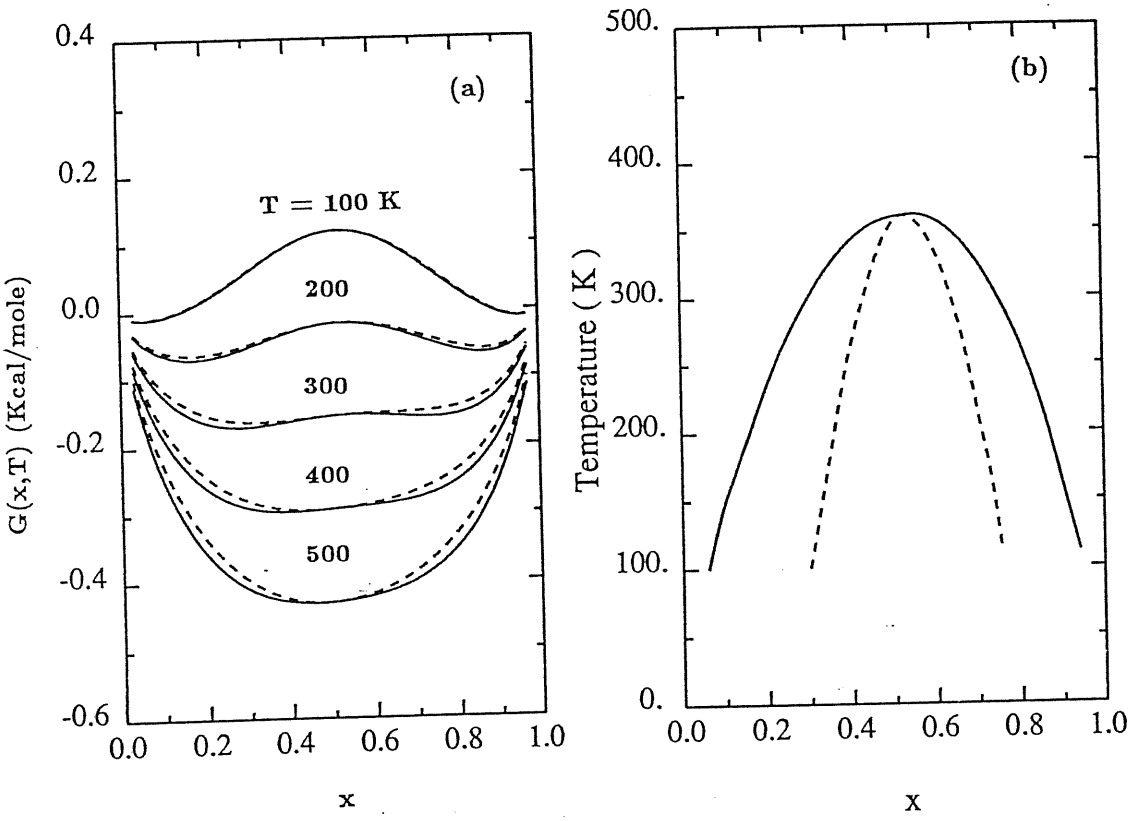

Figure 3.3: Gibbs free energy of mixing as functions of x at different temperatures at $P = 0$. Solid curves: QCA results; dashed curves: CVM results. (b) The phase diagram of Si_xGe_{1-x} alloys at $P = 0$. Solid curve: miscibility gap; dashed curve: spinodal curve.

temperatures (see Fig. 3.2) could be an artifact due to the symmetrization of the dependent variables. We finally calculated the CVM free energy in a non-self-consistent way, using in its expression simply the QCA derived variables z. The results coincide with the one derived completely at QCA level, thus giving us confidence in the accuracy and the reliability of QCA in this system. All the results shown in the following are strictly at the QCA level.

In Fig. 3.3b the phase diagram of the disordered Si_xGe_{1-x} alloys is shown: the instability region is where

$$\frac{\partial^2 F(x,T)}{\partial x^2} < 0 \tag{3.31}$$

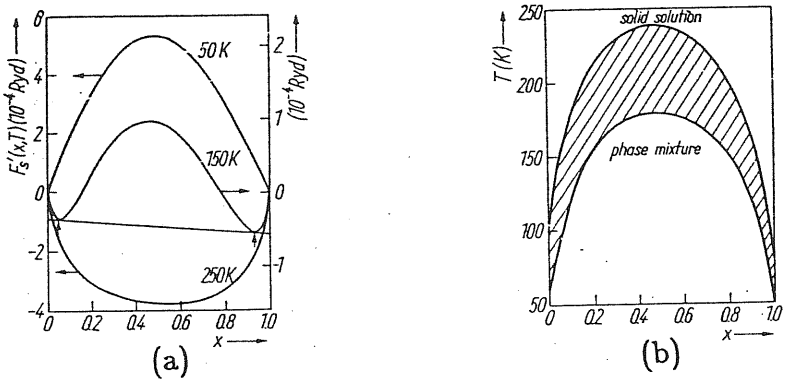

Figure 3.4: (a) Free energy of mixing at 50, 150 and 250 K. (b) The calculated phase diagram. (from Ref. 89)

which is bounded by the spinodal curve (dashed curve) calculated from the values of x at which the second derivative is equal to zero. The miscibility gap (solid curve) is by definition the region where the disordered alloys are metastable and is calculated here from the values of x at which $G(x)$ have common tangent at fixed T. The spinodal curve and the miscibility gap are calculated in the following steps:

- The inversion points and the values of x which have common tangent of $\Delta G(x)$ have been determined at discrete set of T values.
- The critical temperature was determined as the minimum temperature where $\frac{\partial^2 \Delta G}{\partial x^2}$ becomes positive for the whole range of x and the x location of these minima is specified.
- The information we got from the previous points are used as input data to a second-order polynomial interpolation routine to calculate the shown curves for the spinodal curve and the miscibility gap.

The critical temperature above which the disordered alloys are stable in the whole range of x is predicted to be around 360 K (see also Fig. 3.3a). For

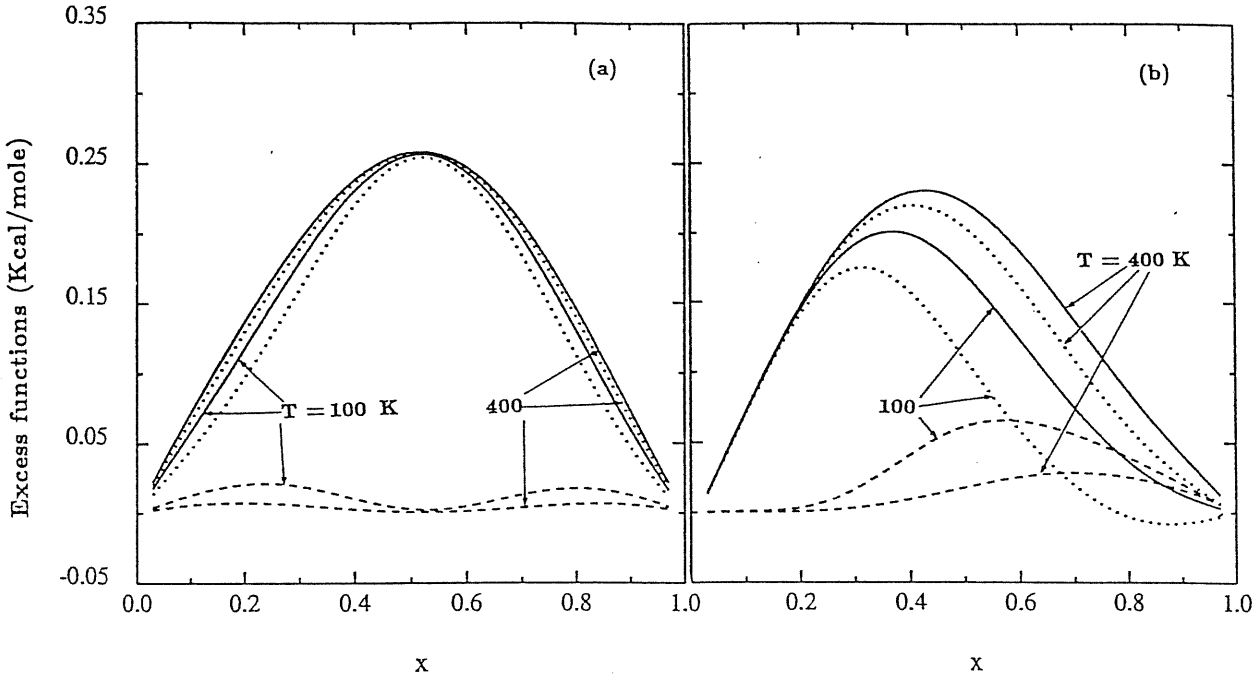

Figure 3.5: Excess thermodynamic functions of mixing at T=100 and 400 K. At $P = 0$ (a) and $P = 30$ Kbar (b). Solid curve: excess Gibbs free energy; dotted curve: enthalpy; dashed curve: entropy.

the sake of comparison we show in Fig. 3.4 the free energy of mixing (a) and the phase diagram (b) of Si_xGe_{1-x} calculated by Soma [89], from which he has concluded that the critical temperature is around 160 K. It should be noticed that in this work they use the second-order perturbation theory to calculate the internal energy (the third and the forth order terms are included in an approximate way [68]), and the completely random distribution to calculate the entropy at all temperatures. The large difference between our and these calculations demonstrates the importance and the need for performing our first-principle calculations.

We show in Fig. 3.5a the excess free energy, enthalpy and entropy of mixing. The dominant features to remark are the small values of the excess entropy, which gives small entropy contribution to G^E (the difference between the solid and the dotted curves). This fact is physically due to the small deviation of the tetrahedral distribution from complete randomness even at small temperatures (see Fig.2). As a consequence both the excess free energy G^E and the interaction parameter Ω (shown in Fig. 3.6a) have a weak T-dependence.

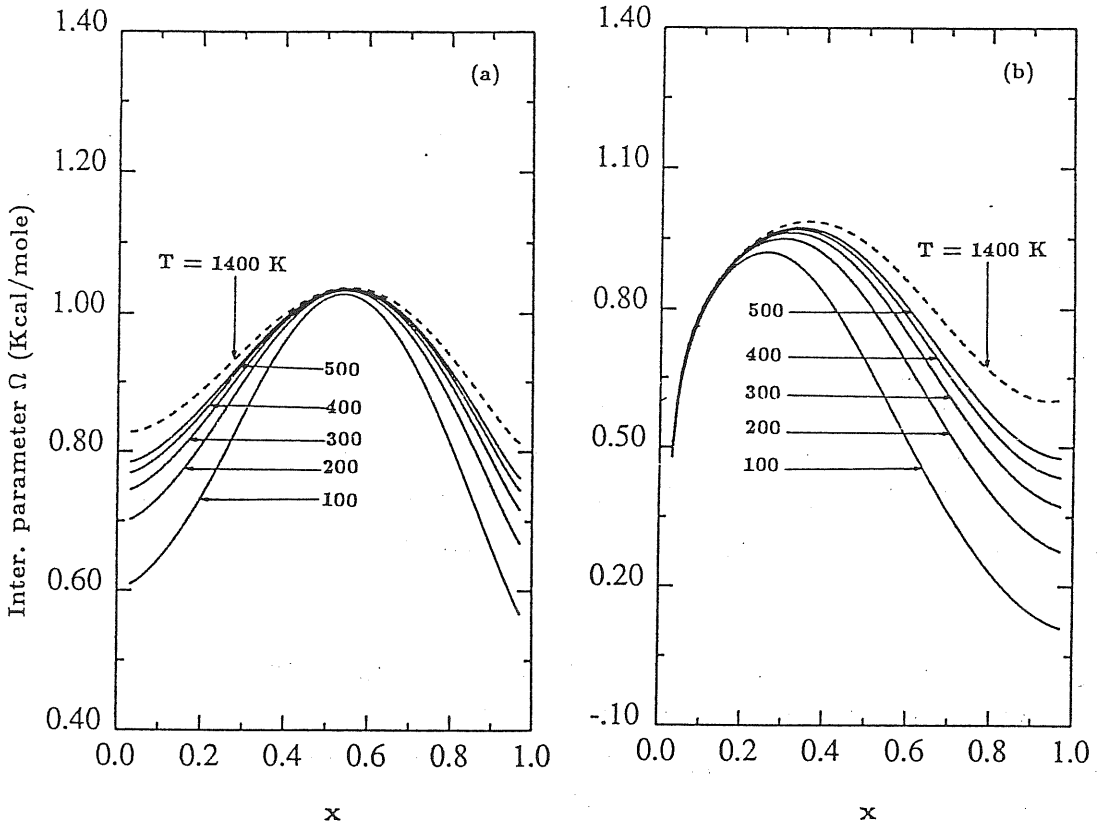

Figure 3.6: Interaction parameter as a function of x at different temperatures. At $P = 0$ (a) and $P = 30$ Kbar (b). Solid curves: up to 500 K; dashed curve: at 1400 K (random distribution).

3.5 The pressure effects

The results reported so far are obtained at $P = 0$. In this section we will study the effects of applying a hydrostatic pressure on the thermodynamic properties. The lattice parameter a of Si and Ge at given P can be determined from the calculated equations of state. Here we will also assume a Vegard's law variation of $a(x)$ between the calculated values of Si and Ge at the same P. The formation energies of each kind of tetrahedra at fixed T is recalculated according to

$$\Delta E_{A_n}(x,P) = E_{A_n}(a(x,P)) - \left(\frac{4+n}{8}E_A(P) + \frac{4-n}{8}E_B(P)\right) \qquad (3.32)$$

and similarly for ΔE_{B_n}, where $E_A(P)$ and $E_B(P)$ are the total energies of the end materials under fixed P. We found that ΔE of the ordered structures decreases by increasing the pressure, but this reduction is not enough to stabilize them (e.g. ΔE for zinc-blende structure is 0.68, 0.66, 0.60, and 0.51 mRy/atom under 0, 50, 70 and 90 Kbar, respectively). Our prediction is therefore that isotropic pressure does not make this compound stable; we comment at this point that uniaxial strain on the contrary has been recently found to stabilize ordered structures in this material [1,10].

At given P the calculations of the thermodynamic properties are carried out as described before, using the formation energies calculated at the same P. As a consequence of the volume reduction by applying hydrostatic pressure the strain energy of the Ge-rich tetrahedra increase. Therefore, the probability distribution of the Si-rich tetrahedra will increase because they have less strain energy.

For the purpose of displaying, all the following results are shown at $P = 30$ Kbar. The probability distributions at different temperatures as functions of x are shown in Fig. 3.7; by comparing it to Fig. 3.2 we see the pressure-induced change in the probability distributions of Si_n and Ge_n clusters, which has a direct effects on the thermodynamic properties. In Fig. 3.5b we show the calculated excess Gibbs free energy, enthalpy and entropy of mixing, to be compared with the zero pressure behavior shown in Fig. 3.5a. The interaction parameter at different values of T as function of x is shown in Fig. 3.6b (notice the difference in scale in Fig. 3.6a and b). The dominant feature to

be noticed is the relatively strong T-dependence in the Si-rich side and the T-independence in the Ge-rich side, the same feature existing also in Fig. 3.5b for the thermodynamic functions.

The Gibbs free energy at different values of T is shown in Fig. 3.8a; this quantity is in general lower than at $P = 0$, having a larger difference in the Si-rich side, and it is mainly due to a reduction in the enthalpy of mixing. The corresponding phase diagram is shown in Fig. 3.8b, where the effects of the pressure on the phase diagram can be seen: the main effect is that the instability region moves toward the Ge-rich side and its width decreases. We show in Fig. 3.9 the critical temperature as a function of P. The behavior is a monotonical increase of $T_c(P)$ with a rather small derivative at pressure up to about 50 Kbar and a steeper increase beyond. This can be understood since the total energy is flat around the equilibrium volumes. Finally we show in Fig.'s 3.10 as functions of x at different values of P, the energy of mixing, interaction parameter and phase diagram of Si_xGe_{1-x} alloys. These results are taken from the work of Soma and co-workers [90], in which they use VCA and their model calculations [68]. It should be noticed that (in addition to the fact that these are semiquantitative calculations) the quasi-monotonic behavior is a result of the complete neglect of the local structural effects.

3.6 Clustering

Because of the difference in bonding between different types of atoms in alloys, the atomic distribution at the lattice sites is usually not completely random, and it depends instead on many factors, such as the system, temperature, pressure and concentration. The deviation from randomness (clustering) has direct effects on the properties of alloys. In spite of this fact the random distribution has been assumed by many workers. To estimate the deviation from randomness different clustering parameters have been used in the literature [31,86]; they are nevertheless intimately related. Here we define a clustering parameter

$$\Delta(x,T) = y_{AB}^{(1)} - x(1-x)$$

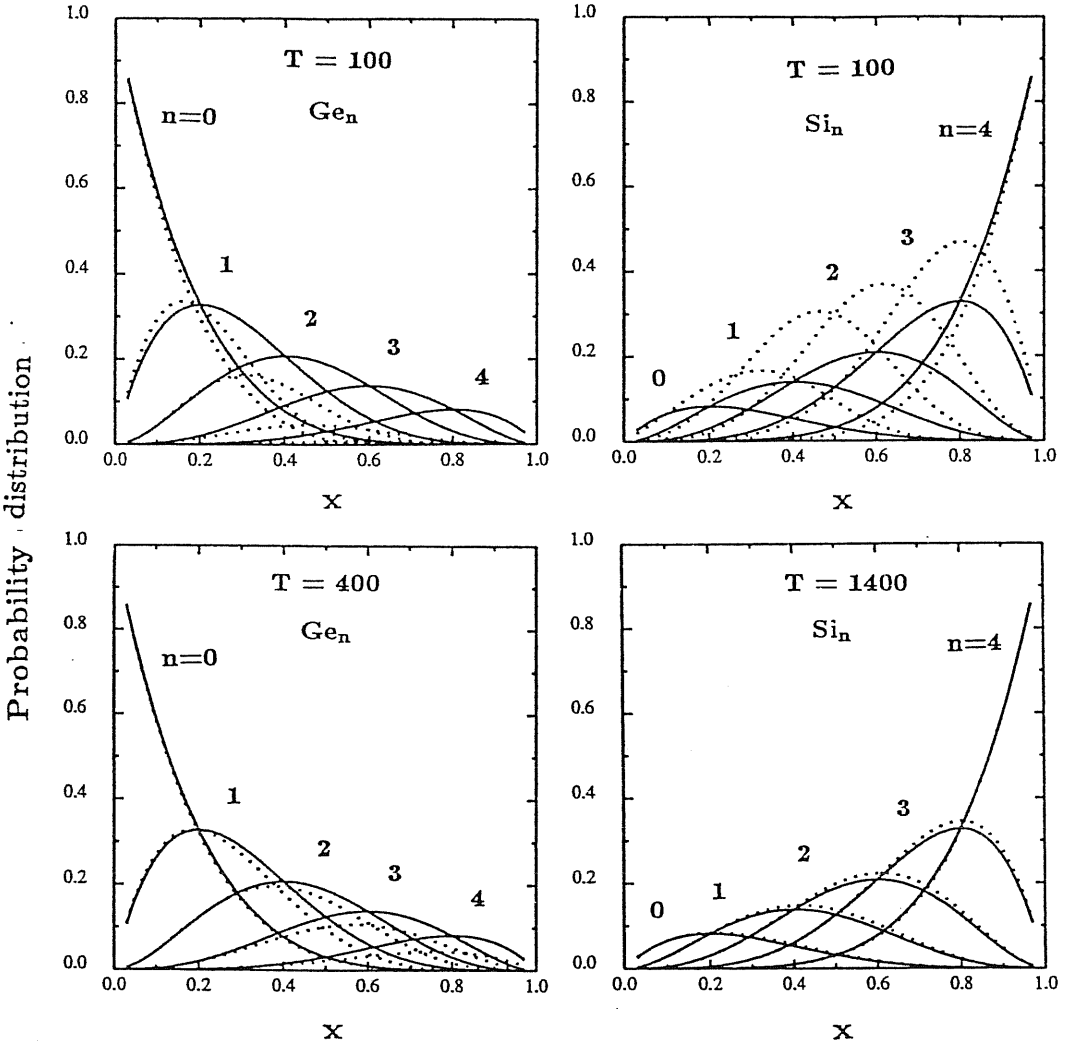

Figure 3.7: The probability distribution of the tetrahedral configurations as functions of the concentration at different temperatures and $P = 30$ Kbar. Dotted curves: QCA results, compared with the Bernoulli distribution (solid curves).

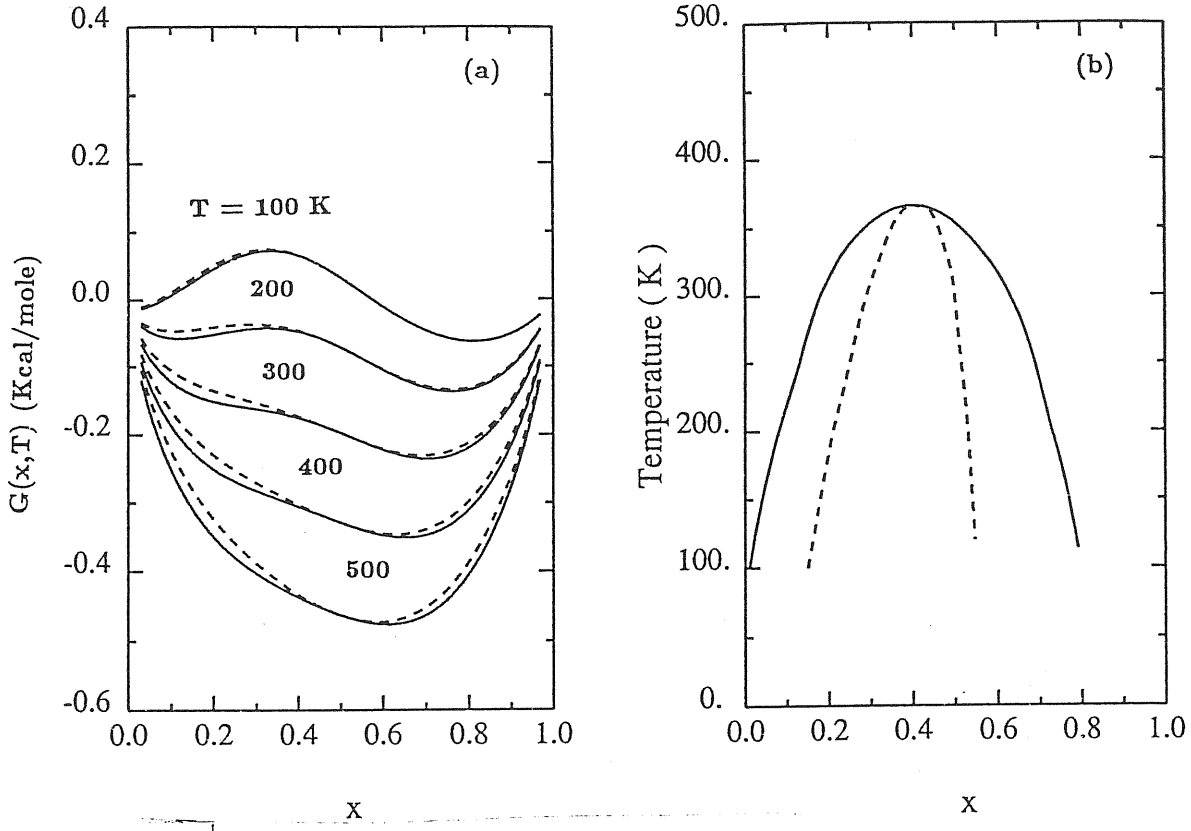

Figure 3.8: (a) Gibbs free energy of mixing as functions of x at different temperatures at $P = 30$ Kbar. Solid curves: QCA results; dashed curves: CVM results. (b) The phase diagram of Si_xGe_{1-x} alloys at $P = 30$ Kbar. Solid curve: miscibility gap; dashed curve: spinodal curve.

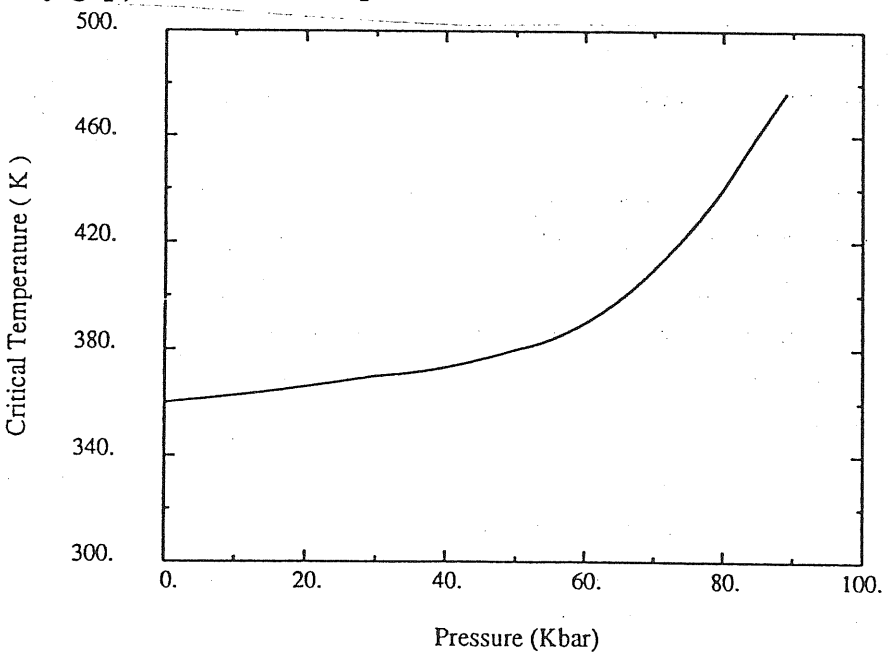

Figure 3.9: The critical temperature as a function of the pressure.

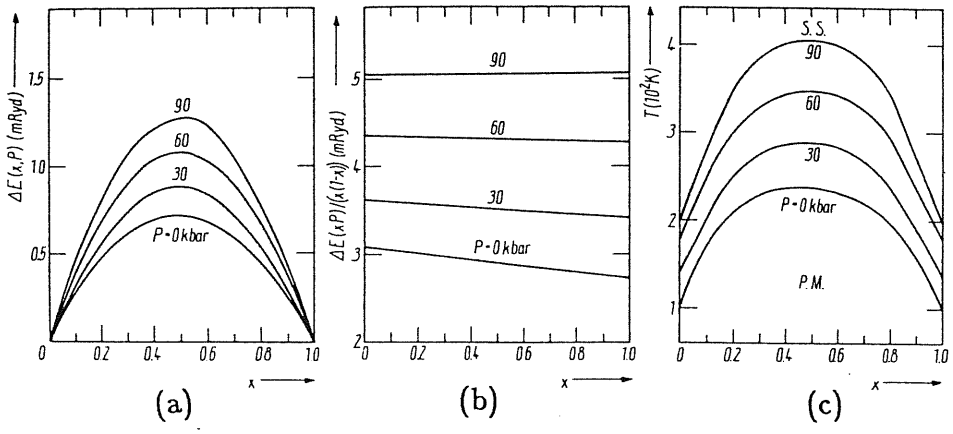

Figure 3.10: Free energy (a), interaction parameter (b) and phase diagram (c) of Si_xGe_{1-x} as functions of x at different values of pressure. (from Ref. 90)

$$= \frac{1}{8}\sum_{jklm}\left((5-n_{1jklm})z_{1jklm}+n_{2jklm}z_{2jklm}\right)-x(1-x) \quad (3.33)$$

as the difference between the calculated and the random values of the first mixed nearest-neighbor bond concentrations. Similar to excess mixed second neighbor pair probability distribution used [31,86] for ternary alloys.

In Fig. 3.11a we show $\Delta(x)$ at different values of T: it has a negative sign near the end points and a positive one around $x = 0.5$. This behavior is different from the one found by Balzarotti and co-workers [27], which is always positive, within modified QCA. We mention also the fact that the simple (i.e. non modified) QCA (for ternaries) gives always a negative deviation [31]. The behavior of Δ in our case can be easily understood. For example, in the Si-rich side the Si-rich tetrahedra have less strain (positive) energy, which tends to increase their probability distribution (see Fig.(1)). As a consequence the values of $y^{(1)}_{SiSi}$ increases on the expense of $y^{(1)}_{SiGe}$ and $y^{(1)}_{GeGe}$. Therefore the negative sign of Δ near the end points is explained. The same arguments can be used to explain the positive sign of Δ around $x = 0.5$. The small tendency to clustering (Δ is one order of magnitude smaller than the values calculated for ternary alloys), i.e. small tendency to ordering in these materials, provides further support to the conclusion of the instability of any coherent structure for bulk

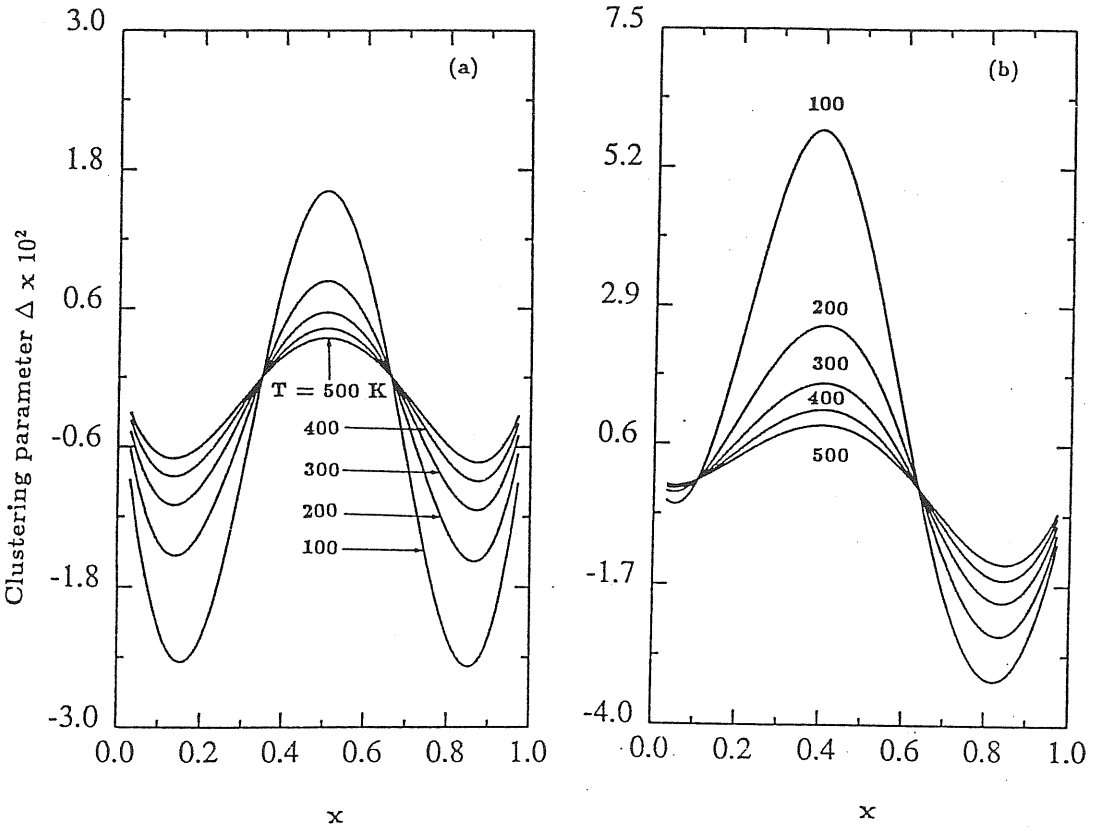

Figure 3.11: Excess first nearest-neighbor pair probability distribution Δ as function of x at different temperatures, at $P = 0$ (a) and $P = 30$ Kbar (b)

Si_xGe_{1-x} alloys.

The effect of applying hydrostatic pressure on the tendency to clustering has been also studied. In Fig. 3.11b we show $\Delta(x)$ at different values of T as a function of x, under 30 Kbar pressure. We found therefore that the pressure has also a drastic effect on the clustering in these materials, because Δ is no more symmetric and the tendency to clustering increases (notice the change in scale in Figs. 3.11a and b). This behavior can be explained as a consequence of the change in the role played by the strain energy.

3.7 Conclusions

A combined electronic structure and statistical mechanical approach has been used to calculate the thermodynamic properties of Si_xGe_{1-x} alloys. The formation energy for each of the 5-site tetrahedral configurations have been calculated

using the local-density approximation and norm-conserving pseudopotentials. Whereas, an approximate entropy of mixing is calculated within the framework of the modified quasi-chemical approximation (QCA) and the cluster variation method (CVM). We draw the following main conclusions:

- Because of our structural model which distinguishes the inside site from the others, the calculated mixed first neighbor pair concentration is not symmetric. The CVM calculations are carried out by symmetrizing all the dependent variables; this leads to unphysical deviation of the CVM probability distributions from randomness at very high temperatures. However we found that QCA free energy coincides with that of CVM calculated using the same QCA probability distributions, which demonstrates the power and the reliability of QCA. The following conclusions are based on this approximation.

- The Gibbs free energy shows a regular-solution like behavior, and the critical temperature above which the disordered alloy is stable for the whole range of concentration is predicted to be around 360 K.

- The interaction parameter shows a weak temperature dependence specially around room temperature, in addition to the weak concentration dependence previously found.

- The tendency to clustering is found to be much smaller than that calculated for ternary alloys [27], which provide additional support for the instability of ordered bulk Si_xGe_{1-x} structures.

- The pressure has a sizable effects on the thermodynamic functions and clustering. The pressure tends to decrease the width of the instability region and to shift it toward the Ge-rich side the; the critical temperature increases by increasing the pressure.

Chapter 4

Stability and Electronic Structure of Si_2Ge_2 (001) and (111)-oriented Superlattices

Superlattices and heterostructures have attracted much interest in both applied and fundamental research. Recent developments in high precision growth techniques have made possible the fabrication of novel materials consisting of layered structures. The degree of control is so advanced now such that strained superlattices, such as Si/Si_xGe_{1-x}, having layer thicknesses down to one monolayer have been grown [14-16] and have been the subject of many experimental and theoretical investigations. These novel structures have been found to have very intriguing structural [1-6] transport [43] and electronic structure properties [19-21]. In particular, we mention here the new quasi-direct optical transitions [14] observed in strained Si_4Ge_4 superlattices grown on the top of Si along the (001) direction. This was the subject of much theoretical investigations, where the band structure of Si_nGe_n (001)-oriented superlattices of different thicknesses has been calculated [91-94].

In this chapter we will consider another aspect of the problem, which is the effects of the growth direction. To this aim, we have studied in some

details two Si_2Ge_2 superlattices along $< 001 >$ and $< 111 >$-directions. The (110)-oriented superlattice has the same crystal structure as that of the (001)-oriented one [95]. It should be emphasized that these are not hypothetical structures, but they can be prepared over $Si_{0.5}Ge_{0.5}$ alloy, which has almost the same lattice parameter. An extensive total energy minimization has been carried out to determine the equilibrium structures and the relative stability. Then, the band structure of the equilibrium structures has been calculated and compared with that of the zinc-blende (Si_1Ge_1 superlattice along both directions) and $Si_{0.5}Ge_{0.5}$ alloy within VCA. The charge density distribution for the lowest conduction band states at some high symmetry points has been calculated. It has been found that both of the superlattices are unstable toward segregation. The (111)-oriented superlattice is relatively more stable than the other one which, in turn, is relatively more stable than the zinc-blende structure. The calculated bond lengths of the (001)-oriented superlattice are found to be in good agreement with that calculated by neglecting the second nearest-neighbor relaxation, and the small ionicity of the Si-Ge bond is negligibly affected by the structural relaxation. For the band structure, it has been found that both of the superlattices are indirect gap semiconductors, and the folding and the symmetry breaking have drastic effects on the charge density distributions corresponding the the lowest conduction band states.

The rest of this chapter is organized as follows. In Sec. 4.1 we describe the crystal structure of Si_2Ge_2 (001) and (111)-oriented superlattices. Sec. 4.2 is devoted to study of the stability and the equilibrium structures of the two superlattices. In Sec. 4.3 the band structures of the relaxed structures are displayed and compared with that of $Si_{0.5}Ge_{0.5}$ alloy within VCA and zinc-blende structure; the level charge density of the lowest conduction band levels at the high symmetry points is also given. Finally, in Sec. 4.4 we give our main results and conclusions.

4.1 Crystal structures

4.1.1 Si_2Ge_2 (001)-oriented superlattice. The lattice structure of this su-

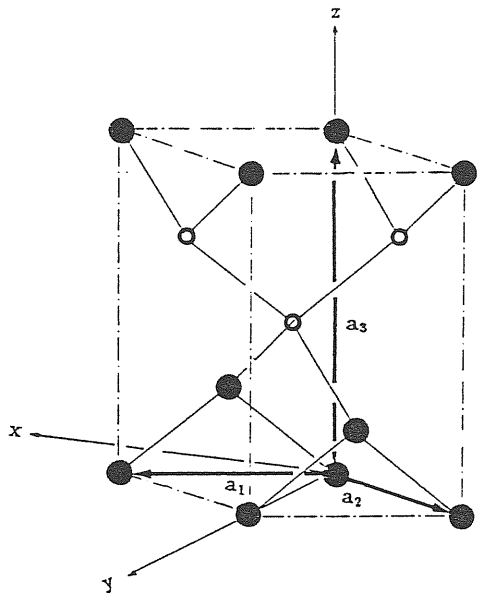

Figure 4.1: Structure of Si_2Ge_2 (001)-oriented superlattice. $a_i(i = 1,2,3)$ are the unit vectors, and they are $a_1 = a(1/2,1/2,0)$, $a_2 = a(-1/2,1/2,0)$ and $a_3 = a(0,0,1)$. Here, a is the lattice constant. The Si-Si, Si-Ge and Ge-Ge bond lengths are assumed to be equal. The four basic atoms in the unit cell are located at $a(0,0,0)$, and $a(1/4,1/4,1/4)$ for Ge, and $a(0,1/2,1/2)$ and $a(3/4,1/4,3/4)$ for Si.

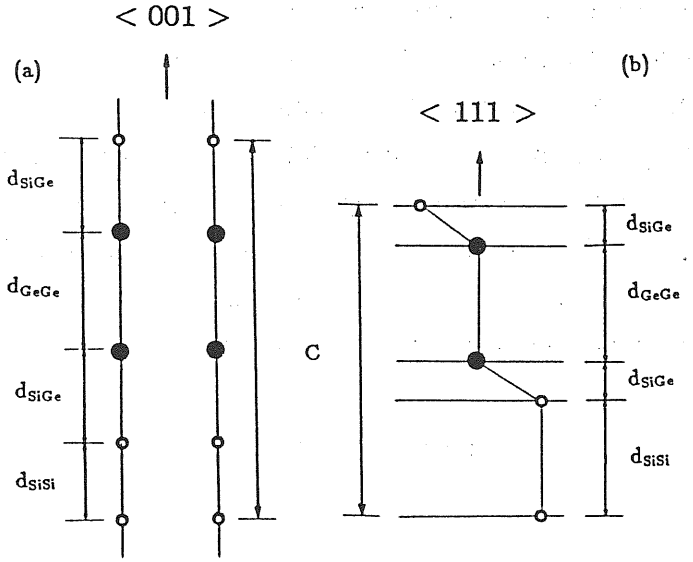

Figure 4.2: Schematic illustration of the studied Si_2Ge_2 superlattices. $d_{ij}(i,j = Si,Ge)$ are the interplanar distances and c is the period along the growth direction. (a) The (001)-oriented superlattice. (b) The (111)-oriented superlattice, for the ideal structure shown in Fig. 4.4, c is equal to $\frac{2}{\sqrt{3}}a_\perp$. In the text we refer to *scaled units*, and we indicate both the rhombohedral and tetragonal structures as ideal when $c/a_\perp = 1$.

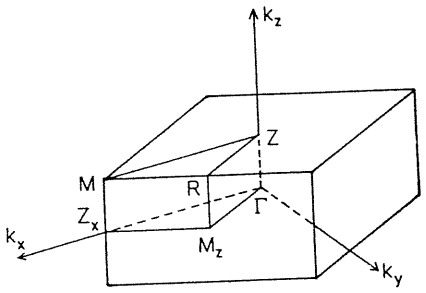

Figure 4.3: The first Brillouin zone of the Si_2Ge_2 (001)-oriented superlattice.

perlattice is obtained by alternating two layers of Si and Ge along the $< 001 >$-direction. The structure is shown in Fig. 4.1. The unit vectors and the atomic positions are shown in the same figure. Here, the bond lengths of Si-Si, Si-Ge and Ge-Ge bonds are assumed to be the same. This structure is a simple tetragonal having C_{2v} symmetry and four atoms per unit cell. The above structure is shown schematically in Fig. 4.2a. It has four independent structural variables, which can be chosen as the lattice parameter normal to the growth direction $a_\perp$ and the three interplanar distances shown in Fig. 4.2.a. The first Brillouin zone (BZ) is shown in Fig. 4.3. Since the unit cell of this structure is two times larger than the unit cell of the diamond structure, the BZ is one half of that of the diamond structure. A direct comparison of the two BZ's are shown in Fig. 2.4. The X and L-points of the diamond structure are folded as follows

- The L-points are not affected by the folding, and they are designated by R.
- The X-points in the (x,y)-plane are also not affected, and they are designated by Z_x.
- The X-points along the z-direction are folded to Γ; the mid-points (001) are designated here by Z.

4.1.1 Si_2Ge_2 (111)-oriented superlattice. The lattice structure of this

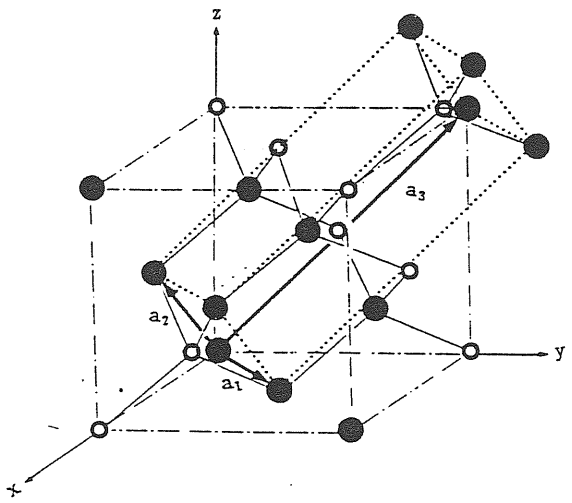

Figure 4.4: Structure of Si_2Ge_2 (111)-oriented superlattice. $a_i(i = 1, 2, 3)$ are the unit vectors, and they are $a_1 = a(1/2, 0, 1/2)$, $a_2 = a(1/2, 1/2, 0)$ and $a_3 = a(0, 1, 1)$. Here, a is the lattice constant. The Si-Si, Si-Ge and Ge-Ge bond lengths are assumed to be equal. The four basic atoms in the unit cell are located at $a(0, 0, 0)$, and $a(3/4, 3/4, 3/4)$ for Ge, and $a(0, 1/2, 1/2)$ and $a(5/4, 5/4, 5/4)$ for Si.

superlattice is obtained by alternating two layers of Si and Ge along the $< 111 >$ direction. The structure is shown in Fig. 4.4. The unit vectors and the atomic positions are shown in the same figure. Here, the bond lengths of Si-Si, Si-Ge and Ge-Ge bonds are assumed to be the same. This structure is a rhombohedral one having D_{3d} symmetry and four atoms per unit cell. The above structure is shown schematically in Fig. 4.2b. The remarkable feature of this structure is that the bond length can take any values without affecting the bond angles. In the total energy minimization this feature is maintained. As a consequence $a_\perp$ and d_{SiGe} are related. Therefore, there are only three independent structural variables, which can be chosen as the $a_\perp$ and the two homopolar bonds (in this case they are equal to the interplanar distances) shown in Fig. 4.2b. Since the unit cell of this structure is two times the unit cell of the diamond structure, the BZ is one half of that of the diamond structure. The X and L-points of the diamond structure are folded as follows

- The L-points along the growth direction are folded to Γ; the mid-points (1/2,1/2,1/2) are designated by L_z.

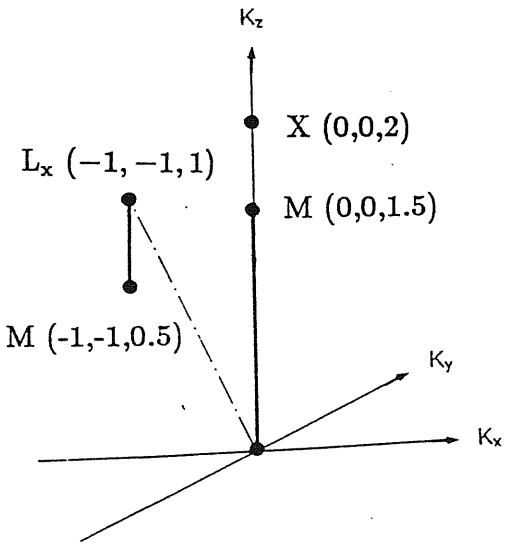

Figure 4.5: Schematic illustration of the folding of the Δ-line of the zinc-blende in the Brillouin zone of the Si_2Ge_2 (111)-oriented superlattice.

- The L-points normal to the growth direction are not affected, and they are designated by L_x.
- The X-points are folded to L_x as shown schematically in Fig. 4.5.

The equilibrium structures and stability of the above structures will be the subject of the next section.

4.2 Stability and equilibrium structures

For the above structures there are four and three independent structural variables for the (011) and (111)-oriented superlattices, respectively. For the former, they could be chosen as $a_\perp$, $c/a_\perp$ and any two of the interplanar distances. For the latter, they could be chosen as $a_\perp$, $c/a_\perp$ and one of the homopolar bonds. To determine the equilibrium structures, we have carried out total energy minimization over the independent variables. For the tetragonal structure this has been done as follows

- At the weighted average lattice parameter and considering $c/a_\perp = 1$, the equilibrium interplanar distances have been determined by total energy

minimization. Since $a_\perp$ and $c/a_\perp$ are kept fixed, the other two independent variables could be any two of the interplanar distances (say d_{SiSi} and d_{GeGe}). About twenty five total energy calculations around the equilibrium have been performed. The results are are least-square fitted to the following quadratic function

$$E(d_{SiSi}, d_{GeGe}) = b_0 + b_1 d_{SiSi} + b_2 d_{GeGe} + b_3 d_{SiSi} d_{GeGe} + b_4 {d_{SiSi}}^2 + b_5 {d_{GeGe}}^2 \tag{4.1}$$

to determine the equilibrium values of d_{SiSi} and d_{GeGe}, from which the d_{SiGe} can be easily obtained.

- The equilibrium values of $a_\perp$ and $c/a_\perp$ are then determined by a similar total energy minimization. The interplanar distances are considered as scaled variables (in units of $a_\perp$), and are assumed to have the same values as calculated above multiplied by the $c/a_\perp$ ratio. About twenty five total energy calculations around the equilibrium have been performed. The results are fitted to a quadratic function similar to the one given in Eq. (4.1), to determine the the equilibrium values of $a_\perp$ and $c/a_\perp$.

Similarly the equilibrium structure of the (111)-oriented superlattice has been determined in two steps:

- As described above, $a_\perp$ and $c/a_\perp$ (see Fig. 4.2b) are first kept fixed. As a consequence, we are left with only one independent variable, which could be any one of the two homopolar bonds (say d_{SiSi}). The value of d_{GeGe} changes by changing d_{SiSi}, while d_{SiGe} is kept fixed. Six total energy calculations have been performed around the equilibrium. The results are least-square fitted to parabola to determine the equilibrium value of d_{SiSi}, and hence d_{GeGe} under this restriction.

- The equilibrium values of $a_\perp$ and $c/a_\perp$ are determined as described above for the tetragonal structure. The only difference is that d_{SiGe} is determined directly from $a_\perp$, while the rest of $c/a_\perp$ is shared by d_{SiSi} and d_{GeGe}; in such a way that d_{SiSi}/d_{GeGe} is kept fixed and equal to the one obtained from the equilibrium values calculated in the previous step.

The results obtained for $a_\perp$, $c/a_\perp$ and the bond lengths of Si-Si, Si-Ge and Ge-Ge bonds for the two structures are given in Tab. 4.1, together with the formation energy ΔE (defined in Eq. (2.2)). The remarkable features to notice are the values of ΔE. The positive sign of ΔE in both superlattice reflects their thermodynamically instability towards disproportionation into pure elements. The (111)-oriented superlattice is found to be relatively more stable that the (001)-oriented one which, in turn, is relatively more stable than the ZB structure, which can be considered as Si_1Ge_1 superlattice in both of the growth directions ($\Delta E(ZB) = 0.21$ kcal/mol, see also Sec. 2.4). This shows clearly the tendency of SiGe system towards segregation. The above finding is in contradiction of what has been recently assumed by Martins and Zunger [10] that the strain free structures (ZB and rhombohedral) are the most stable structures for the SiGe system. According to Zunger and co-workers [9,10], the formation energy can be written as

$$\Delta E = \Delta E_{chem} + \Delta E_{el} \tag{4.2}$$

where ΔE_{el} is contribution to the formation energy resulting from the volume deformation and microscopic strain (bond lengths and angles deformation), and ΔE_{chem} is the contribution from all other *chemical* changes. Since the second contribution to ΔE_{el} is positive, they have assumed that the strain free structures are relatively more stable that the others. Here, we mention that the formation energy depends strongly on the number of the heteropolar bonds (see Sec. 2.4); it is worth to mention that Zunger et al. [10] have arrived to the same conclusion. For the tetragonal structure 50 % of the bond are heteropolar, while they are 100 % and 75 % of the bonds in ZB and the rhombohedral structures, respectively. Therefore, without microscopic strain the tetragonal structure is expected to be the most stable one. However, the strain will tend to destabilize it; a priori it is very difficult to predict its thermodynamic stability. In their work, Martins and Zunger have tried to explain the observed long-range ordered structure (rhombohedral) in strained SiGe grown on the top of Si substrate, but they arbitrarily consider only the structures which are free from microscopic strain. The present work shows instead that tetragonal structures should not be ruled out.

System	$a_\perp$ (Å)	$c/a_\perp$ (Å)	Bond lengths (Å)			Formation energy (kcal/mol)
			Si-Si	Si-Ge	Ge-Ge	
Si_2Ge_2 (001)-oriented superlattice	5.51	0.994	2.35	2.38	2.41	0.10
Si_2Ge_2 (111)-oriented superlattice	5.52	0.990	2.31	2.39	2.41	0.05

Table 4.1: The calculated values of the normal lattice parameter $a_\perp$, $c/a_\perp$ ratio (see Fig. 4.2), the bond length of the equilibrium structures of Si_2Ge_2 (001) and (111)-oriented superlattices.

The calculated bond lengths, shown in Tab 4.1, are in good agreement with these calculated in Sec. 2.5, specially for the (001)-oriented superlattice. It should be emphasized that the calculations reported in Sec. 2.5 are performed by neglecting the second nearest neighbor relaxation. This gives more confidence in our previous calculations.

As a representative we show in Fig. 4.6 the valence charge density of the fully relaxed rhombohedral structure. The charge transfer from Ge to Si atoms is very small. In Sec. 2.5 we have shown that the small ionicity of the Si-Ge bond is not affected by changing the concentration and the chemical environment. From Fig. 4.6 it is evident that it is also not affected by the structural relaxation.

4.3 Electronic structure

In this section we show the energy band structure of the two superlattices under consideration. The calculations are performed using LDA and norm-conserving pseudopotentials [72]. Within LDA, the energy gaps of the semiconductors are underestimated. Some authors have used *artificially* the value α in the $X\alpha$ approximation of the exchange and correlation potential as an adjustable parameter to reproduce the energy gaps of the constituent materials [96,97]. Here, we continue using the Ceperley and Alder results [70,71]. Therefore, in our calculations the energy gaps are underestimated. In the next chapter, we

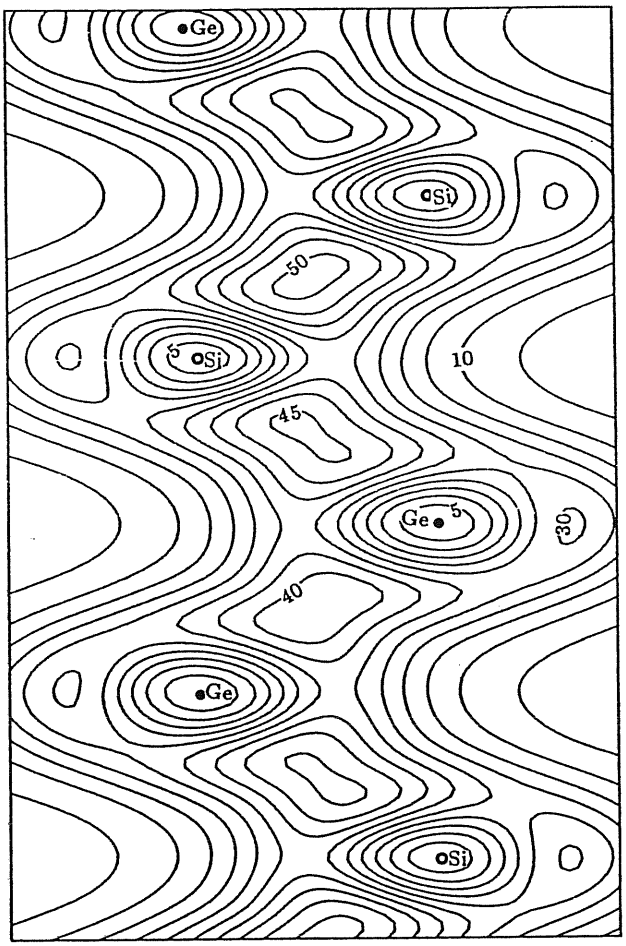

Figure 4.6: Contour plot of the valence electronic density (electron/unit cell) in the [011] plane of the Si_2Ge_2 (111)-oriented superlattice.

show that at the calculated equilibrium lattice parameters the underestimation of the band gaps of Si and Ge is comparable, and correct topology for the band structure of Ge and meaningful variation of the band gaps of Si_xGe_{1-x} alloys with x are obtained. This gives us confidence in the reliability of the calculated band structures for the superlattices, of course not in the calculated values of the energy gaps, but in the other properties, such as, the character of the gap (direct vs indirect).

For the calculation of the structural properties, constant energy cutoff $E_{cut} =$ 12 Ry was enough. It has been found (see next chapter) that in order to achieve good convergence, specially for the Γ_2^c state, a higher E_{cut} is needed. In this calculations we use $E_{cut} = 14$ for the charge density calculations and 17.5 Ry to calculate the band structure.

In the following we give a detailed description of the band structure of the above two superlattices.

4.3.1 Si_2Ge_2 (001)-oriented superlattice

The band structure of the fully relaxed structure along the high symmetry lines is shown in Fig. 4.7. The conduction band has four minima at Γ, R, Z_x and the $\Gamma - Z$ line, which correspond to Γ, L, X and Δ-line of the zinc-blende structure. The calculated band gaps corresponding to the above minima are 0.49, 0.87, 0.35 and 0.37 eV, respectively. So, the above superlattice is an indirect-gap semiconductor. In Fig. 4.8a and b we show a comparison between the band structures of the zinc-blende SiGe and $Si_{0.5}Ge_{0.5}$ alloys within VCA along the Δ-line and the corresponding lines of the above superlattice (the band structure of the first two systems are discussed in details in the next chapter). The important features to notice are:

- In the case of the zinc-blende and VCA the conduction band minima occur at the Δ-line. For the unfolded Δ-line of the above structure the minima moves to the Z_x point, while for the folded one the it occurs at the line. The former has lower energy.
- The folding of the conduction band along the growth direction is not a

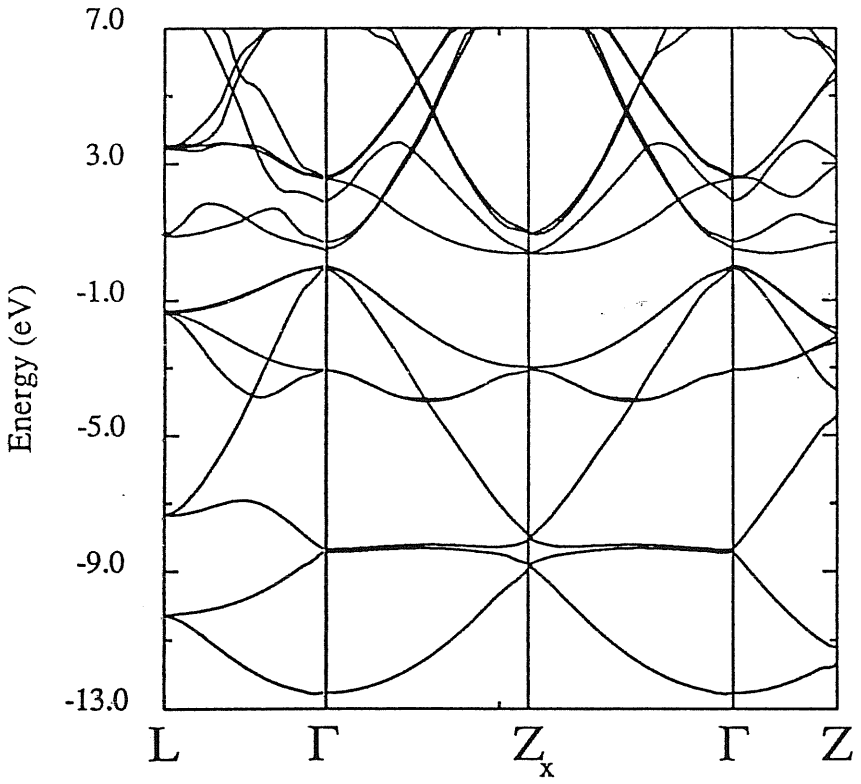

Figure 4.7: The band structure of the fully relaxed Si_2Ge_2 (001)-oriented superlattice along the high symmetry lines.

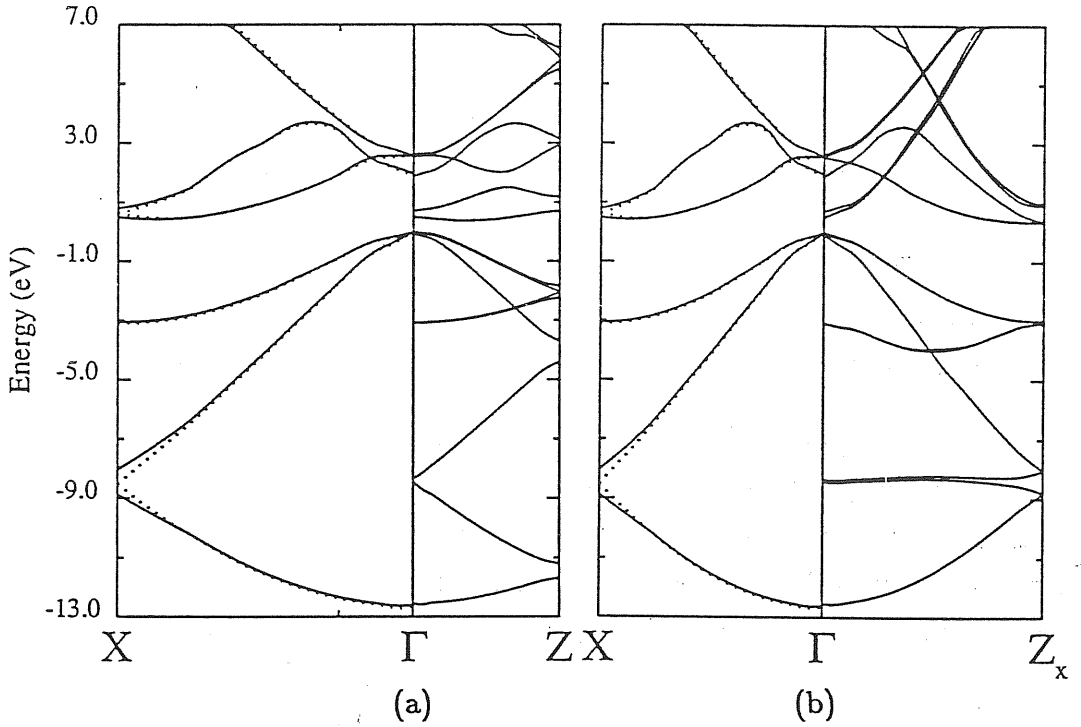

Figure 4.8: Comparison between the band structures along the Δ-line of $Si_{0.5}Ge_{0.5}$ within VCA (dotted lines) and zinc-blende (solid lines) in the left panels, and that of the corresponding folded (a) and unfolded (b) lines of the Si_2Ge_2 (001)-oriented superlattice (solid lines) in the right panels.

simple one. As it is clear from Fig. 4.8 there is an anti-crossing in the conduction band levels. A similar results has been obtained by Nakayama and Kamimura [98] in the $(GaAs)_n(AlAs)_m$ superlattice, and they have shown that it is a consequence of the mixing of the conduction band states.

- The gap which opens due the zinc-blende symmetry at X-point in the valence band disappears in the supercell when the X-point is folded to Γ. While at the unfolded points it shrinks.

To clarify the origin behind the above differences in the behavior of the lowest conduction band along the Δ-line, we have calculated the level charge density which correspond to the lowest conduction band levels at Z_x and Γ. The results are shown in Fig. 4.9a and b. It is evident that they are different. The one which correspond to the lowest conduction band at Γ is concentrated in the interstitial region between similar layers, while the other is more spread. This shows that the mixing with other conduction states are appreciable.

In Fig. 4.10 the band structure of the zinc-blende and VCA along the Σ-line are compared with that of the above superlattice. It is evident that apart from the anti-crossing, the corresponding conduction and valence band are very similar. The level charge density of the lowest conduction band state at R is shown in Fig. 4.11. It is concentrated in the interstitial region between the layers of the interface.

4.3.2 Si_2Ge_2 (111)-oriented superlattice band structure

The band structure of the fully relaxed structure along the high symmetry lines is shown in Fig. 4.12. The conduction band has four characteristic minima at Γ, L_x and along the Γ-L_z and M-L_x lines, which correspond to the Γ, L= $(11\bar{1})$, and the Σ and Δ-lines of the zinc-blende structure. The calculated band gaps corresponding to the above minima are 0.83, 0.39, 0.82 and 0.39, respectively. Therefore, it is indirect gap semiconductor. A comparison between the band structure of the $Si_{0.5}Ge_{0.5}$ alloy within VCA and the zinc-blende along Σ-line and the corresponding lines of the above structure is shown if Fig. 4.13a and b, for the unfolded and folded lines, respectively. From Fig. 4.13a it

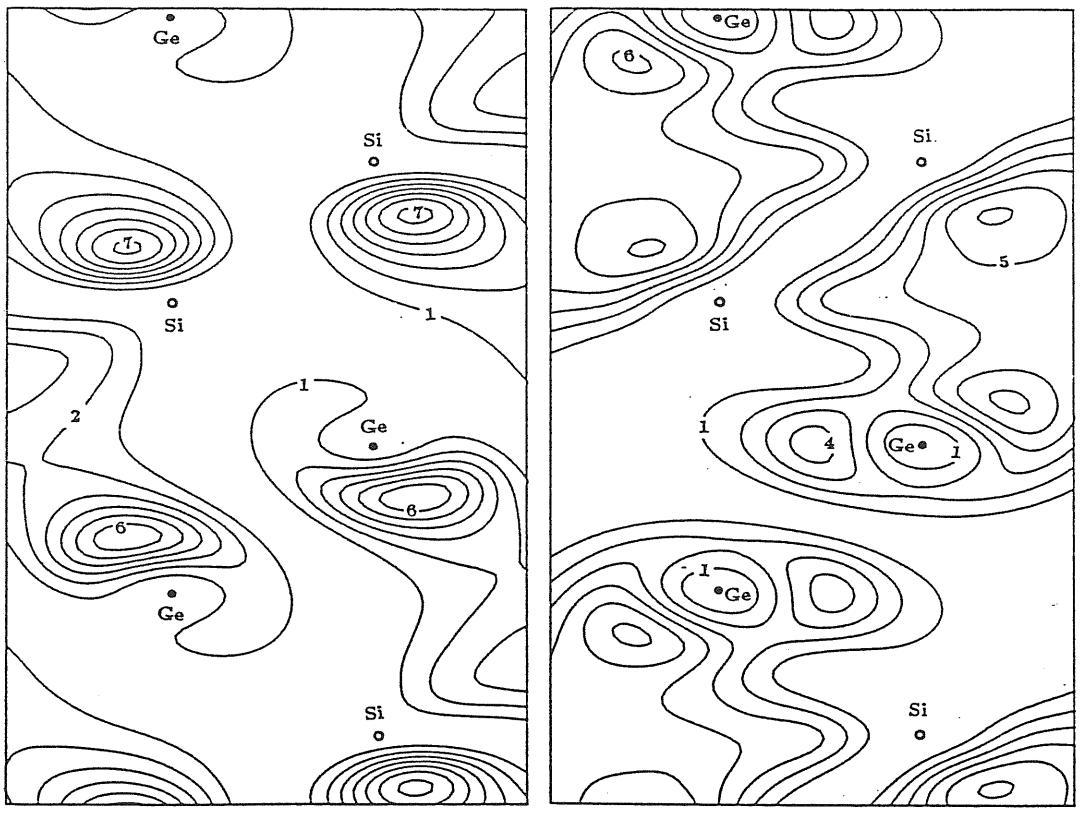

Figure 4.9: The level charge density (electron/unit cell) of the lowest conduction band levels at (a) Γ and (b) at Z_x of Si_2Ge_2 (001)-oriented superlattice.

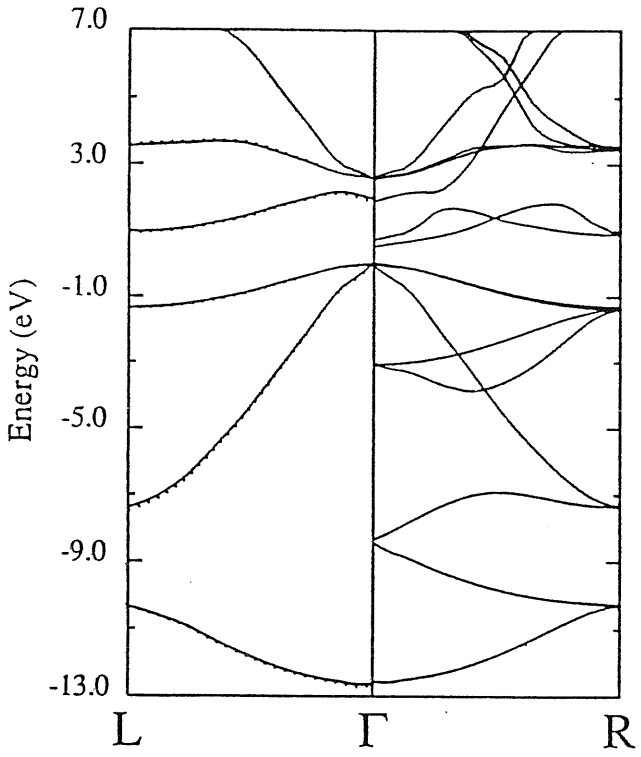

Figure 4.10: Comparison between the band structures along the Σ-line of $Si_{0.5}Ge_{0.5}$ within VCA (dotted lines) and zinc-blende (solid lines) in the left panel, and that of the corresponding line of the Si_2Ge_2 (001)-oriented superlattice (solid lines) in the right panel.

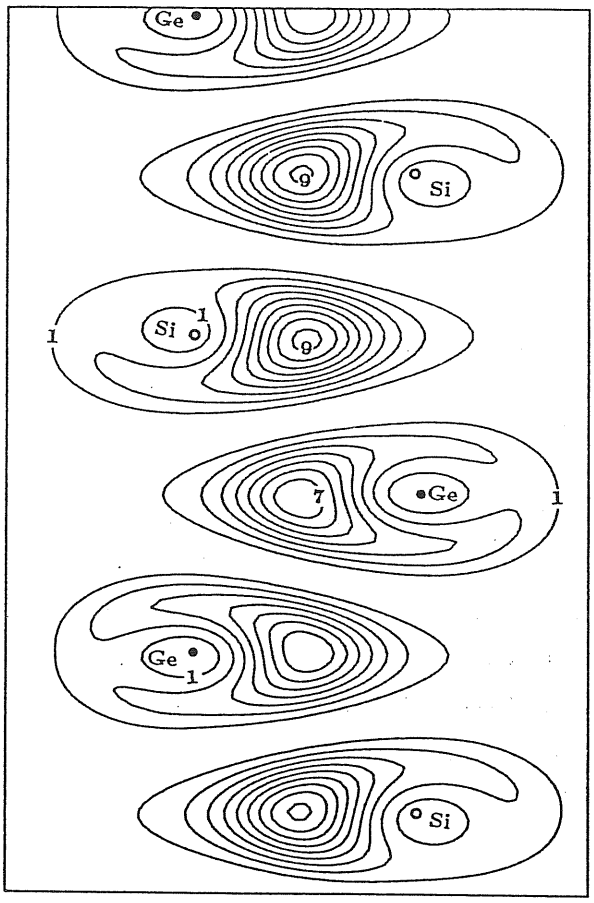

Figure 4.11: The level charge density (electron/unit cell) of the lowest conduction band levels at R of Si_2Ge_2 (001)-oriented superlattice.

is evident that apart from the splitting of the degenerate levels, the unfolded levels of the superlattice are very similar to the corresponding ones for the other structures. From Fig. 4.13b the folding of the conduction and valence bands is very clear. Here, the mixing with other conduction band levels is manifested in the moving of the conduction band minima from Γ (the lowest level at Γ correspond to L_1^c level of the zinc-blende structure) to Γ - L_z lines. The level charge density corresponding to the lowest conduction band levels at Γ and L_x are shown in Fig. 4.14a and b. The remarkable feature to notice here is the large difference between the two distributions. From Fig. 4.14a it is clear that the level charge density of the conduction band level at Γ is concentrated in the interstitial region between the layer of the interface near the Si atoms, while that of the lowest conduction band at L_z is concentrated in the interstitial region between the Ge layers. From Fig.'s 4.9 and 4.14, it is evident that the level charge density distribution of the folded levels is different from that of the unfolded ones.

In Fig. 4.15 we show a comparison between the band structure of the $Si_{0.5}Ge_{0.5}$ alloy within VCA and the zinc-blende along the Δ-line with that of the corresponding lines of the above structure. The band structure of the superlattice along these lines is more complicated than the others; folding and mixing lead to a lot of anti-crossing in the conduction band levels. At L_x the levels at Γ and X-points of the zinc-blende structure coincide, as an example, of the four lowest bands shown in Fig. 4.12 at L_x-point, the first and the fourth correspond to the zinc-blende L, while the second and the third correspond to X-point. The level charge density of the lowest conduction band level at L_x is shown in Fig 4.16. It is mostly concentrated in the interstitial region at the the interface near the Si atoms.

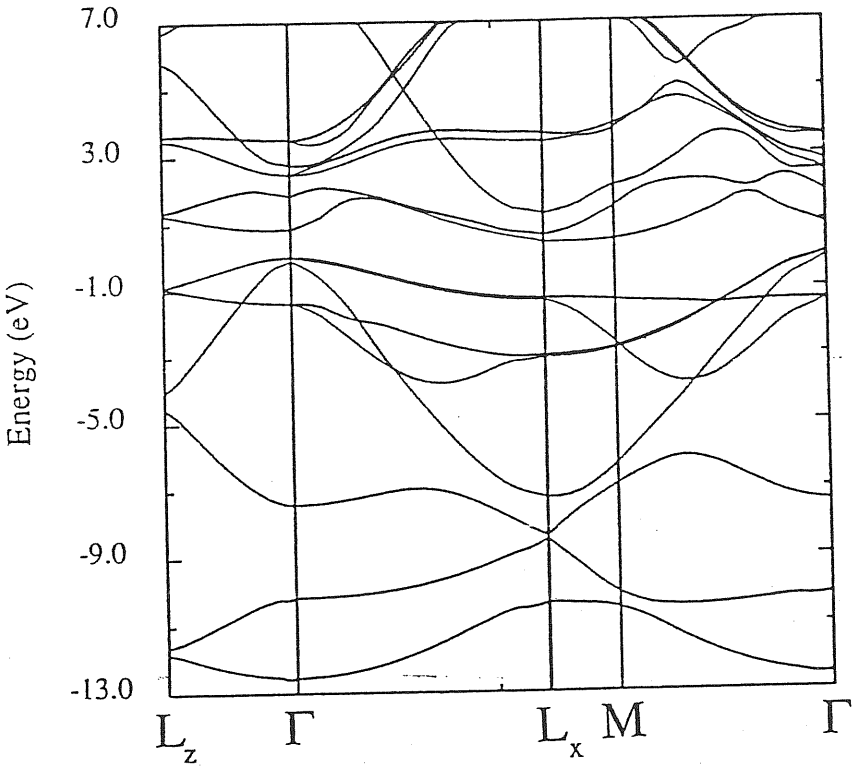

Figure 4.12: The band structure of the fully relaxed Si_2Ge_2 (111)-oriented superlattice along the high symmetry lines.

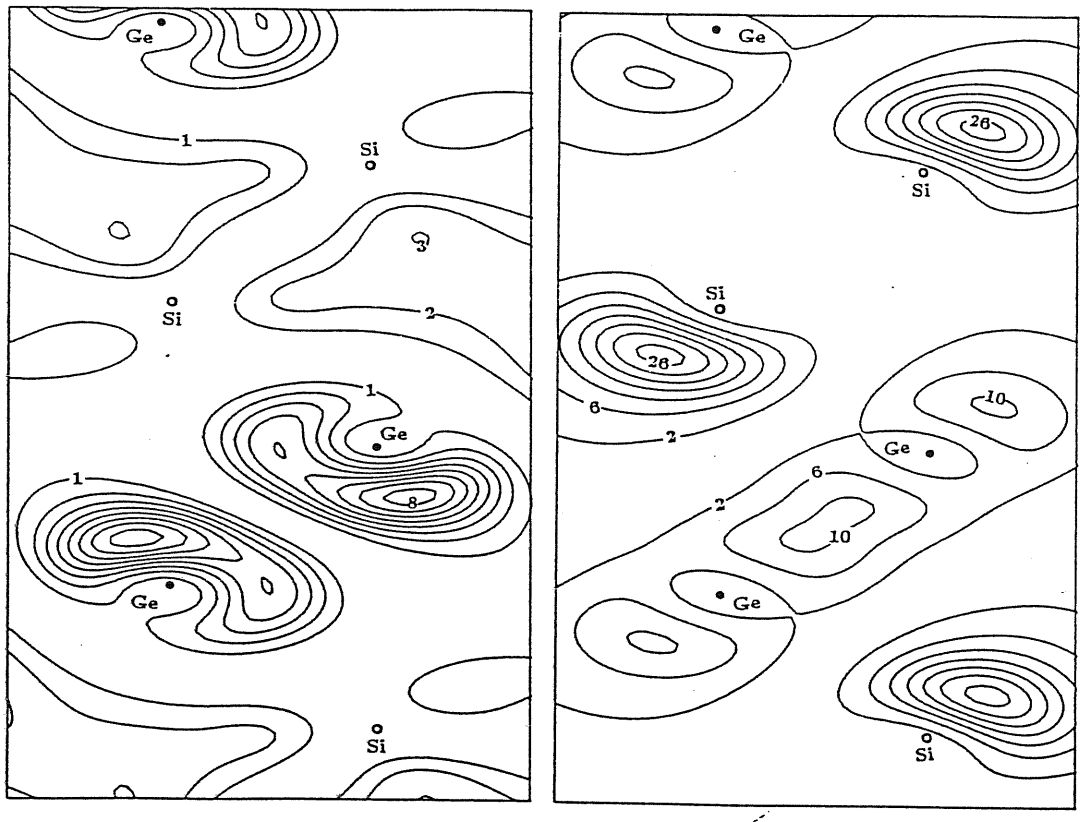

Figure 4.13: The level charge density (electron/unit cell) of the lowest conduction band levels at (a) Γ and (b) at L_x of Si_2Ge_2 (111)-oriented superlattice.

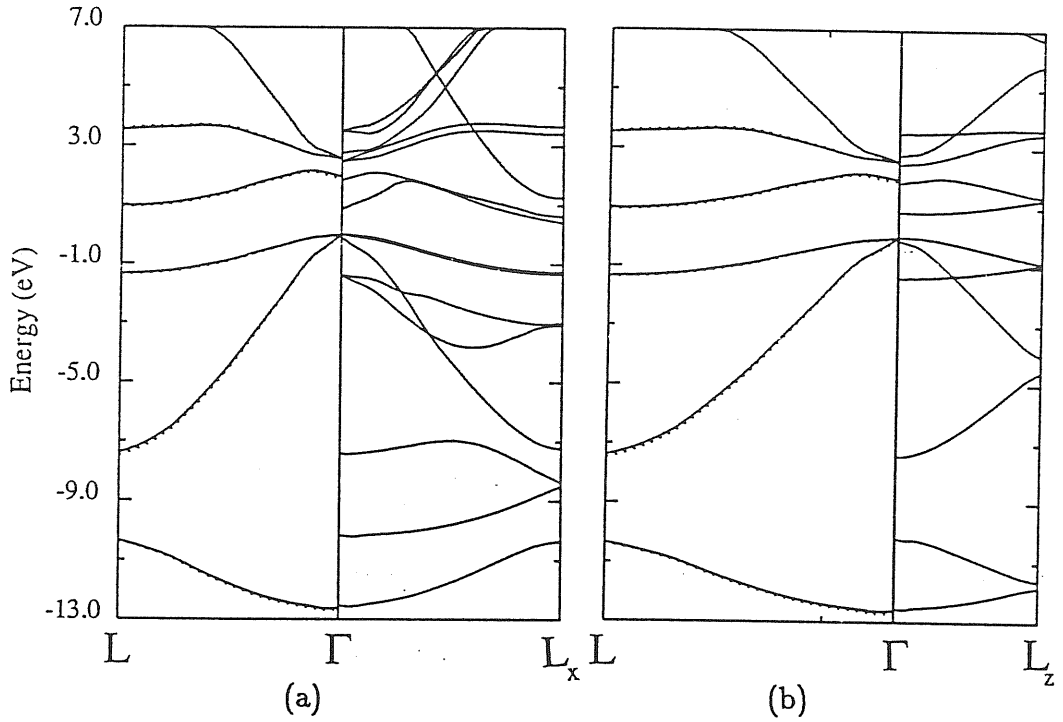

Figure 4.14: Comparison between the band structures along the Σ-line of $Si_{0.5}Ge_{0.5}$ within VCA (dotted lines) and zinc-blende (solid lines) in the left panels, and that of the corresponding folding (a) and unfolding (b) lines of the Si_2Ge_2 (111)-oriented superlattice (solid lines) in the right panels.

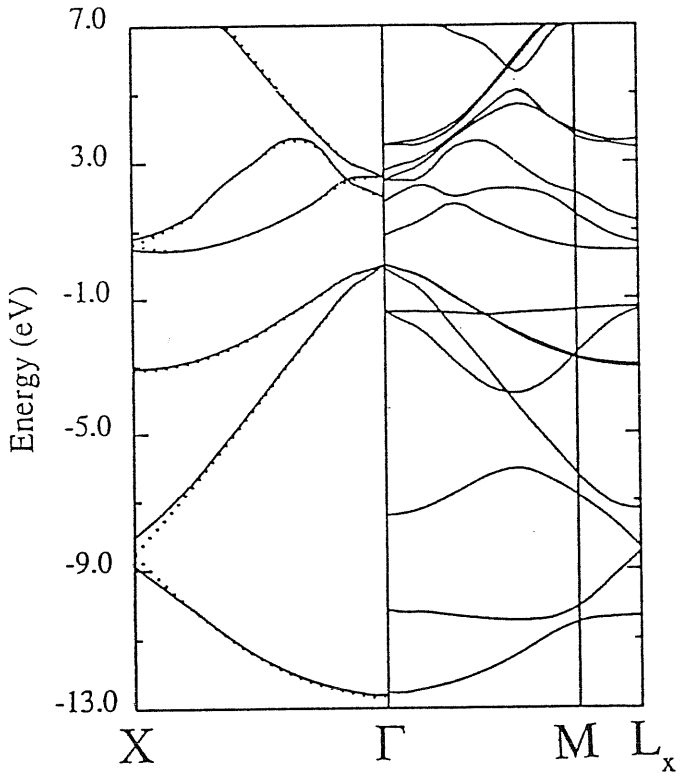

Figure 4.15: Comparison between the band structures along the Δ-line of $Si_{0.5}Ge_{0.5}$ within VCA (dotted lines) and zinc-blende (solid lines) in the left panel, and that of the corresponding line of the Si_2Ge_2 (111)-oriented superlattice (solid lines) in the right panel.

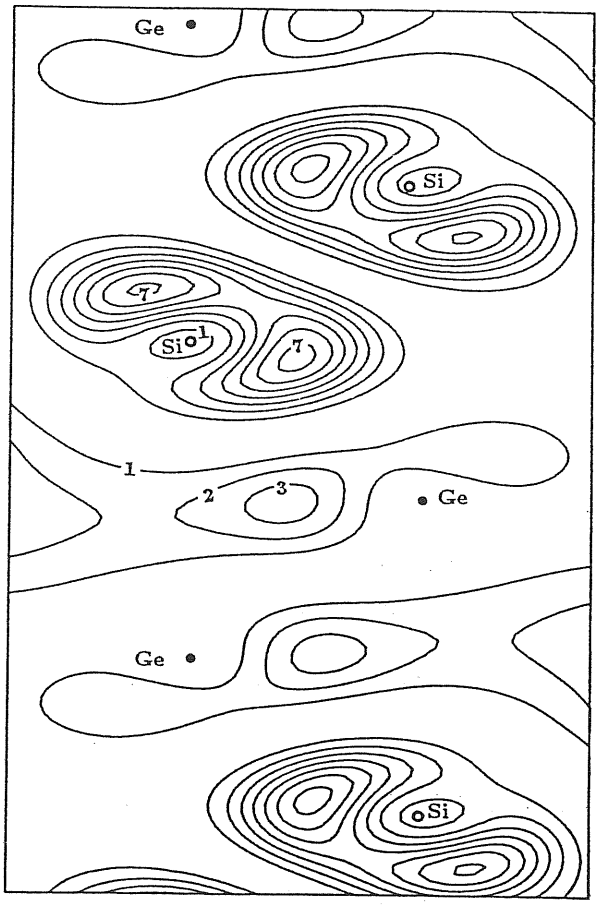

Figure 4.16: The level charge density (electron/unit cell) of the third lowest conduction band levels at L_x of Si_2Ge_2 (111)-oriented superlattice.

4.4 Conclusions

In this chapter we have calculated the stability, equilibrium structure and the band structure at equilibrium of Si_2Ge_2 superlattices grown along the $< 111 >$ and $< 001 >$ directions. The calculations are performed using local density approximation (LDA) and norm-conserving pseudopotentials [72]. In the following we draw our main conclusions:

- Both of the studied superlattices are found to be thermodynamically unstable toward segregation. The (111)-oriented superlattice is relatively more stable that the (001)-oriented one which, in turn, is more stable than the zinc-blende structure.
- The calculated Si-Si, Si-Ge and Ge-Ge bond lengths, specially for the (001)-oriented superlattice, are in good agreement with those calculated by neglecting the second-nearest neighbor relaxation. This demonstrates the reliability of our calculations reported in Sec. 2.5, where second-nearest neighbor relaxation was neglected.
- The small ionicity of the Si-Ge bond (see Sec. 2.5) is found to be unaffected also by the structural relaxation.
- Both of the studied superlattices are found to be indirect gap semiconductors. The lowest level of the conduction band occurs at what we call the Z_x point and the $M - L_x$-line (which correspond to X-point and Δ-line of the zinc-blende structure) for the (001) and (111)-oriented superlattices, respectively.
- Even for such very thin layered superlattice, the mixing between the conduction band states are appreciable, and has direct influence on the conduction band structure. It is responsible, e.g. for the anti-crossing of the levels and the displacement of the conduction band minima.
- The level charge densities of the lowest conduction band levels at the high symmetry points are calculated, and the confinement of the conduction

states is studied. It has been found that it is different for the equivalent levels of the zinc-blende structures, which are either folded or unfolded upon superlattice growth.

Chapter 5

Band Structure

This chapter is devoted to the study of the band structure of Ge, Si and Si_xGe_{1-x} alloys and their pressure dependence. The band structure of Si_xGe_{1-x} alloys is still an intriguing subject, which has been studied using different theoretical techniques [99-102]. Special attention is given here to the self-consistent calculations of Podgorny, Wolfgarten and Pollmann (PWP) [102]. It is well known now that there are serious problems encountered when calculating the band structure of Ge within local density approximation (LDA) (almost 100% reduction of the energy gap and the lowest conduction band edge is calculated to be at Γ rather than at L-point). Using pseudopotentials constructed by them, PWP have obtained roughly 50% reduction of the band gaps of both Si and Ge, and a correct topology of the band structure of Ge. These results appear to be in contradiction with the previous ab-initio calculations [103].

The LDA of the density functional theory (DFT) has been emerged as the most successful tool in describing the ground state properties of inhomogeneous electronic systems, such as atoms, molecules, solids and surfaces. In spite of the fact that the eigenvalues of DFT are formally lagrangian parameters, to be used only in the total energy calculations, they have been used as electronic excitation energies. In the case of semiconductors the calculated energy gaps

are of order 20 - 50% of the observed values. Apart from this reduction, the conduction band structures are usually well reproduced. The shortcoming is now understood as a result of a discontinuity in the exchange and correlation potential [51]. It has been demonstrated that LDA can be used successfully to obtain conduction band related properties [104].

For the band structure calculations of semiconductor alloys VCA has widely been used. In VCA the identity of the alloyed atoms and bonds is completely neglected. In other words, both chemical and structural disorder are neglected. To go beyond VCA different approaches have been proposed, such as coherent potential approximation (CPA) [66], molecular CPA (MPCA) [67], the recursion method [105] and the supercell approach [8]. Each of these approaches has its own problems and limitations. The main disadvantage of the first three is that they are limited to the empirical tight binding method, while the last one is attractive because is allows for more accurate band structure techniques, where the effects of the charge density redistribution and the bond length alternation can be accounted for properly. However, this can be done only at a discrete set of x values and at the price of a large computational effort.

Recently, the pressure dependence of the energy gaps of semiconductors has become a subject of renewed interest. This is because of the new improvements in the experimental techniques, which give more accurate results [112]. And also due to the finding that the results obtained from ab-initio calculations are in good agreement with experiment [107-111], despite the underestimation of the energy gaps within LDA.

Here, we have first shown that the appealing features of the PWP results, which are obtained using the experimental lattice parameters and atomic orbitals expansion of the wave functions, are not reproducible using plane wave expansion. On the contrary PWP pseudopotentials give much worse results than Bachelet, Hamann and Schlüter (BHS) [72] pseudopotentials. Moreover, the appealing features can be obtained using BHS pseudopotentials and the calculated equilibrium values of the lattice constants rather than the experimental ones. This is justified, because we want our calculated crystal to be under zero pressure. The calculated a_{eq} are usually smaller than the experimental values.

Therefore calculating the band structure at the latter is exactly the same as if we were performing these calculations under negative hydrostatic pressure, which is around -15 kbar in the case of Ge. This is very important because of the sizable effects of the pressure on the band structure of semiconductors, specially on the E_0 transition. Using the calculated a_{eq}, our results for the band gaps of Si and Ge are around 40% of the observed values; and a correct topology of the band structure of Ge is obtained. These calculations are performed using BHS pseudopotentials.

Using VCA and Vegard's law variation of $a(x)$ between the calculated a_{eq} of Si and Ge, a meaningful variation of the band gaps with x is obtained. However, we have found that the E_0 and E_2 optical transition show pronounced downward and upward bowing, respectively. While the other transitions show almost linear variation. At $x = 0.5$ the bowing in the E_0 transition is around 0.1 eV. We have found that this can be eliminated via supercell calculations. So, it is to be considered as an artifact of VCA. Moreover, the effects of the ordering, charge density distribution and the bond length alternation have been studied, by performing different supercell calculation at $x = 0.5$.

The pressure coefficients of Ge, Si and Si_xGe_{1-x} alloys are studied: the ab-initio calculated values for the pure materials are in good agreement both with experiment and other similar theoretical calculations, which insures the predictive power of this approach. As a representative of Si_xGe_{1-x} alloys, the pressure coefficients of $Si_{0.5}Ge_{0.5}$ alloys within both VCA and zinc-blende structure are studied. Both systems show Ge-like behavior. Furthermore, the E_0 (the lowest direct transition at Γ) shows a sublinear variation with x, as that observed in the case of Ge [111] and GaAs [112].

The rest of the chapter is organized as follows. In Sec. 5.1 we give detailed comparison between the band structures of the Si and Ge.

Sec. 5.2 is devoted to study the band structure of Si_xGe_{1-x} alloys, within three different approaches (1) Self-consistent VCA calculations (Sec. 5.2.1). (2) Self-consistent supercell approach (Sec. 5.2.2). (3) Empirical pseudopotential VCA calculation (Sec. 5.2.3).

In Sec. 5.3 the pressure dependence of the band gaps of Si, Ge and Si_xGe_{1-x} are calculated and discussed. And finally, Sec. 5.4 contains summary of our main conclusions.

5.1 The band structure of Si and Ge

The band structure of Si and Ge have been widely investigated by many authors, using different theoretical techniques, such as orthogonal plane-waves method (OPW) [113], k.p method by Cardona and Pollak [114], empirical pseudopotential method (EPM) by Cohen and co-workers [115,116], tight-binding method by Chadi [117] and self-consistent density functional and norm conserving (NC) pseudopotential approach [104]. This is to mention only some representative calculations.

Both Si and Ge have the same diamond crystal structure (i.e, the same symmetry point group). In Fig. 5.1 we show the electronic band structure of Si and Ge as calculated using EPM by Chelikowsky and Cohen [115], which are considered as the best fit to the experimental results. Apart from the splitting due to spin-orbit interaction, and in spite of the relatively small ($\sim 4\%$) lattice mismatch, it is evident from Fig. 5.1 that on going from Si to Ge there are two important differences

- Large reduction at k=Γ of the Γ_2 conduction band energy; the difference is 3.1 eV. This makes the direct optical transition at Γ of the same order of magnitude as the indirect transition at L and X-points. It should be noticed that also GaAs has the three transitions of the same order, and there are larger and more serious problems encountered in the band structure calculations using LDA for both Ge and GaAs.
- Large reduction at k=L of the L_1 conduction band energy; the difference is 1.3 eV. As a consequence, Ge is unique among semiconductors in having the lowest conduction band edge at L-point.

The variation of the band gaps on going from Si to Ge, by increasing the

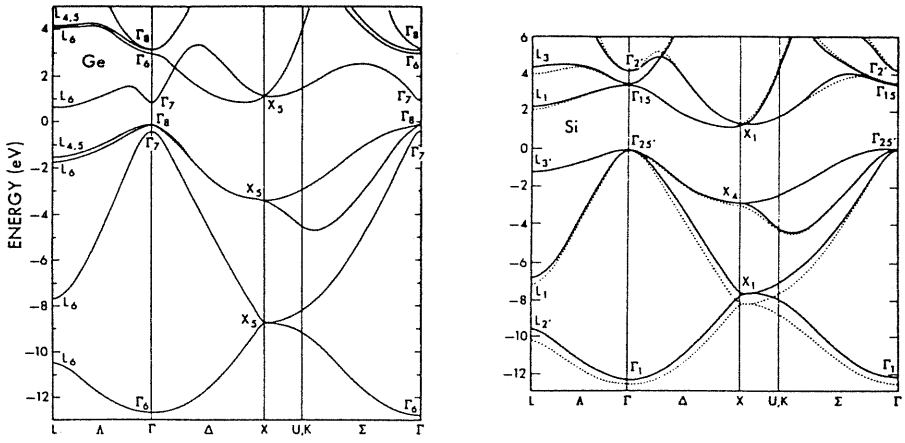

Figure 5.1: Band structures of Si and Ge. In the case of Si two results are presented: nonlocal pseudopotential (solid line) and local pseudopotential (dashed lines). (from Ref. 115)

concentration x of Si_xGe_{1-x} alloys, is a very interesting subject and has been extensively studied both experimentally and theoretically. This will be the subject of the next section.

As we have mentioned above, within LDA the energy gaps of semiconductors are underestimated. It has been found that the reduction of the direct optical gap at Γ is $\sim 100\%$. In addition to this the lowest conduction band edge is at Γ and not at L-point. This problems has been considered as an artifact of LDA. Almost all the above calculations are performed, using the standard BHS pseupotentials, at the experimental lattice parameter. Very recently, PWP have constructed new pseudopotentials for Si and Ge using Kerker scheme [48]. Using these pseudopotentials and atomic orbital expansion of the single particle wave-functions, at the experimental lattice parameter, they have found that for both Si and Ge the direct optical transition at Γ is roughly 50 % of the observed values, and the topological problems encountered in the band structure calculation of Ge are corrected (they got correctly the lowest conduction band edge at L-point). So, what is then the reason for the problems inherent in the band structure calculations of Ge? Is it really LDA, the pseudopotentials or something else? In Tab.'s 5.1 and 5.2 we show the check of the convergence

E_{cut} (Ry)	E_0 (eV)	E_0' (eV)	E_1 (eV)	E_2 (eV)	L_1 (eV)	X_1 (eV)
10	0.50	2.57	1.78	3.84	0.41	0.82
12	0.51	2.55	1.60	3.75	0.20	0.70
14	0.05	2.56	1.55	3.73	0.17	0.70
16	0.02	2.56	1.52	3.72	0.15	0.69

Table 5.1: Check of the convergence of Bachelet et al. with respect to the constant energy cutoff.

E_{cut} (Ry)	E_0 (eV)	E_0' (eV)	E_1 (eV)	E_2 (eV)	L_1 (eV)	X_1 (eV)
10	0.59	2.57	1.89	3.98	0.42	0.75
12	0.39	2.53	1.56	3.81	0.08	0.63
14	-.15	2.54	1.50	3.80	0.06	0.66
16	-.21	2.56	1.47	3.79	0.03	0.65

Table 5.2: Check of the convergence of Podgorny et al. with respect to the constant energy cutoff.

of both BHS and PWP pseudopotentials [1] using plane wave expansion of the the wave functions. The charge densities are calculated using Chadi-Cohen two special points, while the experimental lattice parameter is used. It evident that the reduction in the E_0 optical transition is larger in the case of PWP pseupotential, contrary to what they have reported. The origin of the discrepancy between our and PWP results is unknown to us; but it seems that it is due to a poor convergence of the PWP calculations. For both potentials the drastic reduction occurs above $E_{cut} = 12$ Ry, which supports our explanation of the above conflict. Therefore, the solution of the gap problem for Ge is not in the pseudopotentials suggested by PWP.

It should be noticed that the calculated equilibrium lattice parameter using

[1] We are grateful to PWP for sending us the coefficients of their pseupotentials

Transition	Theo. a_{eq} (eV)	Expt. a_{eq} (eV)
E_0	0.43	0.03
E_0'	2.59	2.57
$X_1^c - \Gamma_{15}^{v\prime}$	0.64	0.69
$L_1^c - \Gamma_{15}^{v\prime}$	0.29	0.16
E_1	1.74	1.54
E_2	3.83	3.73

Table 5.3: Some direct and indirect optical transitions of Ge calculated at the theoretical and the experimental equilibrium lattice constants.

BHS potentials for both Si and Ge are about 1% smaller than the experimental values (see Sec. 2.4). These results are very good as far as the structural properties are concern. But this has drastic effects on the band structure. For example, the fully converged calculations for Ge give $a_{eq} = 5.57$ compared to 5.66 $\AA$ the experimental value. It has been shown also that in the fully converged calculations the quantum mechanical pressure [118] is equal to zero at the calculated equilibrium lattice parameter. Therefore, calculating the band structure at the experimental a_{eq}, for this *theoretical* system, means that we are performing these calculations out of equilibrium ($P = 0$), under around -13 kbar isotropic pressure. The importance of this point comes from the sizable effects of the pressure on the band structure of semiconductors, specially on the E_0 transition (the pressure dependence of the band gaps will be the subject of Sec. 5.3). In Tab. 5.3 we show the energy band gaps of Ge calculated at both the theoretical and experimental lattice parameters, using $E_{cut} = 17.5$ Ry. It should be noticed that the largest effect is encountered, as expected, in the E_0 transition. Therefore, we believe that large portion of the reported problems inherent in the ab-initio calculations of the band structure of Ge is due to the carring out of these calculations out of equilibrium of the *theoretical* system.

Tab. 5.4 contains our calculated values of lowest energy gaps of Si and Ge compared with some other calculations and experiment. The remarkable

System	Transition	Expt.	*Present work*		*PWP*		*WR*	
			value	corr.	value	corr.	value	corr.
Si	E_0	4.19	3.55	0.64	3.22	0.78	- -	- -
	E_0'	3.37	2.54	0.83	2.57	0.80	2.55	0.82
	$X_1^c - \Gamma_{15}^{v\prime}$	1.30	0.56	0.74	–	–	0.64	0.66
	$L_1^c - \Gamma_{15}^{v\prime}$	2.10	1.55	0.55	–	–	1.45	0.65
Ge	E_0	0.89	0.44	0.45	0.43	0.46	0.02	0.87
	E_0'	3.32	2.59	0.73	2.46	0.86	–	–
	$X_1^c - \Gamma_{15}^{v\prime}$	1.30	0.63	0.67	–	–	0.61	0.69
	$L_1^c - \Gamma_{15}^{v\prime}$	0.74	0.29	0.45	0.39	0.35	0.09	0.65

Table 5.4: The calculated values of some direct and indirect optical transitions of Si and Ge, together with the results of Podgorny et al. (PWP) and the results of Van de Walle and Martin (WM), compared with the observed results. The values of the correction term (see text) is also shown.

features to notice are:

- In both our and PWP calculations the correction term (the difference between the calculated and the observed values of the energy gaps) is not a constant, but it is almost equal for the same transition in both systems; except for the E_0 transition, which could be due to the large difference in the value of of E_0 in Si and Ge, and the sensitivity of this transition to the choice of a.

- In both our and PWP calculations the correction term is different for the E_0 and E_0'. Whereas, Van de Walle and Martin (WM) [104] have found that it is the same for the lowest direct transition at Γ for both systems.

- In our calculations the correction term is generally smaller by roughly 0.1 eV in Ge.

- Our results for the lowest energy gaps are $E_g^{Si} = 0.34$ and $E_g^{Ge} = 0.29$ eV (not shown in the table), which are around 60 % out of the experimental values 1.10 and 0.74 eV, respectively.

5.2 The band structure of Si_xGe_{1-x} alloys

In the previous section we show that there are large differences between the band structure of Si and Ge, specially at L and Γ-points, despite the relatively small lattice mismatch. Due to this fact and the technological importance of these systems, the band structure of Si_xGe_{1-x} alloys is an intriguing subject, which has attracted the attention of a lot of researchers in semiconductor physics. Different theoretical approaches have been used, ranging from simple empirical schemes to ab-initio self-consistent calculations [99-102]. From the experimental point of view the band structure of Si_xGe_{1-x} is well established [44,45]. On going from Ge to Si by increasing x, a crossover of the lowest conduction band edge from Ge-like symmetry (L-point) of Si-like symmetry (Δ-line) occurs at $x = .15$ [44]. Another crossover of the direct transition at k=Γ from Ge-like (Γ_2^c state) to Si-like ($\Gamma_{15}^c{}'$ state) takes place at $x = .83$. The variation of the energy band gaps with x is found to be almost linear [45].

The lowest energy gaps of semiconducting alloys are usually smaller than the concentration weighted average of the corresponding band gaps of the constituent materials. The deviation ΔE_g is often expressed phenomenologically by [119]

$$\Delta E_g = bx(1-x), \tag{5.1}$$

where the bowing parameter b is positive, reflecting a downward bowing. For III-V alloys b is in the range ≤ 0.9 eV, and ≤ 2.4 eV for II-IV alloys. Whereas, for Si_xGe_{1-x} it is ~ 0.23 eV for $X_1^c - \Gamma_{15}^{v\prime}$ (XΓ) optical transition; this shows clearly that the energy-gaps bowing in the latter systems is much smaller than in III-V and II-VI alloys. The energy-gaps bowing has been ascribed both to intrinsic interelectronic interactions already present in the hypothetical ordered "virtual" alloys and in the VCA description, and to local structural relaxations. In general, VCA is not expected to reproduce well the bowing; in the case of

Si_xGe_{1-x}, nevertheless, VCA is reasonable because the bowing is small.

In the rest of this section the band structure is calculated self-consistently within VCA and in the supercell approach, and using improved EPM approach.

5.2.1 Self-consistent VCA calculation

Very recently, PWP have provided the first ab-initio self-consistent calculations of the band structure of Si_xGe_{1-x} alloys, using NC pseudopotentials and LDA. In the previous section, we have shown that their results, which are based on atomic orbital expansion of the single particle wave functions, are not reproducible using well converged sets of plane waves. Furthermore, we have shown also that the good features of the PWP calculation can be obtained using the standard pseudopotentials [72], at the calculated lattice constants rather than the experimental ones.

Bearing in mind all the *real* and *artificial* differences between the band structures of Si and Ge discussed in Sec. 4.1, we have carried out ab-initio calculations of Si_xGe_{1-x} alloys. The technical details are the same as described previously in Ch 4. The calculations are performed within VCA in the whole range $0 \leq x \leq 1$, in 0.1 steps of the concentration x, and linear variation of the lattice parameter is assumed (Vegard's law).

In Fig. 5.2 we show the lowest direct (solid lines) and indirect (dashed lines) energy gaps as functions of x. For the sake of comparison we show in Fig. 5.3a the results of PWP, while the experimental results are shown if in Fig. 5.3b. In our results the self-consistently calculated values are designated by circles (open circles for the E_0 transition and closed for the others). The straight lines are drawn by joining simply the end points to guide the eyes. The remarkable thing to notice is the astonishing similarity between the two theoretical results. The major differences is the downward bowing of the E_0 transition and the upward bowing of the E_2 transition in the present calculations, which is absent in the others. This bowing can't be understood as a consequence of the used Vegard's law variation of the lattice parameter of the alloy, while experimentally it shows

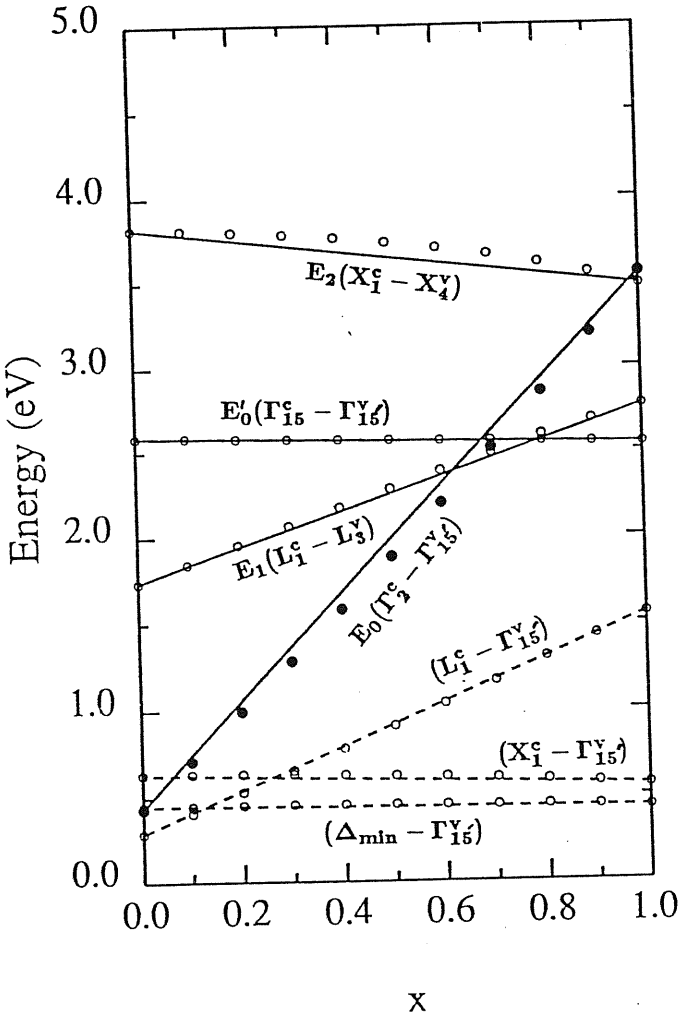

Figure 5.2: Some direct (solid lines) and indirect (dashed lines) optical transitions of Si_xGe_{1-x} alloys as functions of x. Circles: calculated values; straight lines: assumed linear variation drown to guide the eyes.

a downward bowing (see Sec. 2.5). At $x = 0.5$ the bowing is ~ -0.1 eV; only 40 % of it can be attributed to the above effect.

From Fig. 5.3 it is clear that the crossover in the lowest conduction band state occurs at $x = 0.12$ in good agreement with the experimentally determined value $x = 0.15$ [44], We mention also that exactly the same result has been obtained by PWP. These results and others found using different theoretical approaches are given in Tab. 5.6. This shows the predictive power of LDA, despite the shortcomings in the absolute values of the gaps; this predictive power is even better than for approaches that start with experimentally-adjusted gaps.

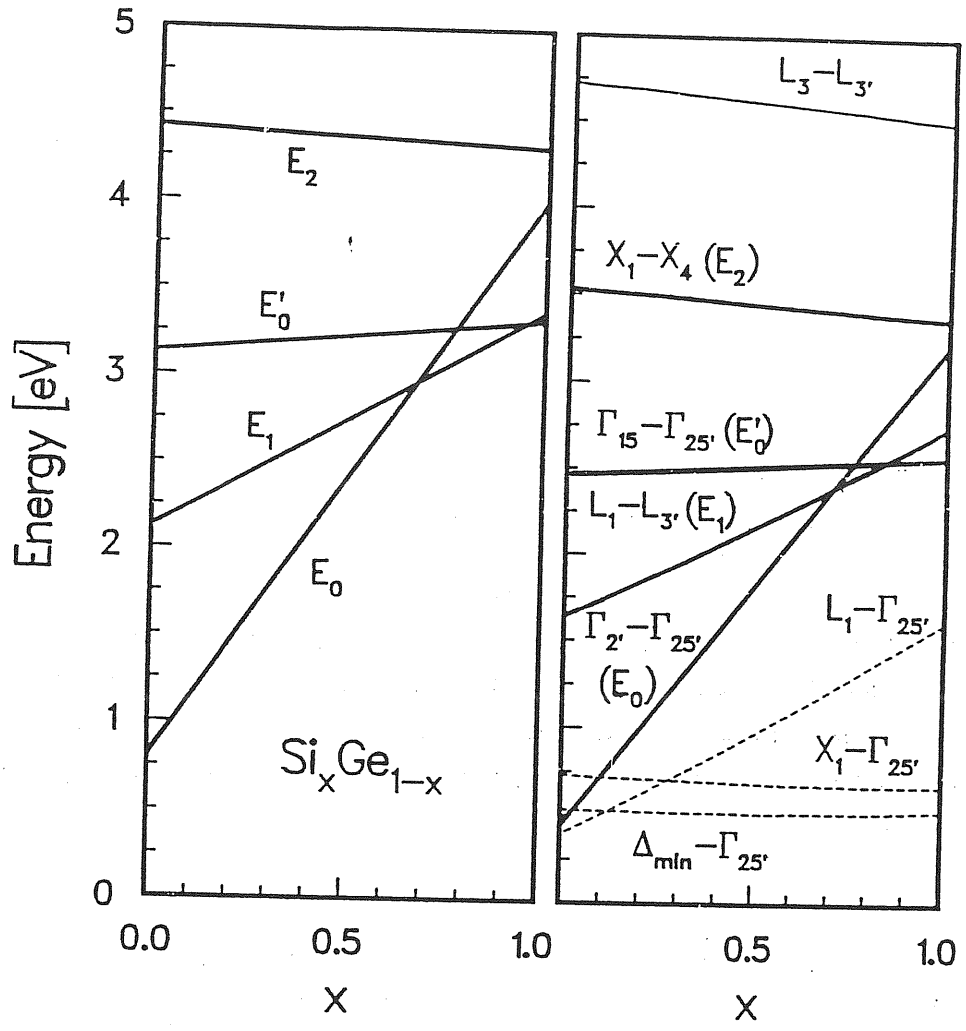

Figure 5.3: Some direct (solid lines) and indirect (dashed lines) optical transitions of Si_xGe_{1-x} alloys as functions of x. (a) The experimental results [45]. (b) The results of Podgorny et al. [102]. (from Ref. 102)

Method	Crossover point
Expt.	0.15[a]
LDA + VCA	0.12[b,c]
k.p	0.25[d]
EPM	0.18[c], 0.21[b]
Tight binding + VCA	0.11[e]
CPA	0.13[f]

a) Ref. 44.
b) Ref. 102.
c) Present work.
d) Ref. 100.
d) Ref. 99.
e) Ref. 120.
f) Ref. 121.

Table 5.5: Crossover point of the lowest conduction band edge from Ge-like to Si-like of Si_xGe_{1-x} alloys, as calculated by different theoretical approaches, compared with experiment.

The variation of the eigenvalues with x is shown in Fig. 5.4; the open circles are the calculated values and the straight lines joining the end values are drawn to show the deviations from linearity. It is evident that most of the upward bowing of the E_2 transition discussed above is due to a downward bowing of X_4 state eigenvalue.

As a representative we show in Fig. 5.5 the band structure of $Si_{0.5}Ge_{0.5}$ alloy within VCA (dotted lines), compared with that having zinc-blende structure (solid lines), the same value $a = 10.346$ a.u has been used in the two cases. This situation is very similar to the case of Ge and GaAs, both systems having the same lattice parameter. It is evident that apart from the splitting of some degenerate states, the two band structures of SiGe systems are equivalent. The $L_1^c - \Gamma_{15}^v$ (LΓ) and E_0 optical transition (not affected by the splitting) are almost the same in both cases. It should be noticed that on going from Ge to GaAs, one founds that, in addition to the splitting of some degenerate states (which is larger than in the SiGe zinc-blende structure), the LΓ transitions behave differently in the systems, since there is an energy difference of order 0.5 eV in the case of E_0 transition and 1.1 eV in the LΓ transition [122]. The above

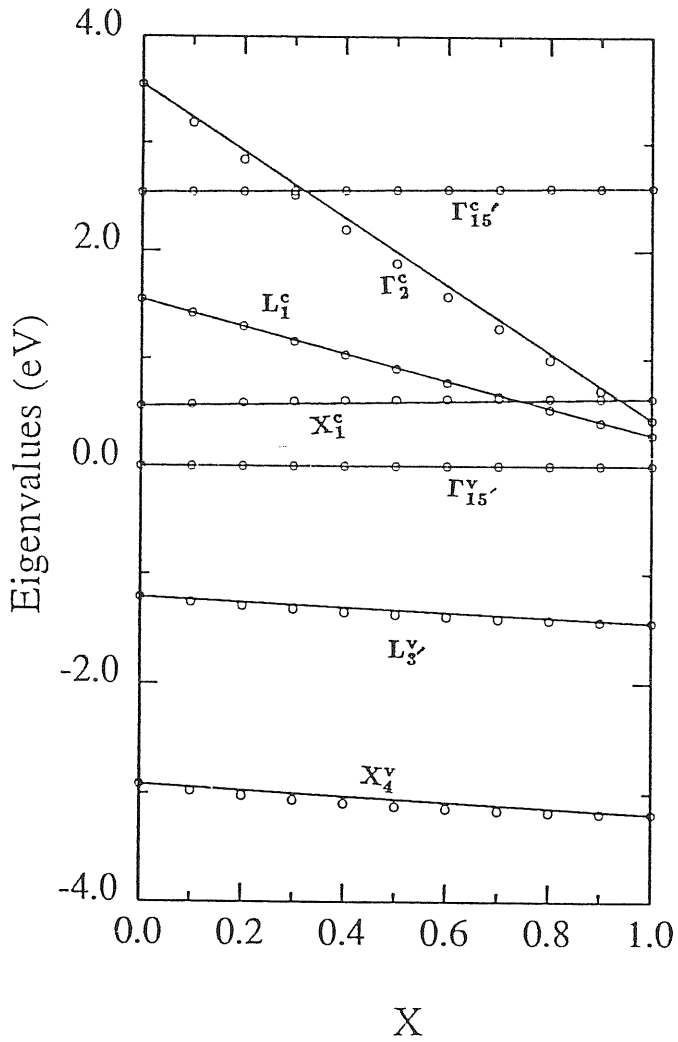

Figure 5.4: The VCA eigenvalues of Si_xGe_{1-x} alloys as functions of x. Circles: calculated values; straight lines: assumed linear variation drawn to guide the eyes.

dated. This will be the subject of the next subsection.

5.2.2 Self-consistent supercell calculations

As we have mentioned before VCA is a kind of zero order approximation, which is valid when the difference in potential of the alloyed materials is small. It is evident from Sec. 2.1 that going beyond this approximation is necessary to obtain good ground state properties. Whereas in the previous subsection we show that it is a good approximation for the band structure and optical transitions calculations. Here, we study the effects of going beyond VCA by considering some SiGe supercells: the effect of the structural relaxation, the type of ordering and the electronic charge density distributions are studied.

For the electronic structure calculations the coherent potential approximation (CPA) is often used as a higher order approximation: CPA takes care of the chemical disorder due to the random distribution of the constituent atoms in the lattice sites. In order to take into account the recently observed bond length alternation (structural disorder), molecular CPA (MCPA) has been developed [67]. The idea behind these approximations is that a complex MCPA effective potential is defined by the condition that a cluster of sites embedded in the effective medium, on average, produces no further scattering. For the simple CPA a single site is embedded in the effective medium. The imaginary part of the potential reflects the fact that alloy quasiparticle states are damped. The main disadvantage of the CPA and MPCA is that they are limited to an empirical tight-binding description. So, they do not take into account the effect of the electronic charge density redistribution.

An alternative approach is through supercell calculations, by introducing an artificial periodic ordering. The advantage of this approach is that it allows the use of modern crystalline band structure techniques, whose predictive power is very accurate. The unit cell in this approach is chosen to represent the most probable local configuration of the alloy. For example, for binary $A_{0.5}B_{0.5}$ the most probable configuration is that each atom is surrounded by two atoms of the same kind and two of the other in the first nearest neighbors shell. The most

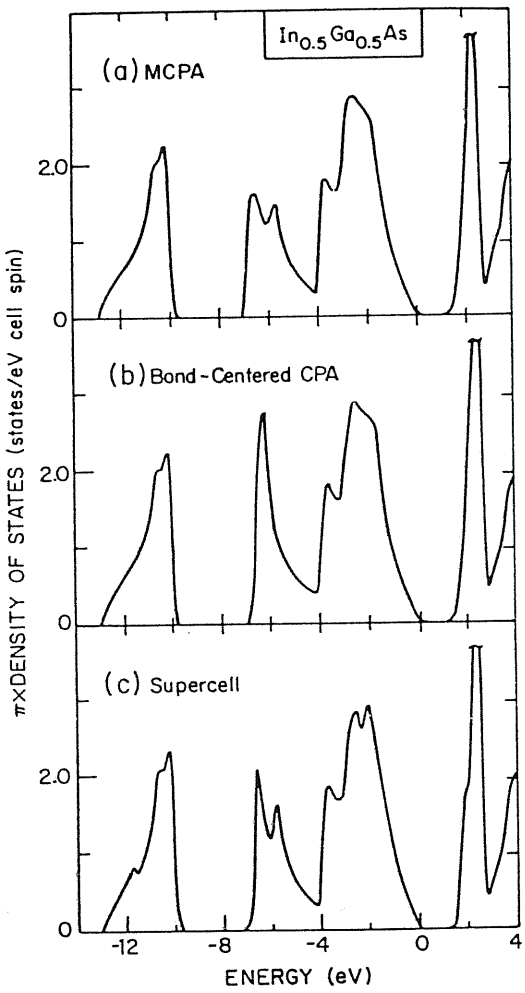

Figure 5.6: Comparison of $In_{0.5}Ga_{0.5}As$ densities of states calculated in (a) MPCA, (b) bond-centered CPA, and (c) supercell approaches. (from Ref. 67)

suitable periodic ordering is along $< 100 >$ direction by alternating two layers of each kind AABBA.. along the ordering direction. Very recently, Lempert, Hass and Ehrenreich [67] have shown that the density of states for $In_{0.5}Ga_{0.5}As$ and $ZnSe_{0.5}Te_{0.5}$ calculated within the supercell approach, are remarkably similar to that calculated by MCPA, except for some additional fine structures. Their results for the $In_{0.5}Ga_{0.5}As$ are shown in Fig. 5.6. The two calculations are done under the same conditions.

The supercell approach is very attractive since it allows for more accurate band structure methods than the tight binding method, such as, LDA or even the more advanced approach which based on the self-energy calculations (i.e.

like the work of Hybertsen and Louie [123]).

To study the effect of the ordering (i.e. the effect of a particular ordered structure or supercell chosen), three different ordered structures with equivalent number of Si and Ge atoms are considered, which are ZB, simple tetragonal and rhombohedral structures. The ZB crystal structure is described in Sec. 2.4.5, and its band structure is shown in Fig. 5.5. Whereas the stability and the band structure of the full relaxed structures of the other two kinds were the subject of Ch. 4. It should be noticed that the local structure is different in the three ordered structures; the number of atoms of different type surrounding a given atom is four for ZB, three for rhombohedral and two for the tetragonal structure. Only the energy gaps at the high symmetry points Γ, L and X of the ZB and the equivalent points after folding in the case of the other structures are calculated. The calculations are performed self-consistently, using LDA and NC pseudopotentials; the technical details are exactly the same as described previously in Ch. 4. Since we are interested here in studying the band structure of the alloys, which have cubic symmetry, the $c/a_\perp$ ratio is taken to be equal to one for both tetragonal and rhombohedral structures. For the sake of meaningful comparison the lattice constant is taken to the same for the three structures; and it is chosen to be $a = 10.386$ a.u., the equilibrium value for ZB. In order to isolate the effects of the ordering we start assuming the following

- The atoms occupy the ideal ZB sites (the local structural disorder is completely neglected).
- The same electronic charge density distribution for the three structures; we have used that of VCA (the effects of the charge density redistribution are discussed below).

In Tab. 5.7 we give the calculated values of some direct and indirect optical transitions for the three structures, compared with that obtained within VCA. The remarkable features to be noticed are:

- For the E_0 transition, the calculated values for the ordered structures are almost equal, and around 0.1 eV higher than that of VCA. It should be

Transition	VCA (eV)	ZB (eV)	Tet. (eV)	Rho. (eV)
E_0'	2.57	2.57	2.58	2.57
E_0	1.91	1.99	2.04	2.01
$X_1^c - \Gamma_{15}^{v\prime}$	0.62	0.66	0.61	0.56
$L_1^c - \Gamma_{15}^{v\prime}$	0.92	0.97	0.96	1.12

Table 5.6: Comparison od some direct and indirect optical transitions of three ordered structures of SiGe (zinc-blende, tetragonal and rhombohedral), and that of $Si_{0.5}Ge_{0.5}$ alloy within VCA.

noticed that in the previous subsection, the pronounced downward bowing of this transition at $x = 0.5$ was of the same order ~ 0.1 eV. Since the three ordered structures give the same value, the pronounced bowing can be attributed to VCA.

- For the rhombohedral structure, the calculated values for the XΓ and LΓ transitions is different from that of the others, this is a consequence of the BZ folding of this particular structure (X $\longrightarrow$ L), and results from the mixing of states, which push the L_1 state up and the X_1 state down in energy. If one is interested in the band structure of the alloy, this *critical* folding should be avoided.

- The remaining transitions are practically the same as the calculated values within VCA; the largest difference is 0.05 eV.

Even at this very rough level of approximation, the supercell approach shows the shortcomings of VCA.

Then, in order to isolate the effect of the charge density redistribution, we have repeated the calculations of the band structure of the tetragonal supercell, using different charge density distributions. The used charge densities are that of the VCA, ZB and the unrelaxed tetragonal structure. In Tab. 5.8 the obtained values of some direct and indirect transition are shown. The remarkable thing to notice is that the calculated values of the same transition are equal,

Transition	Tet. charge density	ZB charge density	VCA charge density
E_0'	2.58	2.58	2.57
E_0	2.04	2.06	2.04
$X_1^c - \Gamma_{15}^{v\prime}$	0.61	0.61	0.62
$L_1^c - \Gamma_{15}^{v\prime}$	0.96	0.96	0.96

Table 5.7: Comparison of some direct and indirect optical transitions of the ideal tetragonal SiGe structure calculated several charge density distributions.

the maximum difference being 0.02 eV. This can understood as a consequence of the very small ionicity of the Si-Ge bond, and it is expected to be system dependent.

To study the effects of the structural relaxation on the band structure of the Si_xGe_{1-x} alloys, in particular on the energy gaps bowing, we have calculated the band structure of the relaxed rhombohedral structure (here also we keep using $c/a_\perp = 1$). The triplet Γ_{15}^v splits into doublet and singlet states, while the doublet X_1^c state splits into two siglet states. For the unrelaxed structure, the difference in energy is 0.01 and 0.17 eV for the Γ_{15}^v and X_1^c states, respectively. Whereas, after relaxation they are 0.05 and 0.27 eV. For the unrelaxed structure, the lowest $X\Gamma$ transition between the splited states is 0.47 eV, while it is 0.56 eV for the weighted average states. In the case of the relaxed structure they are 0.37 and 0.52 eV, respectively. It should be noticed that the observed bowing is ~ 0.1 eV [44]. Therefore, it is evident that large portion of the bowing of the $x\Gamma$ transition is due to structural disorder. We mention here that Jaffe and Zunger [8] have arrived to the same conclusion in the case of ternary alloys.

5.2.3 Empirical pseudopotential calculations

The EPM is nowadays the simplest method for the band structure calculations for semiconductor elements and compounds [115]. Because the pseudopotential from factors are fitted to excited-state spectra, the detailed properties

of the electronic band structure are reproduced accurately. Because of the crystalline periodicity only a few (three in the case of Si and Ge) pseudopotential form factors are needed to represent the crystal potential felt by the valence electrons. For finer details and better agreement with the experimental results, other terms are added to take care of the non-local effects. Since the screening effects are included in these potentials, the transferability to other systems is questionable. Previous EPM calculations of the band structure of Si_xGe_{1-x} alloys have been carried out within the VCA, by simply assuming that the form factors of the alloy potential are the concentration weighted average of the corresponding form factors of Si and Ge. The resultant energy gaps show upward bowing, contrary to the downward bowing observed experimentally [45]. The unreliability of the EPM has been also pointed out by Bergstresser and Van Vechten [124].

Very recently, an extrapolation procedure has been proposed by Bednarek and Rossler (BR) [125], which gives matrix element for phonon-assisted indirect transitions of Si and Ge in good agreement with experiment. This procedure has been checked also by Allen and Cardona [126] by calculating the absolute shift of the energy eigenvalues under hydrostatic pressure, and they show that it is much better than the previous extrapolation schemes (see Fig. 5.7). Since there is a 4 % lattice mismatch between Si and Ge and the lattice constant varies almost linearly between the end points, the lattice constant of the alloy is larger than the lattice parameter of Si and smaller than that of Ge. So, this situation is very similar to the band structure calculation under high pressure [128]. Because of the change in the valence charge density, the change in the screening effects must also be taken into account. One approximation which has been proposed to this effect [129] is

$$V(q) = \frac{1}{\Omega\epsilon(q)} \int V(r) e^{-i\mathbf{q}.\mathbf{r}} d\mathbf{r}, \tag{5.2}$$

where $\epsilon(q)$ is the dielectric function, Ω is the unit cell volume and $V(r)$ is the ionic potential. Thus, multiplying both sides of Eq. (5.2) by $\Omega\epsilon(q)$ we obtain

$$A(q) = \int V(r) e^{-i\mathbf{q}.\mathbf{r}} d\mathbf{r} \tag{5.3}$$

which is independent of the volume and the chemical environment. Since $\epsilon(0)$ is finite for semiconductors, according to BR extrapolation scheme, one has

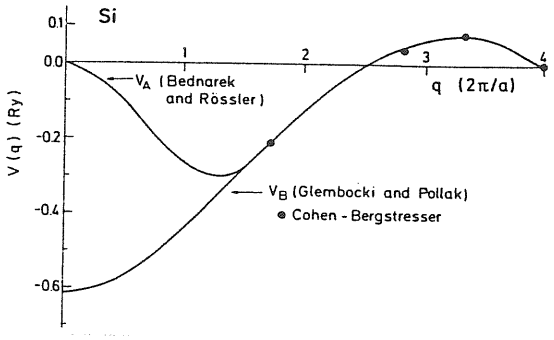

Figure 5.7: Two extrapolation schemes for the empirically determined form factors of Si. V_A is due to Bendarek and Rossler [124], and V_B is due to Glembochi and Pollak [126]. (from Ref. 125)

$A(0) = 0$. Instead of fitting the known V(q) to some form factors, such as that of Cohen and Bergstresser, one can fit the above function $A(q)$. The extrapolation procedure becomes important in the supercell calculation, where the form factors at some new G-vectors do not vanish by symmetry.

We have found that the simple metallic Thomas-Fermi (TF) dielectric function, at the $G \neq 0$ vectors

$$\epsilon(q) = 1 + k_0^2/q^2, \tag{5.4}$$

is sufficient to give excellent pressure coefficient E_0 optical transition (see next section); this agreement is the same as that obtained by Welber et al., using Penn's dielectric function which requires self-consistency loop, since $\epsilon(q)$ is a function of the average (Penn) gap. It should be noticed that semiconductor TF model dielectric function has been derived by Resta [130], but it requires the knowledge of $\epsilon(0)$ for the alloy.

In view of these developments it is necessary to recalculate the band structure of Si_xGe_{1-x} alloys. For this purpose we use the most accurate empirical pseudopotentials of Chelikowsky and Cohen [115]; we consider the local one for Si and the non-local for Ge. The form factors of Si and Ge at each value of x are calculated according to the following

- The values of the function A(q) is calculated at each of the three values

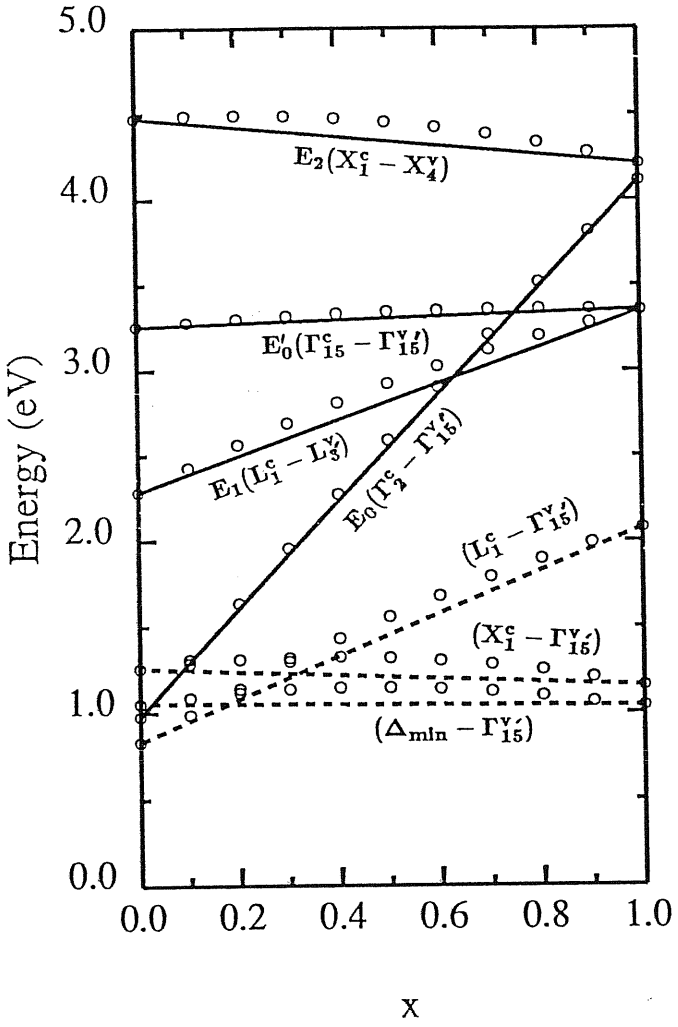

Figure 5.8: Some direct (solid lines) and indirect (dashed lines) optical transitions of Si_xGe_{1-x} alloys as functions of x calculated using empirical pseudopotentials [115]. Circles: calculated values; straight lines: assumed linear variation drown to guide the eyes.

of G which have nonvanishing V(G) in the pure materials, by multiplying by the corresponding $\Omega\epsilon(G)$.

- Following BR scheme, the three nonvanishing values of A obtained above in addition to $A(0) = A(16) = 0$, are fitted to a polynomial of order four. Then the values of A at the G-vectors of the alloy are calculated.

- The form factors of each element is calculated by dividing such values of $A(G)$ for Si and Ge by $\Omega\epsilon(G)$, which corresponds to the alloy.

To calculate the band structure of the alloy we have used VCA; the non-local part of the Ge potential, multiplied by the atomic concentration of Ge, is considered as non-local part of the VCA potential.

In Fig. 5.8 we show some direct and indirect energy-gaps of Si_xGe_{1-x} alloy as functions of x. The circles are the calculated values, and the straight lines are drawn simply by joining the end values to show the deviation of calculated gaps from linearity. We have found almost exactly the same energy gaps for Si_xGe_{1-x} if the effects of the change in screening are not taken into account. This shows clearly that EPM is not a good approach to calculate the band structure of semiconductor alloys, even after taking care of the above improvements.

5.3 The pressure coefficient of Si, Ge and Si_xGe_{1-x}

The study of the pressure dependence of the band structure of semiconductors has become a subject of renewed interest; not only because of the new achievements in the the experimental techniques, such as the development of the diamond-anvil cell and the ruby fluoresence manometer, but also because of the finding that the first-principle ab-initio calculations based on LDA give good account for the pressure dependence of the energy gaps [107-111] and are superior to any previous theoretical technique, such as the semiempirical pseudopotential scheme [128] or the modified version of Van Vechten's dielectric theory [131], despite the severe underestimation of the energy gaps within LDA.

For Ge it has been found that the direct energy gap at $k = \Gamma$ shows a sublinear behavior with pressure. The nonlinearity is attributed to the nonlinearity in the bulk modulus, since it disappears when the gaps is plotted as a function of the lattice parameter. A sublinear behavior has also been recently observed for GaAs. To our knowledge such behavior has not been reported for Si. The XΓ transition has a negative coefficient, unlike the other transitions. This means that it decreases by increasing the hydrostatic pressure, which would imply that at high pressure the system becomes metallic: this in fact does not occur because a structural phase transformation takes place before this stage. Therefore, the reduction of the XΓ energy gap is responsible for the instability of the diamond or the zinc-blende structure at very high pressures. The negative pressure coefficient of the XΓ transition is understood as an effect of the d levels, which lie in energy well above the X minima of the conduction band. By increasing the pressure these levels repel the conduction band at X downward relative to the top of the valence band at Γ (i.e, reducing the XΓ energy gap). Lee, Sanchez-Delesa and Dow have shown that without the d states, the pressure dependence of this transition is not correctly reproduced by the theory. Furthermore, Fahy et al. have shown that the anomalous (positive) sign of the pressure coefficient of this transition in diamond is due to the absence of d states with the same quantum number as the low-lying s and p valence states of the carbon atom.

In this section we will concentrate on the pressure dependence of the energy gaps of Si, Ge and Si_xGe_{1-x} within VCA and having ZB structure. The calculations are performed at the first-principle level. The technical details are exactly the same as described in Ch. 4. The band structure of the above systems has been calculated at six different values of the lattice constant smaller than the equilibrium one. The change in the energy gaps is calculated by subtracting from each of them the corresponding value at a_{eq}. The pressure is determined from the calculated Murnaghan's equations of states

$$P = (B_0/B_0')[(V_0/V)^{B_0'} - 1], \tag{5.5}$$

where V is the volume under pressure P, V_0 is the equilibrium volume ($P = 0$), B_0 and B_0' are the bulk modulus and its pressure derivative. The theoretically calculated parameters V_0, B_0 and B_0', in Sec. 2.4, are used here to calculate P. Therefore, the pressure coefficient determination is fully ab-initio. The calculated changes in the energy gaps of the above systems are least-square fitted to the quadratic equation

$$\Delta E_g = a + bP + cP^2. \tag{5.6}$$

The initial slope of the variation of the energy gaps of Ge are compared with other theoretical results and experiment in Tab. 5.8. Our results are in good agreement with experiment and other self-consistent calculations. In the same table we show the pressure coefficients obtained from Cohen-Bergstresser empirical pseudopotentials, where the change in the screening effects is taken into account as described in the previous section. It should be noticed that the pressure coefficient of the E_0 optical transition is in very good agreement with experiment and with the results of Welber et al. [111], while that of the $X\Gamma$ transition has a positive sign, in contradiction with experiment. This shows the predictive power and the reliability of the ab-initio calculations compared to EPM ones.

The pressure coefficients of the lowest energy-gaps of Si is given in Tab. 5.9. The agreement between our results and other self-consistent results and experiment is also good. The remarkable thing to notice is the similarity between the pressure coefficient of Si and Ge for almost all the energy gaps. Because the

Transition	Present work		CFC [a]	LSD [b]	RBC [c]	Expt.
	SFC	EPM				
E_0	11.95	15.56	12.8	16.19	12.47	$15.3 \pm .5^a, 12.0^a, 12.5^a, 13.0^a$
E_0'	0.66	2.31	0.80	–	–	–
E_1	6.16	8.64	–	6.28	–	7.50^b
E_2	2.76	5.74	–	2.36	–	5.50^b
$X_1^c - \Gamma_{15}^v$	-1.62	2.93	-1.40	-1.11	–	-1.50^b
$L_1^c - \Gamma_{15}^v$	4.27	7.46	4.50	4.90	–	5.00^b

a) Ref. 109.
b) Ref . 110.
c) Ref. 107.

Table 5.8: Comparison of the calculated and measured values of the pressure coefficients of the band gaps at the high symmetry points of Ge. Units are in meV/kbar.

lowest conduction band edge and the direct transitions at $k = \Gamma$ have different characteristics in Si and Ge, their pressure dependence is very different in both systems. For example, the lowest conduction band edge is at $k = L$ for Ge and $k = 0.83X$ for Si (see Sec. 5.1). So, its pressure coefficient is negative in Si and positive in Ge. In Si_xGe_{1-x} the pressure dependence of the lowest direct and indirect transitions will not vary smoothly with respect to x, but it will change suddenly at the crossover points which, in turn, will be pressure dependent. For example, the crossover point of the lowest indirect transition moves rapidly toward the Ge end by increasing the pressure; the crossover of the optical direct transition at $k = \Gamma$ shows the same behavior, but it becomes zero at much higher pressure.

As a representative of Si_xGe_{1-x} alloys, we have studied the pressure dependence of the energy gaps of Si_xGe_{1-x} alloy within VCA and having ZB structure. The calculated pressure coefficients are given in Tab. 5.10. The remarkable features to notice are

- Both systems have more Ge-like behavior; the calculated pressure coefficients are, in general, larger than the weighted average of the correspond-

Transition	Present work		CFC [b]	LSD[a]	Expt.
	SFC	EPM			
E_0	11.52	11.00	11.6	–	–
E_0'	0.45	0.95	0.50	0.48	1 ± 1^a
E_1	4.22	5.85	—	4.45	6.2 ± 0.4^a
E_2	0.70	3.69	—	1.64	3.0^a
$X_1^c - \Gamma_{15}^v$	-1.80	0.93	-1.60	-1.34	-1.5^a
$L_1^c - \Gamma_{15}^v$	3.45	4.70	3.80	3.30	—

a) Ref. 110.
b) Ref. 109.

Table 5.9: Comparison of the calculated and measured values of the pressure coefficients of the band gaps at the high symmetry points of Si. Units are in meV/kbar.

ing values of pure materials.

- The pressure dependence of the energy gaps are not equivalent in both systems. This is a consequence of the difference in the charge density redistributions at high pressure.

In Tab. 5.11, we give the calculated pressure coefficients of the quadratic term in Eq. (5.6) for the lowest direct optical transition at Γ, of Si, Ge and Si_xGe_{1-x} within VCA and having ZB structure. The available experimental and theoretical results are also shown in the same table. It is evident that sublinear variation of this transition observed in Ge is reproduced by the theory, while in Si it shows a linear variation. In both systems of $Si_{0.5}Ge_{0.5}$ alloy a sublinear variation of the above transition is predicted.

5.4 Conclusions

In this chapter we have studied the band structure and its pressure dependence for Si, Ge and Si_xGe_{1-x} alloys, using Local density approximation (LDA) and

Transition	VCA	ZB
E_0	11.84	11.98
E_0'	0.55	0.61
E_1	5.71	5.48
E_2	1.86	1.48
$X_1^c - \Gamma_{15}^v$	-1.78	-1.97
$L_1^c - \Gamma_{15}^v$	4.27	4.15

Table 5.10: Comparison of the calculated values of the pressure coefficients of the band gaps at the high symmetry points of $Si_{0.5}Ge_{0.5}$ within VCA and having ZB structure. Units are in meV/kbar.

System	Theory	Expt.
Ge	$-19.0^a, -20.4^b, -70.4^c$	-45 ± 10^d
Si	-2.0^a	–
VCA	-22.0^a	–
ZB	-10.0^a	–

a) Present work.
b) Ref. 106.
c) Ref. 110.
d) Ref. 111.

Table 5.11: Comparison of the calculated coefficients of quadratic term (in Eq. (5.6) of the lowest optical gap at Γ of Si, Ge and $Si_{0.5}Ge_{0.5}$ alloy within VCA and having ZB structure. The available theoretical and experimental values are also given. Units are 10^-6 eV/kbar.

norm-conserving pseudopotentials. For the alloy, the calculations are performed within VCA and the supercell approach. Some calculations using the EPM have been performed. A similar band structure calculations within VCA has been recently carried out by Podgorny et al. [102], who have obtained roughly the same underestimation of the band gaps of Si and Ge, the correct topology for the band structure of Ge and a meaningful variation of the band gaps of Si_xGe_{1-x} with x. We have found that this calculations is poorly converged and the good results are basically an artifact. In the following we draw our main conclusions.

We have used the standard Bachelet et al. pseudopotentials [72], well converged PW's expansion of the wave functions and the calculated equilibrium lattice constants (this is justified because we want the calculations to performed at zero pressure). Our main results are the following

- For pure crystals:
  1. The calculated energy gaps are $E_g^{Si} = 0.34$ and $E_g^{Ge} = 0.29$ eV, which means about 40% of the experimentally observed values 1.10 and 0.74 eV, respectively.
  2. In agreement with experiment, the band gap of Ge is found to be indirect at L-point.
- For the alloys within VCA we obtained:
  1. A meaningful variation of the band gaps of Si_xGe_{1-x} alloys with x has been found. The crossover point in the lowest optical transition from Ge-like ($\Gamma - L$ transition) to Si-like ($\Gamma - \Delta$-line transition) is found to be at $x = 0.12$, in agreement with the experimental value $x = 0.15$.
  2. It should be noticed that these results are almost the same as the Podgorny et al. results, but here we get such results from a well converged calculations at zero pressure, and using standard ingredients.
- Going beyond VCA, we have performed supercell calculations, all other ingredients are unchanged. Our main findings are:

1. The effects of ordering is discussed by calculating the band structure of three ordered structures (zinc-blende, tetragonal and rhombohedral), which have the same composition $x = 0.5$, using the same (VCA) charge density distribution. Some levels are split; but when taking a suitable average, the calculated band gaps are almost equal in the three structures at the high symmetry points, except for $X\Gamma$ and $L\Gamma$ transitions of the rhombohedral structure. This is understood as a result of the critical folding (X $\longrightarrow$ L) which occurs in this structure. The other band gaps can be used safely as those of the random alloys having the same composition.

2. The calculated values of the E_0 optical transition is almost the same for the above three structures and it is around 0.1 eV higher than that of VCA, which shows a downward bowing of the same order at $x = 0.5$. This shows that even at this level of approximations the supercell approach is better than VCA.

3. Because of the very small ionicity of Si-Ge bond, the effect of the charge density redistribution is negligible. This has been demonstrated by calculating the band structure of simple tetragonal SiGe structure using VCA, ZB and its own charge densities.

4. To study the effect of microscopic structural relaxation, we have compared the band structures of the unrelaxed and relaxed rhombohedral structure ($c/a_\perp$ ration is taken to be equal to one in the two cases). We have found that the $X_1^c - \Gamma_{15}^v$ optical transition is lowered by 0.04 eV in average. Recalling that the observed bowing at $x = 0.5$ for this transition is $\sim$ 0.1 eV, we conclude that large portion of the observed bowing is due to such structural disorder (VCA gives essentially no bowing).

- We have tried some EPM calculation. It has been found that this approach is unreliable for alloys, even after using the best extrapolation scheme and taking into account the change in the screening effects.

- The pressure coefficients of the band gaps at the high symmetry points of Si, Ge and $Si_{0.5}Ge_{0.5}$ alloy within VCA and having ZB structure have been

calculated, by simply repeating the band structure calculations at different lattice parameters smaller than the equilibrium one. The pressure is determined from the calculated equations of state. Our main findings are:

1. The calculated pressure coefficients of Si and Ge are in good agreement with other ab-initio calculations and experiment, in spite of the underestimation of the absolute values of these gaps.
2. For the alloy systems they show more Ge-like behaviors, and they are not equivalent.
3. The lowest direct optical transition at Γ of the alloy system shows a sublinear variation with pressure, similar to that observed for Ge and GaAs.

Appendix A

Full derivation of the CVM entropy expression

The cluster variation method (CVM) gives an approximation for the configurational entropy of the system in terms of the concentration (probability distribution) of a cluster configuration on the the lattice. In Sec. 3.2.2 an expression of the entropy for binary semiconducting alloys within the tetrahedron approximation is given. In binary alloys all the lattice sites are alloyed. Here this expression is derived in two different ways:

I. Following the notations of Sanchez and de Fontaine, the entropy in CVM is given as

$$S = Nk_B \sum_{(r,t)} \gamma(r,t) \sum_{l} \alpha_l(r,t) x_l(r,t) ln x_l(r,t) \qquad \text{(A.1)}$$

where N is the total number of lattice points or sites and k_B is the Boltzman's constant. The index t in (r,t) labels a specific type of r-sites cluster. Since each site can be occupied by either A or B type of atoms, there are generally 2^r configurations of an (r,t) cluster. However, some will be equivalent (In our present case there are ten different configurations of the 5-sites tetrahedron). The variable $x_l(r,t)$ is the concentration of the lth configuration of the (r,t) cluster, and $\alpha_l(r,t)$ is the degeneracy factor, which takes into account the equivalent configurations. The largest clusters to be considered must be chosen in advance in order to calculate the entropy using Eq. (A.1). These clusters are called basic clusters and contain n points. There can be many independent basic clusters with different values of n. The coefficients $\gamma(r,t)$ are given by

$$\gamma(n,t) = -N(n,t)/N \qquad \text{(A.2)}$$

for the basic clusters and by

$$\gamma(r,t) = -N(r,t)/N - \sum_{q=r+1}^{n} \sum_{s} M(r,t;q,s)\gamma(q,s), \qquad 1 \leq r < n \qquad \text{(A.3)}$$

for all other clusters, where $N(r,t)$ is the total number of (r,t) clusters in the system and $M(r,t;q,s)$ is the number of (r,t) clusters contained in a (q,s)

cluster. For any (r', t') cluster which completely contained in (n, t) basic cluster and is not shared by any other basic clusters,

$$N(r', t') = M(r', t'; n, t) N(n, t) \tag{A.4}$$

Using the relationship in Eq.'s (A.2) and (A.3) results in $\gamma(r', t') = 0$. Hence the only nonzero contributions to the entropy come from clusters formed from intersection of two basic clusters, or from intersection of other clusters for which $\gamma(r, t)$ is nonzero.

For the 5-site tetrahedron considered here as a basic cluster for binary alloys with diamond like structure , the tetrahedron surrounding an interstitial site (referred to here bas empty tetrahedron) can be thought as

- A subcluster which has non-vanishing contribution, in spite of not being an overlap of basic clusters; this is because one half of these clsters lies outside the basic clusters.
- Another basic cluster, which is adopted here.

Both choices give the same result. Now, the overlap regions of the two basic clusters can be a second nearest-neighbors (nnn) pair between 5-site and adjacent empty tetrahedra, first nearest-neighbors (nn) pair between two adjacent 5-site tetrahedra and a point if the center of the 5-site tetrahedra are nnn (see Fig. A.1). The values of $N(r, t)$ and $\gamma(r, t)$ are given in Tab. A.1.

(r,t) cluster	$N(r,t)/N$	$M(5,r)$	$M(4,r)$	$M(2(2),r)$	$M(2(1),r)$	$\gamma(r,t)$
5-site tet.	1	- - -	- - -	- - -	- - -	-1
Empty tet.	1	- - -	- - -	- - -	- - -	-1
nnn pair	6	6	6	- - -	- - -	6
nn pair	2	4	- - -	- - -	- - -	2
Point	1	5	4	2	2	-8

Table A.1: The entropy coefficients of 5-site and empty tetrahedra of the diamond structure.

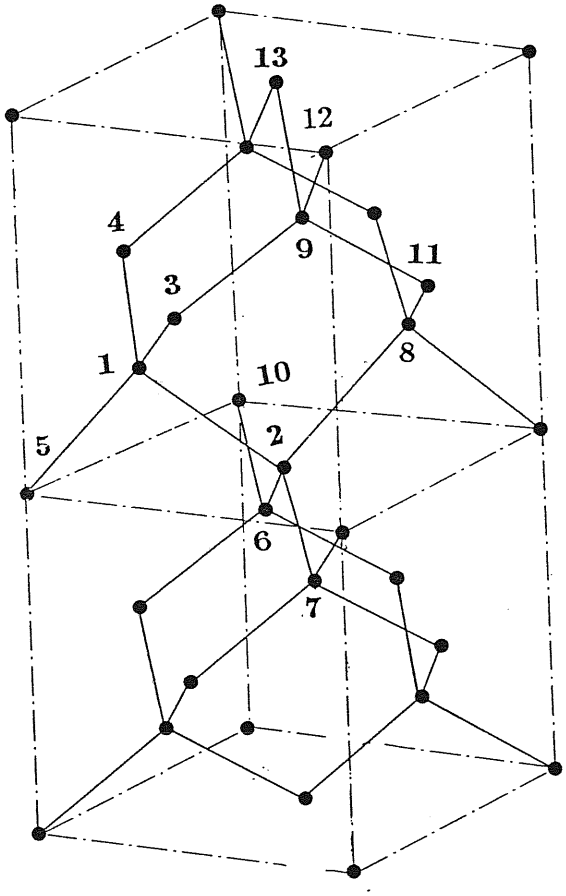

Figure A.1: The diamond structure. A typical 5-site tetrahedral cluster is indicated by the sites numbered 1-5 site 1 is the center of the cluster (cluster 1) and 2-5 are the first nearest-neighbor sites of site 1. Sites 1, 2, 6, 7 and 8 represent another 5-site cluster centered on site 2 (cluster 2) which overlaps cluster 1 at the first-neighbor pair cluster composed of sites 1 and 2. Sites 2, 4, 9 and 10 represent a 4-site cluster centered by vacancy (cluster 0) which overlaps cluster 1 at second-neighbor pair composed of sites 2 and 4. Sites 3, 9, 11, 12 and 13 represent a 5-site cluster (cluster 9) which overlaps with cluster 1 at the one point (site 3).

Using the coefficients of Tab. A.1 and Eq. (A.1), the CVM configurational entropy can be written as

$$S^{(CVM)} = -k_B \left(8 \sum_i x_i ln x_i + \sum_{ijklm} z_{ijklm} ln z_{ijklm} + \sum_{ijkl} w_{ijkl} ln w_{ijkl} \right.$$

$$\left. -2 \sum_{ij} y_{ij}^{(1)} ln y_{ij}^{(1)} - 6 \sum_{ij} y_{ij}^{(2)} ln y_{ij}^{(2)} \right) \qquad \text{(A.5)}$$

where z, w, $y^{(2)}$, $y^{(1)}$ are x are the concentrations of 5-site tetrahedron, empty tetrahedron, nnn pair, nn pair and point, respectively.

II. We can derive the same expression in a different way, thinking of the diamond structure as a bcc structure were one half of the sites are vacant. the vacant sites, in turn, form a second diamond structures. For the standard bcc structure the degeneracy factor [132] per point is

$$g_{bcc} = \frac{\left\{ \begin{array}{c} 1 \quad 2 \end{array} \right\}^4 \left\{ \begin{array}{c} 1 \\ 10 \quad 5 \\ \quad 4 \end{array} \right\}^6 \left\{ \begin{array}{c} \quad 1 \\ 2 \quad 5 \\ 3 \quad 4 \end{array} \right\}^6}{\left\{ \begin{array}{c} 2 \\ 3 \quad 1 \end{array} \right\}^{12} \left\{ \begin{array}{c} \quad 1 \\ 2 \quad 5 \\ 3 \\ \quad 10 \quad 4 \end{array} \right\}^3 \left\{ \begin{array}{c} 9 \quad 6 \\ 8 \quad 1 \quad 7 \\ 2 \\ 3 \quad 4 \quad 5 \end{array} \right\}}, \qquad \text{(A.6)}$$

in the standard CVM notations (e.g. $\{ \bullet\!\!-\!\!\!-\!\!\bullet \} = \prod_{i,j=1}^{n} y_{ij}!$, where n is the number of different types of atoms), where each cluster has been labeled with reference to Fig. A.2

For our modified bcc case, each of the clusters appearing in Eq. (A.6) splits into smaller or equal subclusters as follows

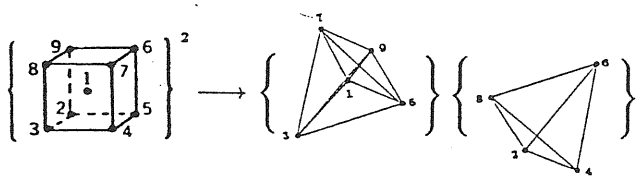

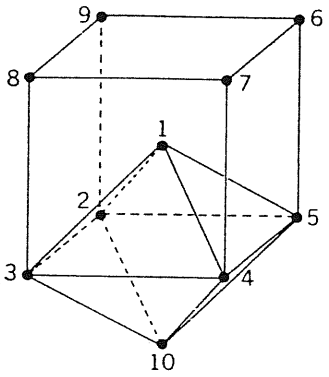

Figure A.2: Basic clusters for the bcc structure.

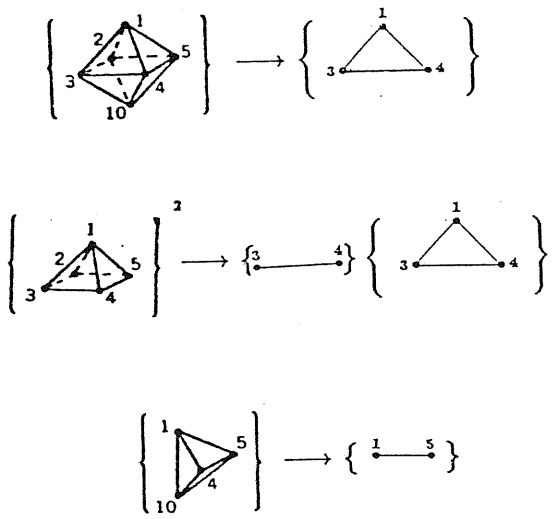

(A.7)

Taking into account the fact that the number of atoms is one half of that of full bcc-structure, the degeneracy factor of the diamond structure having the 5-site tetrahedron as basic cluster is

$$g_{diamond} = \frac{\{ \overset{1}{\bullet}\!\!-\!\!\!-\!\!\bullet\overset{2}{} \}^2 \{ \overset{3}{\bullet}\!\!-\!\!\!-\!\!\bullet\overset{4}{} \}^6 L!^2}{\left\{ \begin{array}{c} \\ \\ \\ \end{array} \right\} \left\{ \begin{array}{c} \\ \\ \\ \end{array} \right\} \{ \cdot \}^8} \qquad \text{(A.8)}$$

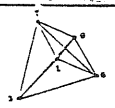

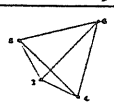

the corresponding entropy expression is exactly the same as that given in Eq. (A.5).

Bibliography

[1] A. Ourmazd and J. C. Bean, Phys. Rev. Lett. **55**, 765 (1985).

[2] T. S. Kuan, T. K. Kuech, W. I. Wang, and E. L. Wilikie, Phys. Rev. Lett. **54**, 201 (1985).

[3] H. R. Jen, H. J. Cherng, and G. B. Stringfellow, Appl. Phys. Lett. **48**, 1603 (1986).

[4] H . Nakayama and H. Fujita, in *GaAs and related compounds* 1985, edited by M. Fujimoto, Inst. Phys. Conf. Ser. No. 79 (Hilger, London, 1986).

[5] T. S. Kuan, W. I. Wang, and E. L. Wilikie, Appl. Phys. Lett. **51**, 51 (1987).

[6] M. A. Shahid, S. Mahajan, D. E. Loughlin and H. M. Cox, Phys. Rev. Lett. **58**, 2567 (1987).

[7] A. Gomoyo, T. Suzuki, K. Kobayashi, S. Kawata, and I. Hino, Appl. Phys. Lett. **50**, 673 (1987).

[8] A. Zunger and J. E. Jaffe, Phys. Rev. Lett. **51**, 662 (1983).

[9] G. P. Srivastava, J. L. Martins and A. Zunger, Phys. Rev. B **31**, 2561 (1985).

[10] J. L. Martins and A. Zunger, Phys. Rev. Lett. **56**, 1400 (1986).

[11] K. Kunc and I. P. Batra, preprint.

[12] S. Ciraci and I. P. Batra, Phys. Rev. Lett. **58**, 2114 (1987).

[13] S. Ciraci and I. P. Batra, Phys. Rev. B **36**, 1225 (1987).

[14] T. P. Pearsall et al., Phys. Rev. B **58**, 729 (1987).

[15] H. Kuwabara, H. Fujiyasu, A. Sasaki and S. Yamada, J. Cryst. growth **72**, 299 (1985).

[16] M. C. Tamargo et al., Appl. Phys. Lett. **46**, 569 (1985).

[17] D. M. Wood , S.H. Wei and Zunger, Phys. Rev. Lett. **58**, 1123 (1987)

[18] A. A. Mbaye, A. Zunger and D. W. Wood, Appl. Phys. Lett. **49**, 782 (1986).

[19] see for example, H. Kamimura and T. Nakayama, Comments Cond. Mat. Phys. **13**, 143 (1987), and Ref.'s therein.

[20] K. Ploog, private communications.

[21] T. Fukui and M. Saito, Jab. J. Appl. Phys. **23**, L521 (1984).

[22] J. C. Mikelson and J. B. Boyce, Phys. Rev. Lett. **49**, 1412 (1982); Phys. Rev. B **28**, 7130 (1983); Phys. Rev. B **31**, 6903 (1985).

[23] A. Balzarotti, M. T. Czyżyk, A. Kisiel, N. Motta, M. Podgorny, M. Zimnal, Phys. Rev. B **30**, 2295 (1984); Phys. Rev. B **31**, 7526 (1985).

[24] A. Balzarotti et al., Proc. of the 18th Int. Conf. on the Phys. of Semic., Stockholm, 1986.

[25] S. Minomura et al, J. Non-Cryst. Solids **59&60**, 541 (1983).

[26] L. Incoccia et al, Phys. Rev. B **31**, 1028 (1985).

[27] A. Qteish and R. Resta, in press.

[28] M. T. Czyżyk et al, Z. Phys. B **62**, 133 (1986); P. Letardi, N. Motta and A. Balzarotti, J. Phys. C **20**, 2853 (1987).

[29] A. R. Miedema, P. F. de Chatel, and F. R. Boer, Physica B&C **100** (1980).

[30] J. A. Van Vechten, in *Handbook on Semiconductors*, Vol. **3**, edited by S. P. Keller (North-Holland, Amsterdam, 1980).

[31] K. A. Jones, W. Porod and D. K. Ferry, J. Phys.Chem. of Solids **44**, 107 (1983).

[32] R. Kikuchi, Physica B **103**, 41 (1981).

[33] G. B. Stringfellow, J. Cryst. Growth **27**, 21 (1974); **58**, 194 (1982).

[34] P. A. Fedders and M. W. Muller, J. Phys. Chem. Solids **45**, 685 (1984).

[35] J. L. Martins and A. Zunger, Phys. Rev. B **30**, 6217 (1984).

[36] A. A. Mbaye, L. G. Ferreira and A. Zunger, Phys. Rev. Lett. **58**, 49 (1987).

[37] L. G. Ferreira, A. A. Mbaye, and A. Zunger, Phys. Rev. B **35**, 6475 (1987).

[38] G. P. Srivastava, J. L. Martins and A. Zunger, Phys. Rev. B **36**, 2902 (1987).

[39] R. Podloucky, H.J.F Jansen, A. J. Freeman, unpublished.

[40] A. Qteish and R. Resta, unpublished.

[41] P. Hohemberg and W. Kohn, Phys. Rev. **136**, B864 (1964).

[42] W. Kohn and L. J. Sham, Phys. Rev. **140**, A133 (1965)

[43] G. Abstreiter, H. Brugger, T. Wolf, H. Jorke and H. J. Herzog, Phys. Rev. Lett. **22**, 2441 (1983).

[44] R. Braunstein, A. R. Moore, and F. Herman, Phys. Rev. **109**, 968 (1968).

[45] J. S. Kline, F. H. Pollak and M. Cardona, Helv, Phys. Acta **41**, 968 (1968).

[46] *Theory of the inhomogeneous electron gas*, edited by S. Lundqvist and N. H. March (Plenum, New York, 1983).

[47] D. R. Hamann, M. Schlüter and C. Chiang, Phys. Rev. lett. **43**, 1494 (1979).

[48] G. P. Kerker, J. Phys. C **13**, L189 (1980).

[49] see for instance, H. T. Yin and M. L. Cohen, Phys. Rev. B **25**, 7403 (1982).

[50] see for example, *Ab-initio calculations of phonon spectra* , edited by J. T. Devreese, V. R. Van Doren and P. E. Camp (Plenum, New York, 1983).

[51] M. Lannoo, M. Schlüter, and L. J. Sham, Phys. Rev. B **32**, 3890 (1985), and Ref.'s therein.

[52] M. L. Cohen, Phys. Scr. **T1**, 5 (1982).

[53] M. L. Cohen, in *Highlights of Condensed Matter Theory*, edited by F. Bassani, F. Fumi and M. P. Tosi (North Holland, Amsterdam, 1985), p. 16.

[54] K. Kunc and R. M. Martin, Physica **117,118** B+C, 511 (1983).

[55] R. M. Martin, in *Electronic Structure, Dynamics and Quantum Structural Properties of Condensed Matter* , edited by J. T. Devreese and P. E. Camp (Plenum, New York, 1985), p. 175; and K. Kunc, *ibid,* p. 227.

[56] R. M. Martin, in *Festkörprobleme (Advances in Solid State Physics)*, Vol. **25**, edited by P. Grosse (Veiweg, Braunschweig, 1985), p. 3.

[57] R. Car and M. Parrinello, Phys. Rev. Lett. **55**, 2471 (1985).

[58] D. de Fontaine, in *Configurational Thermodynamics of Solid Solutions*, edited by H. Ehrenreich, F. Seitz and D. Turnball, Solid State Physics, Vol. **34** (Academic, New York, 1979), p. 73.

[59] D. M. Burley, in *Phase Transition and Critical Phenomena* edited by C. Domb and M. S. Green (Academic, London, 1972), p. 329.

[60] E. A. Guggenheim, *Mixtures*, (Oxford University Press, Oxford, 1952).

[61] V. T. Bublik , S. S. Gorelik, A. A. Zaitsev and A. Y. Polyakov, Phys. Stat. Sol. (b) **66**, 427 (1974).

[62] H. Mariette, Sol. State commun. **38**, 1193 (1981); H. Mareitte, J. A. Kash, and D. J. Wolford, Phys. Rev. B **31**, 5217 (1995).

[63] A. Zunger, Appl. Phys. Lett. **50**, 164 (1987).

[64] N. Churcher, K. Kunc and V. Heine, Solid State Commun. **56**, 177 (1985).

[65] V. T. Bublik and V. N. Leikin, Phys. Stat. Sol. (a) **46**, 365 (1978).

[66] see for example, H. Ehrenreich and L. M. Schwartz, in *Solid State Physics*, edited by H. Ehrenreich, F. Seitz, and D. Turnbull (Academic, New York, 1976), Vol. **31** p. 149.

[67] R. J. Lempert, K. C. Hass, and H. Ehrenreich, Phys. Rev. B **36**, 1111 (1987).

[68] T. Soma, Phys. Stat. Sol. (b) **95**, 427 (1979) and Ref.'s therein.

[69] E. N. Economou,*Green's Functions in Quantum Physics*, springer Ser. solid-state Sci., Vol. **7**, (Springer, Berlin, Heidelberg, New York 1983).

[70] D. M. Ceperley and B. J. Alder, Phys. Rev. Lett. **45**, 566 (1980).

[71] J. Perdew and A. Zunger, Phys. Rev. B **23**, 5048 (1981).

[72] G. Bachelet, D. R. Hamann and M. Schlüter, Phys. Rev. B **26**, 4199 (1982).

[73] A. Baldereschi, Phys. Rev. B **7**, 5212 (1973).

[74] D. J. Chadi and M. L. Cohen, Phys. Rev. B **8**, 5747 (1973).

[75] F. D. Murnagham, Proc. Natl. Acad. Sci. U. S. A. **3**, 244 (1944).

[76] J. P. Dismukes, L. Ekstrom, and R. J. Paff, J. Phys. Chem. **68**, 3021 (1964).

[77] E. K. Abrikosov, V. F. Bankina, L. V. Poretskaya, L. E. Shelimora, E. V. Skudonova, *Semiconducting II-VI, IV-VI and V-VI compounds*, Plenum Press, New York 1969.

[78] L. Nordheim, Ann. Phys. (Leipz) 9, 607 (1931); 641 (1931).

[79] L. Pauling and M. L. Huggins, Z. Kristallogr. Kristallgeom. Kristallphys. Kristallchem. 87, 205 (1934).

[80] C. H. P. Lupis and J. F. Elliot, Acta Met. **15**, 265 (1967)

[81] J. C. Mathieu, F. Durand and E. Bouniem, J. Chem. Phys. **11-12**, 1289 (1965).

[82] K. Mui and F. W. Smith, Phys. Rev. B **35**, 8080 (1987).

[83] H. J. Monkhorst and J. D. Pack, Phys. Rev. B **13**, 5188 (1976).

[84] P. N. Keating, Phys. Rev. **145**, 637 (1966); R. M. Martin, Phys. Rev. B **1**, 4005 (1970).

[85] A. Balzarotti et al. Phys. Rev. B **30**, 2295 (1984).

[86] A. Marbenf and J. C. Guillaume, Revue Phys. Appl. **19**, 311 (1984).

[87] R. Kikuchi, J. Chem. Phys. **60**, 1071 (1974).

[88] C. H. P. Lupis, *Chemical Thermodynamic of Materials.* North Holland, Amsterdam, 1983.

[89] T. Soma, Phys. stat. sol. (b) **95**, 427 (1979).

[90] H. Matsuo Kagaya and T. Soma, Phys. stat. sol. (b) **139**, 427 (1987).

[91] R. People and S. A. Jackson, Phys. Rev. B **36**, 1310 (1987).

[92] L. Brey and C. Tejedor, Phys. Rev. Lett. **59**, 1022 (1987).

[93] M. S. Hybertsen and M. Schlüter, unpublished.

[94] S. Froyen, D. M. Wood and A. Zunger, Phys. Rev. B **36**, 4547 (1987).

[95] D. M. Bylander and L. Kleinman, Phys. Rev. B **34**, 5280 (1987).

[96] A. Taguchi and T. Ohno, Phys. Rev. B **36**, 1696 (1987).

[97] H. Kamimura and T. Nakayama, Comments Cond. Mat. Phys. **13**, 143 (1987), and Ref.'s therein.

[98] T. Nakayama and H. Kamimura, J. Phys. Soc. Jpn. **54**, 4762 (1985).

[99] F. Bassani and D. Brust, Phys. Rev. **131**, 1524 (1963).

[100] E. F. Knstov et al., Sov. Phys. Semicond. **17**, 481 (1983).

[101] D. Stroud and H. Ehrenreich, Phys. Rev. B **2**, 3197 (1970).

[102] M. Podgorny, G. Wolfgarten and J. Pollmann, J. Phys. C **19**, L141 (1986).

[103] G. B. Bachelet and N. E. Christensen, Phys. Rev. B **31**, 879 (1985).

[104] C. G. Van de Walle and R. M. Martin, Phys. Rev. B **34**, 5621 (1986).

[105] H. Holloway and L. C. Davis, Phys. Rev. Lett. **53**, 830 (1984), and Ref.'s therein.

[106] C. O. Rodriguez, E. L. Peltzer y Blanca, and O. M. Cappannini, Phys. Rev. B **33**, 8436 (1986).

[107] C. O. Rodriguez, E. L. Peltzer y Blanca, and O. M. Cappannini, Sol. Stat. Commun. **56**, 575 (1985).

[108] S. Fahy et al., Phys. Rev. B **35**, 5856 (1987).

[109] K. J. Chang, S. Froyen, and M. L. Cohen, Sol. Stat. Commun. **50**, 105 (1984).

[110] S. Lee, J. Sanchez-Dehesa and J. D. Dow, Phys. Rev. B **32**, 1152 (1985).

[111] B. Welber, M. Cardona, Y. F. Tsay, and B. Bendow, Phys. Rev B **13**, 875 (1976).

[112] A. R. Goni, K. Strossner, K. Syassen, and M. Cardona, Phys. Rev. B **36**, 1581 (1987).

[113] See for example the review article of F. Herman, R. L. Kortum, and C. D. Kuglin, Int. J. of Quantum Chem. **15**, 533 (1967).

[114] M. Cardona and F. H. Pollak, Phys. Rev. **142**, 530 (1966).

[115] J. R. Chelikowsky and M. L. Cohen, Phys. Rev. B **14**, 556 (1976).

[116] M. L. Cohen and T. K. Bergstresser, Phys. Rev. **141**, 789 (1966).

[117] D. J. Chadi, Phys. Rev. B **16**, 3572 (1977).

[118] M. T. Yin, Phys. Rev. B **27**, 7769 (1983).

[119] See for instance, A. Onton, J. Luminescence **7**, 95 (1973); Festkörperprobleme **13**, 59 (1973).

[120] E. Erbarut and M. Tomak, Phys. Stat. Sol. (b) **132**, 173 (1985).

[121] S. Krishnamurthy, A. Sher and A. B. Chen, Phys. Rev. B **33**, 1026 (1986).

[122] Landolt-Börnstein, Zahlenwerte and Iunktionen aus naturwissen-schaften und Techhnik, N. S. Vol. **3**, 17a, (Springer Verlag, New York, 1982).

[123] M. S. Hybertsen and S. G. Louie, Phys. Rev. B **34**, 5390 (1986).

[124] J. A. Van Vechten and T. K. Bergstresser, Phys. Rev. B **1**, 3351 (1970).

[125] S. Bednarek and U. Rõssler, Phys. Rev. Lett. **43**, 1296 (1082).

[126] P. B. Allen and M. Cardona, Phys. Rev. B **27**, 4760 (1983).

[127] O. J. Gelmbocki and F. H. Pollak, Phys. Rev. Lett. **48**, 413 (1982).

[128] Y. F. Tsay, S. S. Mirta and B. Bendow, Phys. Rev. B **10**, 1476 (1974).

[129] J. C. Phillips, in *The Fundamental Optical Spectra of Solids*, edited by H. Ehrenreich, F. Seitz and D. Turnbull, Solid State Physics, Vol. **18** (Academic, New York, 1966), p. 55.

[130] R. Resta, Phys. Rev B **16**, 2717 (1977).

[131] S. Y. Ren, J. D. Dow, and D. J. Wolford, Phys. Rev. B **25**, 7661 (1980).

[132] J. M. Sanchez and D. de Fontaine, Phys. Rev. B **17**, 2926 (1978).